THE FLOW PATTERN, SOLIDS SETTLING, AND CHARACTERISTICS OF A SASKATOON, SASKATCHEWAN STORMWATER MANAGEMENT POND

A Thesis

Submitted to the College of Graduate and Postdoctoral Studies

In Partial Fulfillment of the requirements

for the

Degree of Master of Science

in the

Department of Civil, Geological and Environmental Engineering

University of Saskatchewan

Saskatoon, Saskatchewan, Canada

By

Carrie Jane Gillis

PERMISSION TO USE

In presenting this thesis in partial fulfilment of the requirements for a Postgraduate degree from the University of Saskatchewan, I agree that the Libraries of this University may make it freely available for inspection. I further agree that permission for copying of this thesis in any manner, in whole or in part, for scholarly purposes may be granted by the professor or professors who supervised my thesis work or, in their absence, by the Head of the Department or the Dean of the College in which my thesis work was done. It is understood that any copying or publication or use of this thesis or parts thereof for financial gain shall not be allowed without my written permission. It is also understood that due recognition shall be given to me and to the University of Saskatchewan in any scholarly use which may be made of any material in my thesis.

Requests for permission to copy or to make other use of material in this thesis in whole or part should be addressed to:

Head of the Department of Civil, Geological and Environmental Engineering

University of Saskatchewan

57 Campus Drive

Saskatoon, Saskatchewan S7N 5A9

Canada

Or

Dean of College of Graduate and Postdoctoral Studies

University of Saskatchewan

116 Thorvaldson Building, 110 Science Place

Saskatoon, Saskatchewan S7N 5C9

Canada

DISCLAIMER

Reference in this thesis to any specific commercial products, process, or service by trade name, trademark, manufacturer, or otherwise, does not constitute or imply its endorsement, recommendation, or favoring by the University of Saskatchewan. The views and opinions of the author expressed herein do not state or reflect those of the University of Saskatchewan, and shall not be used for advertising or product endorsement purposes.

ABSTRACT

The work described herein took place during 2014 (June 23 to September 30) to investigate the removal efficiency of solids, the settling of solids, and the hydraulics (flow pattern, velocity) within a conventional stormwater pond located in John Avant Park, Saskatoon, Saskatchewan, Canada. The stormwater pond in John Avant Park has a total contributing catchment area of 114.62 ha, from three inlets, one outlet, a man-made aeration stream, and an aeration fountain.

Programmable ISCO 6700 series automated stormwater samplers equipped with ISCO 750 acoustic Doppler area velocity flow modules were installed in the inlet and outlet manholes to measure the water level and velocity. Stormwater samples were collected within 24 hours for concentration and particle size distribution analysis, following each of 14 rain events that occurred during the measurement period. A hand corer and a water depth to sediment surfaces measurement apparatus (telescopic pole with foot) were used to investigate spatial variances in the particle size distribution and accumulation of settled solids. A robotic total station and a three dimensional prism were used to track drogues to investigate pond hydraulics. For comparison, camera equipment was used and calibration points were surveyed to evaluate the movement of drogues using concepts from large scale particle tracking velocimetry (LSPTV) along with visual observations.

In total, 82 mm of rainfall was recorded over the field season, resulting in an inflow to the pond of approximately 66,517 m^3, as measured from the inlets. The total outflow from the pond was approximately 154,150 m^3, where 86,943 m^3 of the outflow was not accounted for as inflow measured in the inlets. It was found that the stormwater pond had a total solids removal efficiency of -67%, indicating a higher concentration of solids were leaving the pond than entering. Solids sampled from the pond's outflow had a higher concentration of finer particles than the inflow,

suggesting the pond was more effective at removing larger particle sizes. From the negative removal efficiency and the higher concentration of finer particles in the outflow, it was determined that resuspension of finer grained solids (clay, silt size) potentially occurs.

From 51 sediment depth measurements taken throughout the pond it was estimated that the pond is accumulating approximately 1 cm of solids per year, based on when the pond went into service in the late 1980s. It was found that over the summer season, from June 24 to August 25, the spatial distribution of sediment thickness slightly differed. The thickness of core samples varied from approximately 10 cm to just over 30 cm, where the clay liner of the pond was captured in some cores and not others such that the cores themselves could not be used to indicate depth. Core samples were predominately comprised of sand, with coarser particles (sand, gravel) located closer to the inlets and the periphery. Finer particles (silt, clay) were more predominant further away from the inlets.

Drogue tracking was performed on five different occasions throughout the field season to evaluate pond hydraulics (flow pattern, velocities) using surveying with a robotic total station, concepts from Large Scale Particle Tracking Velocimetry (LSPTV), and visual observations. The flow path and velocity of drogues were found to be predominately related to the wind speed and direction. Results from this field investigation suggest that short-circuiting could occur when the wind direction is from the inlets to the outlet during rain events or baseflow conditions as drogues were seen to travel in this direction under those conditions.

ACKNOWLEDGEMENTS

I would like to acknowledge the Natural Sciences and Engineering Research Council (NSERC) of Canada for funding this project. I would also like to acknowledge the Association of Professional Engineers and Geoscientists of Saskatchewan for their Continuing Education Grant for members of the Association. Many thanks go to my supervisors Kerry Mazurek and Gordon Putz who offered a wealth of knowledge and always made time to answer questions and to have encouraging and helpful discussions. Their understanding and patience as I maintained working while completing my graduate studies will never be forgotten and was greatly appreciated. Thank you also to the other members of my graduate committee James Kells and Warren Helgason for your helpful input and feedback and to Cory Albers for your advice and direction. This project would not have been possible without the help and input of Dale Pavier, Adam Hammerlindl, Brendan Pokoyoway, and the field support provided by Andrew Pan, Scott Coleville, Mina Ahadi, Balew Mekonnen, Mahmud Amin, and Rocky Chowdhury.

I would also like to acknowledge my husband John Hugh for the years of support and encouragement. Thank you also to my family for always believing in me and supporting me throughout my studies. Last not least, I will be forever thankful to my good friend and former colleague Joy Agnew. Thanks for the emotional support, being that extra little push when I needed it most, and helping to instill in me the confidence that I needed. Thank you all so very much.

TABLE OF CONTENTS

PERMISSION TO USE…….…….... i

DISCLAIMER……. ii

ABSTRACT……. iii

ACKNOWLEDGEMENTS…….. v

TABLE OF CONTENTS……. vi

LIST OF TABLES……...…… viii

LIST OF FIGURES…….……...……... x

LIST OF NOTATIONS…….....…….. xiv

Chapter 1 INTRODUCTION……... 1

1.1 Objectives…….. 3

1.2 Project Scope……. 4

1.3 Organization of the Thesis……. 4

Chapter 2 LITERATURE REVIEW…… 5

2.1 City of Saskatoon Stormwater Requirements Overview…….. 5

2.2 Inflow to and Outflow from a Stormwater Management Pond……. 5

2.3 Settling of Solids within a Stormwater Management Pond…….. 11

2.4 Flow Pattern in a Stormwater Management Pond……. 14

2.4.1 Tracers…….. 14

2.4.2 Particle Image Velocimetry and Particle Tracking Velocimetry……..... 15

2.4.3 Drogues……. 20

Chapter 3 METHODOLOGY…….. 23

3.1 Field Site Characteristics……... 24

3.2 Meteorological Data Collection……. 25

3.3 Inflow and Outflow Sampling……... 27

3.4 Settled Solids Investigation……... 38

3.5 Flow Pattern and Velocity Investigation……... 45

Chapter 4 ANALYSIS, RESULTS, AND DISCUSSION……... 52

4.1 Analysis of Rainfall Events……...……..... 52

4.2 Pond Inflows and Outflows……...…… 57

4.3 Total Solids Analysis for Flow in Inlets and Outlet……..…….. 65

4.4 Settled Solids Investigation Within the Pond……... 74

4.5 Investigation of the Flow Pattern in the Pond…….. 86

Chapter 5 CONCLUSIONS AND RECOMMENDATIONS……. 105

LIST OF REFERENCES……..... 111

APPENDIX A RAINFALL HYETOGRAPHS…….. 122

APPENDIX B INLET AND OUTLET CONCENTRATION WITH FLOW……..... 128

APPENDIX C PARTICLE SIZE DISTRIBUTION DATA…… 131

APPENDIX D POND SEDIMENT THICKNESS MEASUREMENTS……. 133

APPENDIX E POND SEDIMENT PARTICLE SIZE DISTRIBUTION……... 136

LIST OF TABLES

Table 3-1 Major research project activities and sub-activities……...…….. 23

Table 3-2 Particle size distribution of pond sediment classifications……...…….. 37

Table 4-1 Rain events recorded by the tipping bucket rain gauge and the status of Inlet 1, 2, and 3 (I1, I2, I3 respectively) and Outlet sampler measurements during, and following these rain events…...…… 55

Table 4-2 Maximum water levels, velocities, and flow rates for the three inlet pipes over the data collection season ……...……. 60

Table 4-3 Event mean concentrations (EMCs) and total discharge volume (V_T) for the inlets and Outlet, used to determine the site mean concentration (SMC), load of total solids (L), and the total removal efficiency of the pond.……..……... 67

Table 4-4 Using collinearity equation calibration coefficients to back calculate calibration points to test the accuracy of the method……. 89

Table 4-5 Tracking drogue velocity, inlet flows, and Outlet flow for the July 17, 2014 drogue tracking event.……... 93

Table 4-6 Tracking drogue velocity, inlet flows, and Outlet flow for the August 20, 2014 drogue tracking event…… 94

Table 4-7 Tracking drogue velocity, inlet flows and Outlet flow for the September 3, 2014 drogue tracking event…… 96

Table 4-8 Tracking drogue velocity, inlet flows, and Outlet flow for the September 19, 2014 drogue tracking event…….. 97

Table 4-9 Summary of forces on the drogue…… 103

Table C-1 Particle size distribution of total solids sampled over the summer sampling season in 2014……...…….…….. 132

Table D-1 June 2014 sediment depth measurements along with the corresponding northing and easting survey coordinates ……...…….. 134

Table D-2 August 2014 sediment depth measurements with the corresponding northing and easting survey coordinates ……...…….…… 135

Table E-1 June stormwater pond sediment particle size distribution ……...……... 137

Table E-2 August stormwater pond sediment particle size distribution ……. 138

Table E-3 Individual sample data from particle size distribution analysis for June and August samples of 2014…….…….. 139

LIST OF FIGURES

Figure 3-1 Plan view of the John Avant Park stormwater management pond in Erindale, Saskatoon, Saskatchewan, with arrows depicting approximated locations of inlets (arrows into pond) and Outlets (arrows out of pond) (Adapted from Google Maps, 2014)…….……..... 25

Figure 3-2 Tipping bucket rain gauge mounted to a stand along with the data logger protected in an enclosed box ……..……. 27

Figure 3-3 An ISCO 6712 series automated stormwater sampler with 12 V battery attached……. 28

Figure 3-4 Manufacturer's intake strainer for stormwater to enter the ISCO sampler pumping system ……... 29

Figure 3-5 Adapted intake strainer design (left) initially used for project shown in the inlet pipe at the bottom of the manhole (right)……...…..……. 30

Figure 3-6 ISCO 750 area-velocity modules installed upstream of the intake strainer initially used for the project…….. 32

Figure 3-7 Pipe (left) conveys stormwater from the catchment area to the manhole (right, top-down view)……...…….. 32

Figure 3-8 Broad crested weir in the bottom of the Outlet manhole, with area-velocity module installed on the side of the manhole upstream of the weir……..... 33

Figure 3-9 (Left) ISCO samplers and batteries with tie strap and chain assembly hung in manholes for easy retrieval (right) ……... 34

Figure 3-10 (Left) Retrieval of ISCO 6700 samplers for data logging, sample bottle exchange, and battery exchange (center), and return to the manhole (right)…...……..... 35

Figure 3-11 Full sample bottles from the ISCO 6700 series samplers (left), and an individual example of a sample bottle containing a sample (right)……. 35

Figure 3-12 Gilson Vibratory Sieve Shaker (left) and Hoskin Scientific mechanical sieve shaker (right) used for particle size distribution testing of solids…… 36

Figure 3-13 Hydrometer (left) and graduated cylinders used for determining the particle size distribution of solids…….…… 37

Figure 3-14 Sample/measurement locations within the pond perimeter and locations of the three inlets and Outlet.……..…….. 39

Figure 3-15 Taut cable secured at both banks of the pond (left), where stakes were then surveyed to determine the ground coordinates from which the sample distances from the stakes were measured (right)..... 40

Figure 3-16 Wildco hand corer with extension pole attached, used to take core samples of pond sediment..... 41

Figure 3-17 Telescopic pole with metal foot used to take depth measurements..... 42

Figure 3-18 Core sample with visible clay liner and water trapped between clay liner and cap (left), along with no longer intact sample prior to drying..... 43

Figure 3-19 Surveying the water elevation of the pond as part of the sediment depth measurement procedure..... 44

Figure 3-20 Example of a drogue that was constructed..... 46

Figure 3-21 Three-dimensional prism (left) and Leica robotic total station (right) used to track the prism-attached drogue..... 47

Figure 3-22 Camera set up at an oblique angle overlooking the stormwater pond with the drogues in the flow..... 48

Figure 4-1 Inter-event time plot to determine the number of rain events over the season and the time separating rain events..... 53

Figure 4-2 Recorded precipitation from the first rainfall to the last rainfall over the measurement period..... 56

Figure 4-3 Definition sketch for the finite crested-weir located at the Outlet, with the Outlet from the pond (left), and the Outlet to the storm sewer distribution system (right).. 59

Figure 4-4 Inlet and Outlet pipe flow rate and measured precipitation amounts for the July 17 to 18, 2014 rain event, where flow in the inlets reached a maximum approximately 3.75 hours after the start of precipitation, as determined by the first tip of the tipping bucket rain gauge..... 61

Figure 4-5 Inlet and Outlet pipe flow rate and measured precipitation amounts for the July 24, 2014 rain event, where flow in the inlets reached a maximum approximately 10 hours after the start of precipitation, as determined by the first tip of the tipping bucket rain gauge..... 61

Figure 4-6 Inlet and Outlet pipe flow rate and measured precipitation amounts for the July 24, 2014 rain event, where flow in the inlets reached a maximum approximately 10 hours after the start of precipitation, as determined by the first tip of the tipping bucket rain gauge..... 62

Figure 4-7 Determination of baseflow from the Outlet…… 64

Figure 4-8 The variation of total solids concentrations with flow rate for Inlet 2 over all rain events……. 70

Figure 4-9 Total solids concentration and flow rate with the time from the start of precipitation for the July 17-18, 2014 rain event……...……... 71

Figure 4-10 Total solids concentration and flow rate with the time from the start of precipitation for the July 24, 2014 rain event……...……..……. 71

Figure 4-11 Particle size distribution of solids in the inlets and Outlet of the John Avant Park stormwater pond…….. 73

Figure 4-12 Measured in June existing pond bottom elevation, which indicates the distribution of sediment over the pond, where the design pond bottom elevation was 499.0 m …… 76

Figure 4-13 Measured in June existing pond bottom elevation with a 20 cm contour interval, where the design pond bottom elevation was 499.0 m…….…….. 77

Figure 4-14 Measured in August existing pond bottom elevation, which indicates the distribution of sediment over the pond, where the design pond bottom elevation was 499.0 m……... 78

Figure 4-15 Measured in August existing pond bottom elevations with a 20 cm contour interval, where the design pond bottom elevation was 499.0 m……..……. 79

Figure 4-16 Percentage of gravel by mass throughout the pond, from June (left) and August (right) measurements (5% contour intervals)……...…… 80

Figure 4-17 Percentage of sand by mass throughout the pond, from June (left) and August (right) measurements (10% contour intervals)……...……... 81

Figure 4-18 Percentage of silt by mass throughout the pond, from June (left) to August (right) measurements (1% contour interval)…….. 82

Figure 4-19 Percentage of clay by mass throughout the pond, from June (left) to August (right) measurements (1% contour intervals)……... 83

Figure 4-20 Percentage of sediment mass less than 50 microns throughout the pond, from June (left) to August (right) measurements (2% contour interval)…….…… 84

Figure 4-21 MathCad example of finding collinearity equation camera calibration coefficients, shown as matrix (Q), from the September 19, 2014 drogue tracking event…….. 88

Figure 4-22 Example of a photo from the camera set up for LSPTV during the September 19, 2014 drogue tracking event…….. 92

Figure 4-23 September 3, 2014 drogue tracking using the robotic total station and the 3D prism, where arrows near the drogue flow paths indicate direction of drogue movement, and the arrows N, E, S, W indicate north, east, south, and west directions……. 95

Figure 4-24 September 19th drogue tracking using the robotic total station and the 3D prism, where arrows near the drogue flow paths indicate direction of drogue movement, and the arrows N, E, S, W indicate the north, east, south, and west directions..... 97

Figure 4-25 Definition of forces on the drogue…….. 99

Figure 4-26 Drogue tracking showing the leading drogue with the shallowest fin, with drogues with deeper fins lagging in order of depth…….. 104

Figure A-1 Hyetograph for the rain event beginning at 11:00 July 9, 2014…… 123

Figure A-2 Hyetograph for the rain event beginning at 19:15 July 17, 2014…….. 123

Figure A-3 Hyetograph for the rain event beginning at 8:40 July 24, 2014…… 124

Figure A-4 Hyetograph for the rain event beginning at 12:00 July 25, 2014…….. 124

Figure A-5 Hyetograph for the rain event beginning at 3:47 August 20, 2014……..... 125

Figure A-6 Hyetograph for the rain event beginning at 10:50 August 24, 2014…….. 125

Figure A-7 Hyetograph for the rain event beginning at 19:21 September 2, 2014…….. 126

Figure A-8 Hyetograph for the rain event beginning at 1:01 September 8, 2014…… 126

Figure A-9 Hyetograph for the rain event beginning at 5:57 September 13, 2014…….. 127

Figure B-1 Relationship of total solids concentration and flow rate in Inlet 1…… 129

Figure B-2 Relationship of total solids concentration and flow rate in Inlet 2…… 129

Figure B-3 Relationship of total solids concentration and flow rate in Inlet 3…… 130

Figure B-4 Relationship of total solids concentration and flow rate in the Outlet…….. 130

LIST OF NOTATIONS

A	Cross-sectional or projected area
A_{bd}	Projected area for the bottom-half of the drogue float
ADV	Acoustic Doppler Velocimeter
ADCP	Acoustic Doppler Current Profiler
b	Weir width (also equals b_c)
BMP	Best Management Practice
C_{aw}	Drag coefficient
C_d	Discharge coefficient or dimensionless drag coefficient
C_{dbu}	Drag coefficient for the top-half of the drogue float
C_i	Sampled concentration of solids of time interval i
C_v	Approach velocity correction coefficient
d	Diameter
EMC	Event Mean Concentration
F_{bs}	Drag force on the submerged bottom-half of the drogue float
F_{bu}	Drag force on the unsubmerged top-half of the drogue float
F_f	Drag force on the drogue fin
Fs	Drag force on the line connecting the drogue float and fin
g	Acceleration of gravity
h_1	Water level upstream of weir
H_1	Total energy head
I1	Inlet 1
I2	Inlet 2
I3	Inlet 3
IETD	Inter-event time definition
l	Length of weir in the direction of flow
L	Mass loading over the season
LSPIV	Large Scale Particle Image Velocimetry
LSPTV	Large Scale Particle Tracking Velocimetry
O	Outlet
PIV	Particle Image Velocimetry
PTV	Particle Tracking Velocimetry

Q	Flow rate
R	Removal efficiency (%)
SMC	Site Mean Concentration
TSS	Total Suspended Solids
TS	Total Solids
TDS	Total Dissolved Solids
u	Time-averaged velocity above the water surface at elevation z, or easting
u_*	Shear velocity
U_f	Water velocity at the depth of the drogue fin
U_s	Water velocity at the water surface (due to wind)
v	Velocity
V_i	Total volume of water discharged over time interval i
VSS	Volatile Suspended Solids
V_T	Total volume of water discharged from inlets and Outlet over season
W	Wind velocity at the elevation of the drogue float
W_{10}	Wind velocity at 10 m elevation above the water surface
y	Water level
z	Elevation
z_o	Roughness height due to waves
κ	Von Karman's constant
ρ_{air}	Density of air
ρ	Density of water
τ	Shear stress
ν	Viscosity of wind

Chapter 1

INTRODUCTION

Stormwater management ponds have been designed and constructed not only to store urban runoff and attenuate peak flows during rain events, but also to improve the water quality entering receiving surface waters such as rivers, lakes, and wetlands. During a rain event, urban runoff carries garbage (litter), emission deposits from vehicles, fecal matter, fertilizers, and pesticides, which can contain contaminants such as metals, nutrients, bacteria, and solids (Kantrowitz and Woodham 1995). These contaminants can be a major contributor to the pollution and contamination of receiving waters (Birch *et al.* 2006). Contaminants can also be a major nuisance to nearby residents as pollutants can lead to odors and poor visual esthetics.

In the Canadian Prairies, stormwater management ponds are often enjoyed by paddlers and their surrounding areas also serve as residential park. Typically, housing surrounding stormwater management ponds is considered prime real estate with increased property value (Wakelin *et al.* 2003). Developers often market lots surrounding stormwater management ponds as backing onto a freshwater urban lake, often leading to misconceptions of their actual purpose (Wakelin *et al.* 2003). Water quality in these ponds is therefore of utmost importance to nearby homeowners, where odors and poor pond aesthetics often lead to complaints to the municipality.

Stormwater management ponds may remove suspended solids and their associated contaminants through sedimentation. When incoming urban stormwater runoff enters the pond from the collection system through inlet pipes, the flow velocity is reduced and suspended solids settle out. The proportion of suspended solids that settles out is a function of the design volume and functionality (geometry, flow pattern) of the pond (Birch *et al.* 2006). Therefore, effective

stormwater management pond designs will help to minimize contamination of receiving waters. Many Canadian provinces and municipalities have put forward guidelines or best management practices (BMPs) to specify stormwater treatment to reduce the mass of pollutants entering receiving waters and to reduce the peak flow. For example, the City of Calgary (2011) requires that at least 85% of total suspended solids (TSS) with particle sizes of 50 μm or greater be removed from stormwater before stormwater enters receiving surface waters for water quality and aquatic protection. Lake Tahoe in California has set total maximum daily loads for particle sizes under 16 μm, where water is only allowed to enter the lake via infiltration from very large sedimentation basins (Kayhanian *et al.* 2012).

Case studies on stormwater management ponds have examined the removal efficiencies of typical contaminants found in urban runoff such as major ions (chloride, calcium, bicarbonate), metals (aluminum, chromium, copper, lead, mercury, zinc), nutrients (ammonia-nitrogen, nitrate-nitrogen, nitrite-nitrogen, organic-nitrogen, phosphorous, orthophosphate-P), dissolved solids, suspended volatile solids, total suspended solids, biochemical oxygen demand, chemical oxygen demand, and fecal coliforms (Kantrowitz and Woodham 1995; Birch *et al.* 2006; Pettersson and Lavielle 2007). Although studies have assessed the contaminant removal efficiencies of stormwater management ponds (Birch *et al.* 2006; Kantrowitz and Woodham, 1995) and the hydraulic retention times using dye tracers (Barter 2003; Hanna 1989), there has been less work examining the flow patterns within ponds (Shilton 2001).

The flow pattern within a stormwater management pond will influence both the location and particle sizes of solids that settle. Ineffective flow patterns may contribute to short-circuiting or dead-zones within the pond, consequently reducing the retention time which could compromise treatment efficiencies. Accumulated sediment in the pond may also contribute to decreased

retention times due to a reduction in storage volume, or even potential negative removal efficiencies if settled solids become re-suspended. Increased aquatic vegetation within a pond may also influence flow behavior, which ultimately affects the settling of solids.

Collecting field data to gain an understanding of the flow patterns within a stormwater management pond and how it might influence the particle size and removal efficiency of settled solids will help guide future pond designs. Detailed information on typical solids concentrations in pond inflow and outflow, characteristics of storms, flow patterns, and where sediment has deposited can also help with numerical modelling of flow within a pond, which will be attempted as part of the larger project of which this work is a component.

The field-based research discussed herein was conducted at the John Avant Park stormwater management pond in Erindale, Saskatoon, Saskatchewan, Canada. The John Avant Park stormwater pond was chosen because of its accessibility, representative size, proximity to the University of Saskatchewan, fewer inlets and Outlets than comparable ponds (less equipment needed), and the availability of a secure location to set up a rain gauge and data logger for precipitation measurements.

1.1 Objectives

There were three major objectives of this work:

(1) To determine the Erindale stormwater management pond's removal efficiency of solids and the removal efficiency of solids by particle size;

(2) To determine the spatial distribution of solids accumulation within the stormwater management pond, solids accumulation rate, and the particle size distribution of accumulated solids; and

(3) To determine the flow pattern within the Erindale, Saskatoon stormwater management pond and how it might affect the distribution of settled solids within the pond.

1.2 Project Scope

The scope of this project included inflow and outflow sampling for solids concentration and particle size, investigating the settled solids in the stormwater management pond, and investigating the internal flow pattern of the stormwater management pond. The scope of this project did not include investigating the removal efficiency of nutrients, heavy metals, or bacteria. Measuring the residence time of the pond was also not included in the project scope.

1.3 Organization of the Thesis

The thesis is organized as follows. Chapter 2 is a literature review outlining requirements for stormwater management set by the City of Saskatoon, as well as research that has been conducted on stormwater solids, the settling of solids in stormwater management ponds, and related research pertaining to flow patterns and velocities. Next, Chapter 3 outlines the methodology used to conduct the field work for this project, including all data collection and procedures used for sample analysis. Chapter 4 then presents the data analysis, and discusses the project results. Finally, Chapter 5 consists of concluding remarks and recommendations for future research.

Chapter 2

LITERATURE REVIEW

A number of studies have examined the removal efficiency and particle size distribution of solids present in stormwater inflow to a stormwater management pond. Studies have also assessed the spatial distribution of sediment, particle size distribution of sediment, and flow patterns within stormwater management ponds. In this chapter, City of Saskatoon stormwater management requirements are reviewed along with these topics.

2.1 City of Saskatoon Stormwater Requirements Overview

For all new developments, the City of Saskatoon (2012) requires that stormwater runoff is routed through a conveyance, storage, and treatment system, which is completely separate from the sanitary sewer system. Saskatoon's stormwater pond design protocol requires the accommodation of a 1 in 2 year return period rainfall event for the minor components of the stormwater management system (manholes, piping, catch basins, outfall structures) and the accommodation of a 1 in 100 year return period rainfall event for the major components of the stormwater management system (overland street drainage, detention facilities, park land, *etc.*) (City of Saskatoon 2012). These stormwater management ponds often have multiple inlets and Outlets, vegetation, aeration systems (fountains), and vary in size and shape.

2.2 Inflow to and Outflow from a Stormwater Management Pond

To improve the quality of stormwater runoff before it enters receiving surface waters (rivers, lakes, wetlands), the emphasis is often put on the removal of solids. Ideally, solids are removed through a reduction in velocity that promotes sedimentation in a stormwater management pond. Stormwater management ponds are typically designed for a specific residence time to allow for the settling of solids from stormwater runoff before resident water is discharged to receiving

water bodies (Hvitved-Jacobsen *et al.* 1994; Greb and Bannerman 1997; Birch *et al.* 2006; Selbig *et al.* 2013). Typically, the larger the pond volume to runoff volume ratio, the higher the treatment efficiency of contaminants and the settling of solids (Hvitved-Jacobsen *et al.* 1994). The removal of solids is of concern since associated organic and inorganic contaminants bound to particulates can become disassociated from the particle causing long-term toxicity or negative environmental and aquatic effects in receiving waters (Gettel *et al.* 2011). Solids that are not removed from stormwater can also lead to increases in surface water turbidity, decreasing the penetration of light and inhibiting the growth of plant species (Kantrowitz and Woodham 1995).

The particle size distribution of solids entering a stormwater management pond is one of the major factors impacting the removal of contaminants due to the influence particle size has on the settling velocity and contaminant loading (Kim and Sansalone 2008; Selbig *et al.* 2013). Solids or particles present in stormwater influent have been found to range from the size of 0.004 mm to 2.0 mm (Greb and Bannerman 1997). In Madison, Wisconsin, Greb and Bannerman (1997) found a distribution of 50.5% clay, 40.2% silt, and 0.3% sand, with a median grain size of 0.002 mm (clay size) in stormwater runoff. The median particle size, however, is likely to vary by rain event and site as others have found the median particle size of solids in urban runoff to range from 0.029 mm to 0.3 mm depending on the rain event (Kim and Sansalone 2008). In the effluent of a stormwater management pond, typically higher percentages by mass of the smaller particle sizes are present than in the influent (Greb and Bannerman 1997). One study in Florida found that 65 to 99% of the effluent flows throughout a season consisted of particles less than 0.075 mm (Kim and Sansalone 2008). It has been suggested that knowing the particle size distribution of solids in urban runoff can help improve the selection and design of stormwater treatment systems for the removal of fine particles, as the settling of fine particles will be related to Stoke's law (Greb and Bannerman

1997; Kayhanian *et al.* 2012); however, Stoke's law assumes laminar flow which is very unlikely to be true in the case of stormwater management ponds, and that the law applies to the settling of single particles and not groups of particles.

Many contaminants of concern can be bound to the solids present in stormwater. Typically 60-80% of phosphorous and between 30-80% by mass of certain heavy metals are bound to suspended solids in highway and stormwater runoff (Hvitved-Jacobsen *et al.* 1994). Fine particles are of concern since they often have higher levels of bound pollutants due to increased particle surface area-to-volume ratios when compared to larger particles (Kayhanian *et al.* 2012; Selbig *et al.* 2013). The high surface area-to-volume ratio of fine particles results in a higher pollutant load for a specified volume when compared to the same volume of coarser particles, since the pollutant will account for a greater portion of the total volume with the finer particles (Lodhi and Acharya 2014).

Some researchers have investigated the relationship between the particle size of solids and bound contaminants. Vaze and Chiew (2004) investigated the nutrient loads associated with particular particle sizes of solids in urban stormwater and found that the majority of total phosphorous (40% by mass) and total nitrogen loading (50% by mass) was associated with solids ranging from 11 μm to 150 μm in diameter. Lodhi and Acharya (2014) found similar results for particulate bound phosphorous, where higher concentrations were associated with particles less than 20 μm in diameter. Smaller particles have also been found to account for the majority of metal loads for sediment. Zhao *et al.* (2010) found that smaller particles (<250 μm) accounted for over 80% of road sediment metal loads. Kayhanian *et al.* (2012) found that even smaller particle sizes (<38 μm) accounted for a very low mass fraction (10% by mass) of particle bound concentrations of metals such as copper, lead, and zinc for vacuumed road sediment. In their findings, Selbig *et*

al. (2013) found that higher concentrations of metals (iron, manganese, zinc, copper, chromium, lead, nickel, arsenic, cadmium) were found in the silt fraction of sediment when compared to the sand fraction for stormwater bed, stormwater suspended, street dirt, and stream bed sediment.

Typically, in the analysis of stormwater samples, water is evaporated off and the solids remaining are referred to as the total solids (TS) of the sample (Droste 1997). The total solids can therefore be used to refer to all solids, but can also be further broken down into two main categories (total suspended solids (TSS) and total dissolved solids (TDS)) based on the mass of solids that pass (TDS) or do not pass (TSS) through a 2 μm pore size filter (Droste 1997; EPA 2012). Both TSS and TDS can further be categorized based on the portion of solids that are either volatile or fixed, where the mass of volatile solids of the sample is the portion of the sample that burns at 550 to 600°C, typically representing the organic fraction, and the fixed portion is the remainder that does not burn-off (Droste 1997). Kayhanian *et al.* (2012) note that particles smaller than 10 μm are typically not captured in stormwater management ponds. Since TDS are not typically captured in stormwater management ponds, TSS are typically the focus of studies investigating the removal of solids. TSS levels can vary substantially but within the same order of magnitude. TSS concentrations from storm sewer outfalls sampled from a variety of Saskatchewan communities were shown to range from 129 mg/L to 350 mg/L (Water Security Agency, 2006).

There are inconsistencies in the literature as to how the removal of solids by stormwater management ponds is calculated and reported on, but it is most commonly reported as a removal efficiency. In some cases the removal efficiency is defined based on inflow and outflow concentrations (mass/volume) (Pettersson and Lavieille 2007; Birch *et al.* 2006) and in other cases it is defined using inflow and outflow loads (mass) (Kantrowitz and Woodham 1995). Regardless of the definition used for the removal efficiency, a negative removal efficiency refers to a higher

concentration or load in the outflow than in the inflow, and a positive removal efficiency refers to a higher concentration or load in the inflow than in the outflow (Pettersson and Lavieille 2007; Kantrowitz and Woodham 1995).

Even if a stormwater management pond is efficient at removing TSS, fine to coarse settled solids can become re-suspended with wind and waves, resulting in lowered or even negative removal efficiencies (Wakelin *et al.* 2003), where negative removal efficiencies indicate higher contaminant loads present in the outflow than the inflow. Kantrowitz and Woodham (1995) assessed stormwater management pond removal efficiencies over six rain events in Florida, where they calculated the removal efficiency as the change in load divided by the inflow load for a detention pond. They found that four of the six rain events were associated with negative TSS removal efficiencies, with an average removal efficiency of -20%. Over the six storms, the removal efficiency of TSS ranged from -162% to over 63% and the greatest removal efficiency was associated with the two smallest storms in the season suggesting the high variability of removal efficiency between rain events (Kantrowitz and Woodham 1995). Birch *et al.* (2006) also found a wide range in the removal efficiency (-12% to 93%) of TSS between rain events, thought to be due to highly variable loads of TSS entering the stormwater management pond. In their research, Birch *et al.* (2006) defined the removal efficiency as the average weighted concentration of the inflow divided by the outflow. Pettersson and Lavieille (2007) took a similar approach using a concentration to define the removal efficiency of a stormwater pond. They determined the site mean concentration (SMC) for a specific contaminant, calculated as the pollutant mass divided by the stormwater volume, and defined the removal efficiency as the difference between the site mean concentration for the inflow and outflow divided by the inflow. In their research, Pettersson and Lavieille (2007) found only positive removal efficiencies were apparent for TSS (61% to 77% over

the entire study), where negative removal efficiencies were only reported for other contaminants such as certain nutrients and heavy metals. Anderson *et al.* (1996) assessed removal efficiencies of TSS and TDS using a mass balance approach over an entire field season for specific rain events and for baseflow conditions, where baseflow conditions refer to dry weather outflow from a pond. Baseflow during dry weather conditions may be a result of groundwater inflow to the pond or the pond elevation being higher than the outflow control structure (weir, level of Outlet, *etc.*). Anderson *et al.* (1996) found that TSS removal was -55% for baseflow and 42% for events, and TDS removal was 4% for baseflow and -11% on average for all events. The negative removal efficiencies during baseflow were thought to be a result of a fountain in the pond, which would re-suspend clay and fine silt particles (Anderson *et al.* 1996).

In longer term studies, removal rates of various pollutants have also been found to vary between years, likely due to changes in pond morphology including changes induced by increased vegetation and sediment accumulation (Pettersson and Lavieille 2007). In one study it was found that the removal efficiency of particulate pollutants (TSS, volatile suspended solids (VSS), lead) did not change over a 7 year period; this was thought to be a result of increased aquatic vegetation in the pond that likely improved the settling of solids despite the reduction of pond treatment volume brought on by 15 to 20 cm of accumulated solids over the seven years (Pettersson and Lavielle 2007). Seasonal variations also have been shown to elicit changes in the removal efficiency of particulate pollutants such as TSS, VSS and particulate bound lead. An increased removal efficiency of TSS, VSS, and lead was found during the summer period when compared to the autumn and winter, which are attributed to increased aquatic vegetation during the summer months (Pettersson and Lavielle 2007). Specifically, it has also been found that the highest removal efficiencies of TSS were associated with earlier or later on in the summer season compared to the

fall when aquatic vegetation that promoted settling decays (Pettersson and Lavieille 2007). Removal efficiencies have also been found to decrease following particularly windy days when resuspension likely occurs (Wakelin *et al.* 2003).

The literature suggests that data from multiple rain events should be used when evaluating the removal efficiency of a stormwater management pond, as the removal efficiency of contaminants is rain event and treatment system specific (Greb and Bannerman 1997; Pettersson 1999; Selbig *et al.* 2013). Therefore, it is important that each stormwater pond is treated individually with regards to the removal efficiency of contaminants; there are no general typical values for the removal efficiency of stormwater contaminants.

2.3 Settling of Solids within a Stormwater Management Pond

When solids enter the stormwater management pond through the inlet pipes, the cross-sectional area of the flow increases, causing a reduction in flow velocity and the settling of solids and attached contaminants. The accumulation of settled solids causes a loss of active treatment volume and a reduced retention time if sediment is not periodically removed (Fyfe *et al.* 2007); it can even lead to chemical or physical resuspension of contaminants (Pettersson and Lavieille 2007). Increased aquatic vegetation can also affect the pond hydraulic characteristics and consequently the settling of solids (Pettersson and Lavieille 2007). Plants in a stormwater management pond design can play an important role in treatment, as they can adsorb organic pollutants (removing if harvested), heavy metals, or pathogenic bacteria (Wakelin *et al.* 2003). Plants can also play a role in reducing currents and wind influence which could otherwise lead to the re-suspension of solids (Braskerud 2001; Wakelin *et al.* 2003; Pettersson and Lavieille 2007). Plants have also been found to reduce short-circuiting by altering flow patterns, potentially leading to an increased detention time (Braskerud 2001).

It has been found that the sediment accumulation within a stormwater management pond will vary by site and design, and that each pond has its own design and actual removal efficiency (Heal *et al.* 2006). Pettersson and Lavieille (2007) suggested that, over a seven year period, the reduction in treatment volume associated with sediment accumulation may have been responsible for observed reduced removal efficiencies of contaminants. Although the periodic removal of settled solids is recommended, removal is often not performed as it constitutes a very costly management activity that may include downtime of the stormwater management pond. Some researchers have studied the spatial sediment distribution to focus sediment removal management activities on dominant settling areas of the stormwater management pond. Such research helps reduce costs by focusing management activities to particular pond areas and potentially improves future stormwater management pond designs for easier management access. Heal *et al.* (2006) assessed the sediment distribution within a stormwater detention basin along the axis of the pond (from inlet to Outlet and across the pond at the midpoint). As shown in their sediment maps, Heal *et al.* (2006) found that the area around the pond inlet was associated with the greatest accumulation of sediment, where sediment depth at the inlet increased by approximately 0.25 m in a four year period (approximately 0.06 m/year) within that area. The areas of the pond farther away from the inlet showed very little change in the sediment depth as particles from incoming stormwater settled out near the inlets (Heal *et al.* 2006).

Marsalek *et al.* (1997) took core samples from various locations in a 0.5 hectare stormwater management pond constructed within a stream and found that the pond had accumulated, on average, 0.02 m of solids per year over the 10 years it had been in use. The accumulated solids in the pond had ultimately reduced the treatment volume of the pond by 13% over the 10 year period (Marsalek *et al.* 1997).

The particle size range observed for a core sample taken from the pond will depend on the location from which the sample was taken. It has been generally found that coarser particles settle closer to the inlet and finer particles settle closer to the Outlet. In a study by Marsalek *et al.* (1997), the particle sizes of sampled sediment ranged from 0.24 μm to 8 mm. Near the inlet of the stormwater management pond the deposited sediment was primarily sand (70.6% by mass) and gravel (29% by mass) with only a small portion of clay (0.4% by mass), whereas finer sediment was generally found closer to the Outlet (54% clay, 41% silt, and 5% sand) (Marsalek *et al.* 1997).

Kayhanian *et al.* (2012) also investigated the spatial particle size distribution within three stormwater management ponds and found that as core sample distance increased from the inlet to the Outlet, the particle size distribution of sediment core samples decreased, indicating coarser particles were settling closer to the inlet. It was discovered that accumulated sediment near the inlet was responsible for the largest mass of all particle size ranges, including the two extremes which were less than 38 μm and greater than 1000 μm (Kayhanian *et al.* 2012). The majority of particle mass for sediment core samples near the mid-point between the inlet and Outlet had particle sizes less than 250 μm, and near the Outlet the majority of the mass had particles that ranged from 38 μm to 75 μm.

The information in the literature is lacking with regards to relationships between the sediment distribution within a stormwater management pond and the flow pattern, despite such relationships being investigated for other types of settling ponds. For example, Fyfe *et al.* (2007) investigated the flow pattern and sediment accumulation in a dairy shed waste stabilization pond; however, only the sediment accumulation (not the particle size distribution) was investigated, and the relationship between the spatial sediment distribution and flow patterns was not discussed.

2.4 Flow Pattern in Stormwater Management Ponds

Traditional stormwater management ponds are susceptible to dead zones and short-circuiting, which reduce the effectiveness of the pond at removing contaminants (Shaw 1997; Pettersson *et al.* 1998; Glen and Bartell 2010). Dead zones are regions where there is no water exchange between incoming and resident stormwater, ultimately reducing the effective treatment volume and detention time (Pettersson *et al.* 1998). Short-circuiting occurs when incoming contaminants travel from the inlet to the Outlet with very little dispersion, resulting in a shortened retention time and consequently a reduced removal efficiency of contaminants (Glenn and Bartell 2010; Shaw *et al.* 1997). Dead zones and short-circuiting generally occur when the pond geometry and/or the positioning of the inlet pipes promote a flow pattern within the pond that does not effectively utilize the entire treatment volume for contaminant removal. It is suggested that altering the flow pattern to remove dead zones may result in improved removal efficiencies for contaminants (Pettersson *et al.* 1998).

Short-circuiting can be investigated using tracers; however, alternative methods are required to visualize the internal flow patterns of a stormwater management pond. Methods to measure flow velocities in a variety of surface water applications have included the use of Doppler instrumentation, surveying drogues, and large scale applications of particle image velocimetry (PIV) or particle tracking velocimetry (PTV). Some methods are too expensive, impractical, or have not yet been used to investigate the flow pattern in stormwater management ponds.

2.4.1 Tracers

Researchers have commonly used tracers, injected at the inflow, to measure the retention times of stormwater management ponds and wetlands, where typically the tracer concentration is measured over time at the inlet and the Outlet (Persson 2000; Holland *et al.* 2004). It has been

suggested that the use of these tracer concentration methods ultimately treat the stormwater management pond as a "black box" (Spencer *et al.* 2011). A newer tracer method has used clay labelled with a holmium tracer, intended to mimic the deposition of pond sediment for comparison with a sediment transport model (Spencer *et al.* 2011). For the clay tracer method, pond sediment is sampled throughout the pond area and analyzed for holmium, where the montmorillonite clay can be used to understand cohesive sediment transport in a field stormwater management pond, as the clay tends to form flocs (Spencer *et al.* 2011). Although these tracer methods can be used as an indicator for short-circuiting and dead zones, depending on the sampling methods used, they cannot necessarily be used to determine real-time internal flow patterns and internal flow velocities for field-scale applications as flow paths of tracers cannot be seen clearly due to the lighting conditions. Tracer methods do not necessarily allow for tracer plume visualization and the collection of samples containing varying tracer concentrations within the flow may not be practical.

2.4.2 Particle Image Velocimetry and Particle Tracking Velocimetry

There are a few potential methodologies for examining the velocity field in a pond. At the laboratory-scale, there are two imaging techniques that utilize surface tracers and laser-based systems to non-intrusively visualize and measure velocity fields in flows: particle tracking velocimetry (PTV), which involves tracking individual particle tracers between images, and particle image velocimetry (PIV), which involves assessing the movement of groups of tracer particles (Fujita *et al.* 1998). Both PIV and PTV were developed to investigate flows at the laboratory scale, using light sources for illumination, video equipment, and data processing to obtain flow measurements.

At the field-scale, large-scale particle image velocimetry (LSPIV) or large-scale particle tracking velocimetry (LSPTV) has been used for a field of view up to hundreds of square meters. LSPIV has been used to determine the velocity field in shallow surface waters or for ice in applications such as full scale or physically modelled rivers and physically modelled reservoirs (Creutin *et al.* 2003; Muste *et al.* 2005; Fox *et al.* 2006; Kantoush and Schleiss 2009; Muste *et al.* 2011; Daigle *et al.* 2013), whereas LSPTV has been used to determine surface water velocity fields in a lake (Admiraal *et al.* 2004). The use of LSPIV is now widespread for non-intrusively determining time-averaged surface velocities and the scale of turbulence structures in laboratory and open channel flows, which is important in predicting contaminant mixing, scour, and sediment deposition (Fox *et al.* 2006; Fox and Patrick 2008; Kantoush *et al.* 2011). Many researchers have found that flow measurements produced from LSPIV and similar imaging methodologies are comparable to Doppler instrumentation and current meters (Dermisis and Papanicolaou 2005; Muste *et al.* 2004; Muste *et al.* 2011). The benefits of using LSPIV or LSPTV have been argued over single or multiple point sampling techniques such as Acoustic Doppler Velocimeters (ADV), Acoustic Doppler Current Profilers (ADCP), and Electromagnetic Current Meters, which are considered to be more intrusive, time-intensive, and require personnel to enter the water in a boat under potentially dangerous conditions (storms, flooding, *etc.*) (Fox and Patrick 2008). In contrast, LSPIV and LSPTV can be performed from the shore without the requirement to have a probe within the flow (Creutin *et al.* 2003; Muste *et al.* 2011; Muste *et al.* 2014).

Both LSPIV and LSPTV use relatively inexpensive video-based equipment and natural lighting for video recording of tracer particles that are either naturally occurring (foam, boils caused by light turbulence, ice blocks, light floating debris) or artificial (Eco-foam, corn starch, colored mulch *etc.*). Although either naturally occurring or artificial tracers can be used, their use

should take into account environmental conditions, such as wind, that may affect the free-surface of the flow (Muste *et al.* 2011). When conducting LSPIV or LSPTV in the field, wind or calm, mirror-like surfaces with reflections, glare and shadows have been noted to interfere with the processing of natural tracers, so that artificially seeded tracers may be preferred (Muste *et al.* 2011).

LSPIV differs from LSPTV in the number of tracer particles that are used, which defines the algorithm used for image processing; lower concentrations of tracers will typically require data processing using LSPTV techniques rather than LSPIV techniques (Fujita *et al.* 1998). If LSPIV is used, sufficient tracer particles are needed to statistically correlate successive images using recognizable tracer particle patterns and tracer displacements (Fujita *et al.* 1998; Cruetin *et al.* 2003; Meselhe *et al.* 2004. Dermisis and Papanicolaou 2005; Muste *et al.* 2008; Muste *et al.* 2011; Muste *et al.* 2014). For LSPIV, too few tracer particles can cause issues for image processing, since similar tracer patterns may not be apparent to correlate between successive images, whereas too many tracer particles could be problematic due to agglomeration affects which have been attributed to surface tension (Fox *et al.* 2006; Admiraal *et al.* 2004; Muste *et al.* 2011; Kantoush and Schleiss 2009). Tracer particles have also been shown to be influenced by boundary effects, where particles adhere to the walls of a flume, resulting in unusable data (Fox *et al.* 2006; Admiraal *et al.* 2004).

Once the flow surface has been seeded with an appropriate concentration of tracer particles, depending on LSPTV or LSPIV methods for data processing, the flow surface is recorded using a wide-angle lens video camera with an appropriate resolution for the scale, and a suitable time lapse between successive images. It has been recommended that the flow surface for LSPIV or LSPTV should be recorded at an oblique angle to minimize non-ideal lighting conditions in the outdoor

environment caused by sun glare, shadows, too strong or poor illumination, which can interfere with data processing (Muste *et al.* 2008; Muste *et al.* 2014).

Once images of tracer particles are recorded, both LSPIV and LSPTV require image distortion correction to correct for field scale distortions that are a result of a wide-angle camera lens and geometric distortions from recording at an oblique angle (Fujita *et al.* 1997; Fujita *et al.* 1998; Muste *et al.* 2008). Fujita *et al.* (1997) first described a methodology for correcting these camera distortions for LSPIV, which has been used for image analysis in a variety of applications (Fujita *et al.* 1998; Creutin *et al.* 2003; Muste *et al.* 2004; Muste *et al.* 2008; Muste *et al.* 2014); it has also been used to correct for image distortion in photogrammetry (Jeyapalan 2004; Wolf *et al.* 2014).

The methodology described in Fujita *et al.* (1997) involves surveying at least six real-world coordinates of fixed points (trees, posts, manholes, points on/near water surface *etc.*) seen in camera images for calibration. Daigle *et al.* (2013) investigated two alternative methods of acquiring real world coordinates. The first method did not rely on surveying equipment or fixed points, whereas the second method did not rely on points on the water surface. In the first method, an object of known dimensions (square plate) is placed on the flow surface in the image at varying points within the field of view, thereby creating a local reference system for real-world physical dimensions of pixels. The dimensions are then interpolated for all of the pixels along the flow surface. In the second method, crosses with measured dimensions were installed and surveyed above the flow surface, and one cross was installed at the edge of the river near the flow surface.

Once the points are surveyed, a transformation matrix is defined to relate the real-world coordinates of points seen in the images to the known image coordinates (horizontal and vertical pixel locations) through calibration constants, typically using software such as Matlab (Fujita *et*

al. 1997; Erdbrink 2007; Daigle *et al.* 2013). The transformation matrix of constants can then be used to calculate the new real-world coordinates corresponding to the image pixel coordinates of tracer particles (Erdbrink 2007; Daigle *et al.* 2013). Velocity vectors are then calculated from the calculated real-world coordinates associated with image pixel coordinates of tracer particles. For LSPIV, identifiable tracer particle patterns in successive images are statistically correlated to determine velocity vectors, whereas for LSPTV individual tracer particles are compared between successive images to determine velocity vectors (Fujita *et al.* 1998; Meselhe *et al.* 2004; Admiraal *et al.* 2004).

If using LSPIV for a full scale stormwater management pond application, it would require hundreds if not thousands of seeded or naturally occurring tracer particles. The seeding of such large quantities of tracer particles (oranges, tennis balls, *etc.*) at a public recreation site is not necessarily feasible and at a stormwater management pond naturally occurring tracers may be non-existent. In contrast, LSPTV requires the seeding of only a few tracer particles, which facilitate their retrieval, where there is a lower likelihood of residential complaints or interference from park users. Most LSPIV applications have been for velocity measurements in rivers (Fujita *et al.* 1998; Creutin *et al.* 2003; Muste *et al.* 2011). For lakes, other researchers have used LSPTV to minimize tracer concentration requirements and issues with processing data (Admiraal *et al.* 2004). However, regardless of the number of surface tracers used, these only represent the velocity at the water surface. Surface velocities have then been used to estimate the mean velocity under the assumption that the mean depth-averaged velocity is 85% or 88% of the surface velocity for a river (Muste *et al.* 2005; Dermisis and Papanicolaou 2005) or using the power law for lakes (Admiraal *et al.* 2004). Admiraal *et al.* (2004) estimated depth-averaged velocities using the 1/7 power law, where the mean velocity was estimated to be approximately 7/8 of the surface velocity; however,

it was noted that this method of depth averaging velocities is not valid for non-uniform flow. Tracer particles that would be indicative of the vertical velocity distribution and not just the surface velocity would therefore be ideal.

2.4.3 Drogues

Drogues, which consist of a float, line, and fin(s) below the water surface, have been used to assess below-surface water currents or flow patterns in a variety of applications, including stormwater management ponds, water reservoirs, lagoons, and waste stabilization ponds (Anderson *et al.* 1996; Pettersson 1998; Hanna 1989; Shilton and Bailey 2006; Fyfe *et al.* 2007). They have also been used in favor of dye tracers as they can be used to observe flow paths and flow patterns over large, field-scale distances in a cost effective manner, where their movement has even been found to accurately follow injected tracer dye (Barter 2003). For determining flow patterns, drogues may be also preferred due to their cost effectiveness over Doppler systems (Shilton and Bailey 2006; Fox and Patrick 2008). In drogue tracking studies, one marked drogue is generally surveyed every 5 to 10 seconds to determine the coordinates using survey instrumentation and markers (colors, sails, *etc.*) for differentiation (Myers *et al.* 1982; Hanna 1989; Pettersson 1998; Fyfe *et al.* 2007). The coordinates of the drogues at sequential times are then used to determine velocities (Pettersson 1998; Myers *et al.* 1982; Fyfe *et al.* 2007). A newer method of drogue tracking involves using a global positioning system (GPS) for each drogue (Barter 2003), but at a higher cost. However, since these drogue tracking studies have taken place, survey instrumentation has become increasingly advanced. Robotic total stations, which can lock-onto and then track a three dimensional prism may potentially be used for drogue survey applications to minimize the labor and cost, with improved accuracy of coordinate measurements.

Drogue tracking studies have indicated that counter-clockwise or clockwise vortex-like flow patterns were often apparent in ponds or lagoons, with lower velocities towards the center of the circulation pattern and higher velocities along the edge, where flow patterns are similar regardless of flow intensity (Hanna 1989; Fyfe *et al.* 2007; Pettersson *et al.* 1998). It has been noted that in laboratory experiments, even once drogue movements indicated a steady-state flow pattern, every so often the predictable pattern would change for a period of a few hours from one circulation cell to two (Shilton and Bailey 2006).

Although drogue tracking can be used to determine flow patterns and velocity with high repeatability, wind and vegetation can impact tracking. Pettersson *et al.* (1998) noted that vegetation caused drogues to become trapped. Wind has also been noted to have an effect on drogue movement, with the greatest influence near the center of the pond or at far distances from the inlet(s) and shore (Barter 2003; Fyfe *et al.* 2007). To obtain depth-averaged velocity measurements when using drogues, drogues with fins at different depths at and below the water surface have been used (Pettersson *et al.* 1998).

The general procedure of tracking one or two drogues by surveying yields very limited data, while tracking a larger number of drogues at various depths over a long period of time tends to give a better representation of the flow pattern (Myers *et al.* 1982). When tracking larger numbers of drogues, care must be taken to ensure the lines of the drogues do not become tangled (Pettersson *et al.* 1998). However, as surveying individual drogues may only be feasible with a small number of drogues, alternative tracking methods need to be used for larger numbers. The combination of surveying and camera use has been used to track the movement of larger numbers of drogues, but only at the laboratory-scale for a model pond (Shilton and Bailey 2006). Combining surveying and video-imagery techniques from LSPTV may therefore enable the tracking and

velocity determination of all drogues at the field-scale. The use of LSPTV for tracking drogues at various depths to allow for the determination of a vertical velocity profile has not yet been used at the laboratory or field-scale.

Chapter 3

METHODOLOGY

There were three major project activities that took place to examine the removal efficiency, settling of solids, and flow pattern within a stormwater management pond located in Erindale, Saskatoon. One project activity involved measuring the flow rates, solids concentration (total solids), and particle size distribution of inflow and outflow samples from the inlets and Outlet of the stormwater management pond. This also involved collecting meteorological (precipitation amounts, wind speed and wind direction) data. The second project activity consisted of sampling the settled solids throughout the pond and estimating the depth of settled solids and particle size distribution of the accumulated solids at each sampling station. The third project activity involved using a combination of surveying and techniques from LSPTV to track drogues to investigate pond flow patterns and to estimate velocities in the pond at different depths. Each project activity consisted of a number of sub-activities and these are listed in Table 3-1.

Table 3-1. Major research project activities and sub-activities

Activity	Sub-activities involve the measurement or determination of:
1. Inflow and Outflow Sampling to Determine Solids Removal Efficiency	• Collection of meteorological data (precipitation, wind speed and direction) • Removal efficiency of solids by particle size • Total mass loading of solids • Mass loading and particle size distribution • Whether resuspension may be occurring • Flow rates of pond inflow and outflow (hydrographs)
2. Investigation of Settled Solids	• Spatial variation and particle size distribution of sediment • Dominant pond areas for solids removal according to particle size • Accumulated sediment depth
3. Investigation of Flow Patterns and Velocities	• Internal circulation and flow patterns • Internal velocities • Relationship between velocity, flow pattern, and spatial distribution of settled solids

3.1 Field Site Characteristics

The John Avant Park stormwater management pond in Erindale, Saskatoon, as shown in Figure 3-1, has three inlets and one Outlet. At the Outlet, there is a broad-crested weir for water level control (personal communication, A. Hildebrandt, City of Saskatoon, January 2014). Inlets 1, 2, and 3, have inside diameters of 525 mm, 750 mm, and 1050 mm, respectively. An Outlet pipe with an inner diameter of 1050 mm conveys the water to the broad-crested weir in the Outlet manhole. Downstream of the weir there is a circular pipe to convey the outflow to the city's stormwater distribution system. At this stormwater management pond, there is also a fountain and a man-made stream for aeration. The aeration systems had not been part of the original design, but were later installed due to low levels of dissolved oxygen (personal communication, G. Mak, AECOM, January 2014). The fountain aeration system was not in use over the summer of 2014 during project fieldwork, but the stream was still in use.

The design features of the pond include a normal water design depth of approximately 1.86 m, with a high water design depth of approximately 3.1 m. There is an additional 0.6 m above the high water level allowed for freeboard (personal communication, A. Hildebrandt, City of Saskatoon, January 2014). The pond has a maximum width of 194 m and a maximum length of approximately 233 m, with an estimated surface area of 29,400 m^2 at the normal depth. There are 4 main catchment areas that contribute to stormwater runoff entering the pond: Inlet 1 has a catchment area of 9.67 ha; Inlet 2 has a catchment area of 21.40 ha; Inlet 3 has a catchment area of 71.99 ha, and the pond itself has a catchment area of 11.56 ha (personal communication, H. Azinfar, City of Saskatoon). In addition, there is a small catchment area (2.82 ha) that conveys stormwater runoff directly to the Outlet manhole such that solids present in the stormwater runoff entering this manhole do not settle out in the stormwater management pond. The John Avant Park

stormwater management pond was designed and commissioned in the late 1980s. The bottom of the pond therefore contains approximately 25 years of accumulated settled solids, as there has been no known dredging.

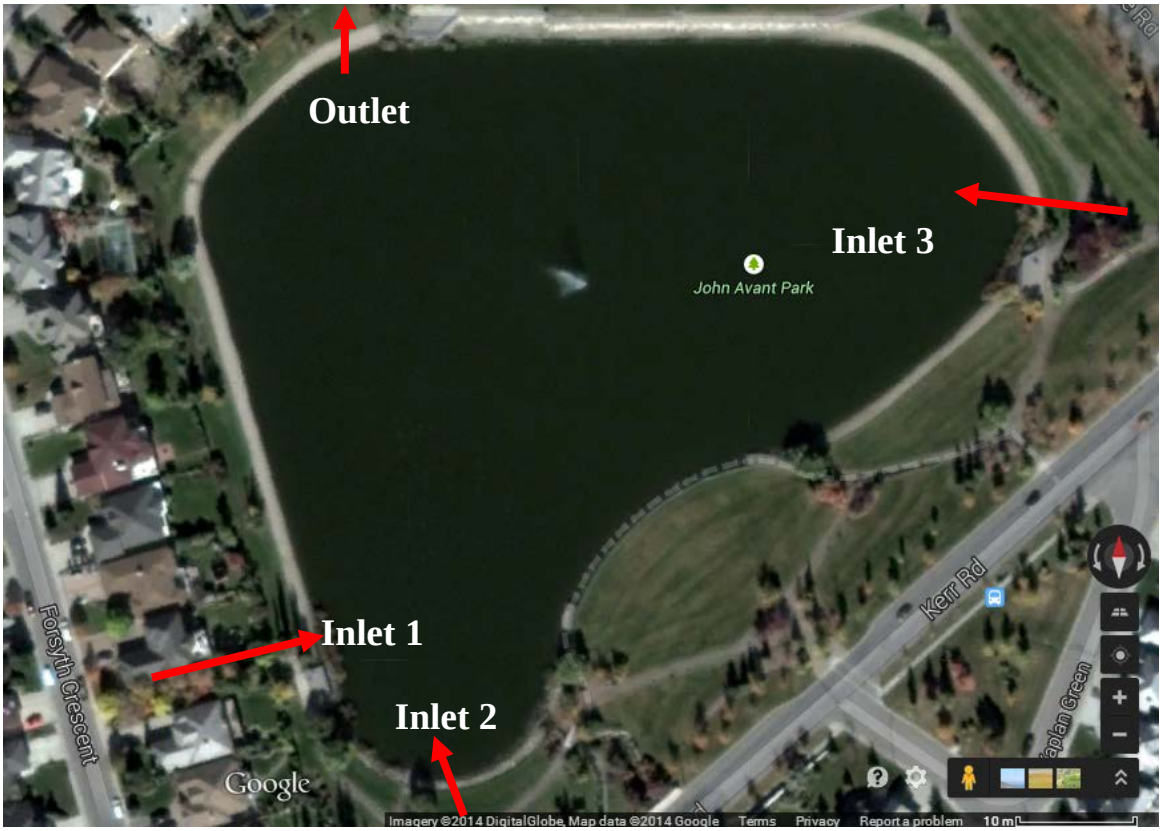

Figure 3-1. Plan view of the John Avant Park stormwater management pond in Erindale, Saskatoon, Saskatchewan, with arrows depicting approximate locations of inlets (arrows into pond) and Outlet (arrow out of pond) (Adapted from Google Maps, 2014).

3.2 Meteorological Data Collection

The rainfall from each rain event during the study period was measured using a leveled tipping bucket rain gauge (model TR-525USW, Texas Electronics, Inc.) mounted approximately 2.4 m above ground level (Figure 3-2), and programmed to count the number of tips for 15 minute intervals. This tipping bucket rain gauge model has an accuracy of +/- 1% for rainfall intensities of 50 mm/hour or less (Texas Electronics n.d). A data logger (Campbell Scientific Inc.) was used

to record the rainfall data; it was installed on the rain gauge mount in a protected box. The rain gauge was located approximately 240 m away (52°8’32” N, 106°33’31”W) from the site (52°8’20” N, 106°33’52” W). The location of the rain gauge was chosen since it was a known personal residence and was thought to be more secure for the equipment than at the public site. The rain gauge was located in an open space where it was not expected to be affected by trees. It should be noted that the rainfall would be expected to vary throughout the catchment area for the stormwater management pond.

The wind speed and direction was monitored and manually recorded prior to and during each drogue tracking event using a hand-held anemometer (Kestrel 4500 Pocket Weather Tracker) with the capability of measuring wind direction as well as speed. The anemometer was held at an elevation of approximately 2 m above ground surface, at a location immediately beside the pond, when taking measurements. The Kestrel 4500 Pocket Weather Tracker has an accuracy of +/- 3% and a range from 0.4 to 60.0 m/s.

Figure 3-2. Tipping bucket rain gauge mounted to a stand along with the data logger protected in an enclosed box.

3.3 Inflow and Outflow Sampling

Contaminants in the inflow and outflow of stormwater management ponds are often sampled using automated stormwater samplers such as those manufactured by ISCO or Sigma (Anderson *et al.* 1996; Greb and Bannerman 1997; McLeod 2007). Some automated samplers also have add-on instruments with the capacity to measure water level and velocity, and therefore flow rates in the inlet and Outlet pipes for the stormwater management pond can be calculated. Some researchers have used filters in a system capable of backwashing, pumping water into a series of filters, and then collecting the samples for total solids (Selbig *et al.* 2013); this method of sampling, however, does not allow for the acquisition of flow data for the calculation of total solids loads or typical contaminant concentration comparisons to the hydrograph.

Stormwater sampling and flow measurements for this project were performed using programmable automated ISCO 6700 and 6712 samplers (Figure 3-3) similar to other studies (Kantrowitz and Woodham 1995; Gettel *et al.* 2011; Birch *et al.* 2006; Pettersson and Lavieille 2007). The sampling protocol involved sampling for a full range of rainfall events (varying precipitation amounts and intensities) during the study period as recommended by Alberta Environmental Protection (1999).

Figure 3-3. An ISCO 6712 series automated stormwater sampler with 12 V battery attached.

The ISCO samplers can be programmed to automatically take up to 24 - 1 L samples at varied intervals (1 minute to 99 hours) until all bottles contained in the sampler are full and require replacement. For sampling for this project, the ISCO samplers were programmed to sequentially sample at 10 minute time intervals for the first 12 bottles, and then 30 minute time intervals for the remaining 12 bottles. Shorter time intervals were chosen for the beginning of the rain event to

acquire samples representative of the first flush, which is associated with the highest contaminant concentration due to the immediate mobilization of particle-attached contaminants during a rain event (Alberta Environmental Protection 1999). To sample stormwater, the ISCO samplers have a peristaltic pump with 3/8" inner diameter tubing and a maximum suction head of 8.5 m. An intake strainer, shown in Figure 3-4, serves as the sampler intake at the end of the tubing, through which water is pumped to the sample bottles.

Figure 3-4. Manufacturer's intake strainer for stormwater to enter the ISCO sampler pumping system.

It had been suggested that the manufacturer's intake strainer collects samples that are not representative of particle sizes entrained in the flow, with an over-sampling of coarser particles due to a design based on the assumption of fully-mixed, turbulent conditions (Gettel *et al.* 2011). The manufacturer's intake strainer also was reported to have a tendency to be pushed to the water's surface under higher flow conditions, where one study required a weighted intake so air did not become entrained in the sample (McCleod 2007). As a result of these reports, an adapted intake strainer was initially designed for this project, as shown in Figure 3-5, based on the design of Gettel *et al.* (2011). Gettel *et al.* (2011) had designed and performed sampling experiments in the laboratory with four modified intake strainers. They found an alternative design, using the same

principles shown in Figure 3-5, permitted the acquisition of samples with the most representative particle size distribution for particles entrained in the flow. The intake strainers were placed into the inlet and Outlet pipes, with the exception of Inlet 1 (I1) where such placement was not possible due to the small size of the pipe.

Figure 3-5. Adapted intake strainer design (left) initially used for project shown in the inlet pipe at the bottom of the manhole (right).

Although the adapted intake strainer shown in Figure 3-5 worked well under laboratory testing in the flume at the University of Saskatchewan, the violent nature of water flow in the stormwater pipes combined with air entrainment led to insufficient sampling. With the modified intake strainer, entire samples would consist of air or only a portion of a sample would be taken. Therefore the adapted intake design was abandoned for the manufacturer's intake strainer (Figure 3-4). The manufacturer's intake strainer naturally became entrained in the flow downstream, performing better than the modified intake strainer.

The ISCO samplers were programmed to initiate and continue sampling as long as the water depth in the pipe was higher than a specified trigger depth, indicating runoff from a rain event. The water depth was measured using an ISCO 750 area-velocity module, which uses acoustic Doppler technology to determine the depth of flow and average velocity in the pipe. The ISCO 750 area-velocity module has a velocity accuracy of +/- 0.03 m/s for velocities ranging from

-1.5 m/s to 1.5 m/s and an accuracy of +/- 2% for velocities ranging from 1.5 to 6.1 m/s. The depth measurement of the sensor has an accuracy of 0.008 mm from water depths ranging from 0.01 m to 1.52 m. The trigger water depth for sampling at the inlets was set using a trial and error approach to determine when the water depth was sufficient to not sample air and to have all three inlet samplers initiating sampling simultaneously to collect data representative of the entire rain event with similar sample times for each inlet. The trigger depth was therefore different depending on the inlet, and required continuous monitoring especially after particularly dry periods. The trigger depth was determined based on the minimum level of sampling that would obtain a full 1 L water sample, without simply sampling air due to low water depths in the pipe.

Several stormwater pipes conveying water from each catchment area discharged into each inlet manhole, which then discharged through each inlet pipe to the stormwater management pond. To obtain the water level and velocity data necessary to calculate flow rates in the inlets, ISCO 750 Area-Velocity modules were installed by a contractor on metal brackets (Figure 3-6). The metal brackets were installed upstream of the intake strainer in the inlets for Inlet 2 (I2) and Inlet 3 (I3). The location of installation within the pipe was chosen to minimize the influence of turbulence past the invert, without flow disturbance induced by the intake strainer. For Inlet 1 (I1) and Inlet 3, however, the installation of the ISCO Area-Velocity module in the inlet pipe proved difficult. For Inlet 1, the inlet pipe diameter was too small to install the ISCO 750 Area-Velocity module, so it was installed in a stormwater pipe that discharged into the manhole (upstream of the inlet). The installation in the upstream stormwater pipe in Inlet 1 was likely still representative of the majority of flow into the stormwater pond, as the other two stormwater pipes discharging into the manhole captured immediate runoff from the road only and therefore had very small catchment areas. Inlet 3 was located below the surface water elevation of the pond and was therefore

completely submerged only allowing installation of the ISCO 750 Area-Velocity module at the edge of the inlet (where it met the manhole). A typical top-down view of the manhole upstream of a pipe inlet to the pond is shown in Figure 3-7, where the pipes shown are the upstream stormwater pipes from the catchment area that discharge into the manhole, and the concrete inlet pipe that discharges into the stormwater pond is at the bottom of the manhole. Each inlet manhole differs in the number of pipes conveying water from the catchment area.

Figure 3-6. ISCO 750 area-velocity modules installed upstream of the intake strainer initially used for the project.

Figure 3-7. Pipe (left) conveys stormwater from the catchment area to the manhole (right, top-down view.

The water level in the pond was controlled by a broad-crested weir, measuring 2.413 m across at its width, located in the manhole downstream of the pond and the Outlet pipe. The weir is shown in Figure 3-8, where the length of the weir in the direction of flow was assumed to be 0.3 m (based on ladder rung observations), as this could not be measured due to the force of the flow over the weir. The ISCO 750 Area-Velocity module was installed immediately upstream of the weir using a bracket mounted on the wall of the manhole, as shown in Figure 3-8. During installation, the Outlet ISCO sampler was programmed to zero the water level to the crest of the weir.

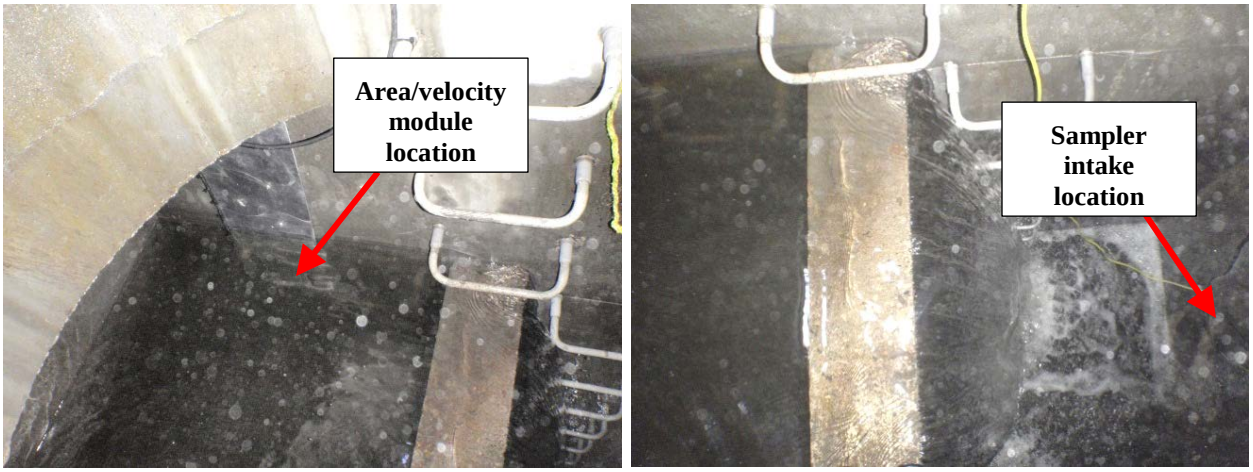

Figure 3-8. Broad crested weir in the bottom of the Outlet manhole, with area-velocity module installed on the side of the manhole upstream of the weir.

Once the ISCO 750 area-velocity modules and intake strainers were installed, the connected ISCO samplers and batteries were hung inside the manholes using a chain and tie strap assembly for easy retrieval, as shown in Figure 3-9. For retrieval of the samplers from the manholes, first, personal protective equipment was donned and signs and safety cones were set-up on the road near the manhole. The manhole cover was then removed, following which the ISCO

sampler was attached to a winch and pulley system on a wooden 4” x 4” post to raise and then lower the samplers out of the manhole (Figure 3-10). A field computer with installed Flowlink™ software was then connected to the sampler to retrieve sample times, pipe water level data, pipe velocity data, and information on program interruptions from the ISCO 6700 sampler data loggers. During sampler retrieval, the 12 volt battery powering the sampler would be exchanged for a fully recharged battery and the full sample bottles (Figure 3-11) would be collected and exchanged with empty bottles.

Figure 3-9. (Left) ISCO samplers and batteries with tie strap and chain assembly hung in manholes for easy retrieval (right).

Figure 3-10. (Left) Retrieval of ISCO 6700 samplers for data logging, sample bottle exchange and battery exchange (center), and return to the manhole (right).

Figure 3-11. Full sample bottles from the ISCO 6700 series samplers (left), and an individual example of a sample bottle containing a sample (right).

To determine the solids concentration in the sample bottles collected from the ISCO samplers, the water volume of each sample was measured, the sample weight was taken, and then the sample was dried in an oven for a minimum of 24 hours to ensure water had evaporated. Once the water had evaporated, the mass of solids was measured. The concentration of solids was then calculated for each sample.

The particle size distribution of solids was also analyzed to assess the particle size removal efficiency of the pond over the entire season. To determine the corresponding particle size

distribution of solids mechanical sieve shakers (Figure 3-12) and a 152H hydrometer (Figure 3-13) were used following ASTM D422-63 (1998) (*Standard Test Method for Particle-Size Analysis of Soils)*. For the mechanical sieve shakers, a Gilson Vibratory 3-inch Sieve Shaker and a larger Hoskin Scientific sieve shaker were used. The mass of sample remaining on the larger sieves was less than the ASTM standard called for, so to scale down the procedure for the smaller sample size, smaller diameter sieves were used.

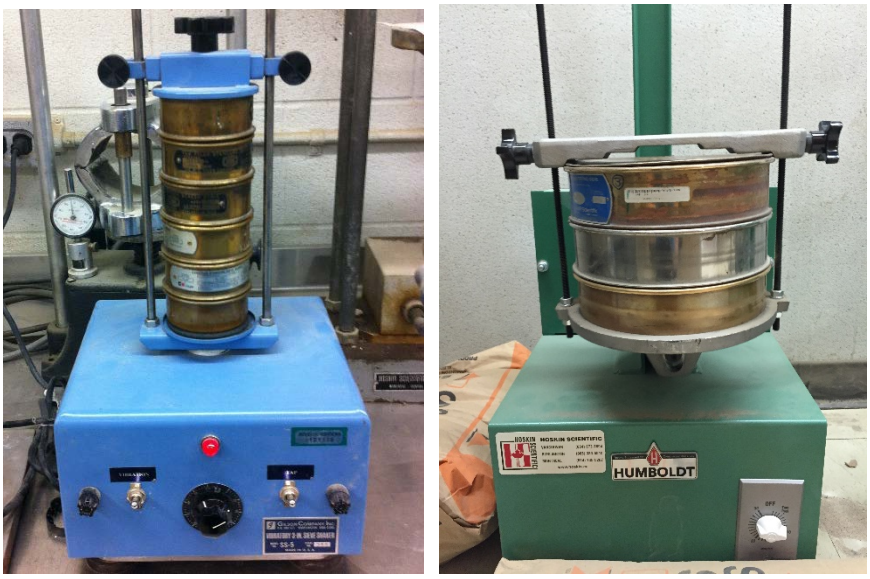

Figure 3-12. Gilson Vibratory Sieve Shaker (left) and Hoskin Scientific mechanical sieve shaker (right) used for particle size distribution testing of solids.

Figure 3-13. Hydrometer (left) and graduated cylinders used for determining the particle size distribution of solids.

When performing the hydrometer analysis, it was assumed that the specific gravity of solids was 2.65 (soils comprised of quartz minerals). However, organics within the sample and solids-bound contaminants (e.g. heavy metals) may have influenced the specific gravity such that it may not have been 2.65. A specific gravity less than 2.65 would have led to a hydrometer corrections with a higher percentage of finer particles, whereas a specific gravity greater than 2.65 would have led to hydrometer corrections with a higher percentage of coarser particles (ASTM Standard D422-63, 1998). For the hydrometers, the zero correction was measured to be 2.5 and the meniscus correction was 0.5. The USDA (1993) *Soil Survey Manual* was used to determine the classification of solids based on their particle size as indicated in Table 3-2.

Table 3-2. Particle size distribution of pond sediment classifications.

Classification	Particle Size (mm)
Gravel	76.0 to 2.0
Sand	2.0 to 0.05
Silt	0.05 to 0.002
Clay	Less than 0.002

3.4 Settled Solids Investigation

Settled solids in the John Avant Park stormwater management pond were sampled to determine spatial and particle size variations in deposited sediment, dominant areas for sediment removal, the relationship between flow patterns and spatial distribution in sediment, and the accumulated sediment depth. For investigating the sediment, core samples, a total station surveying instrument, a telescopic pole with a levelled foot attached, and particle size analysis equipment similar to that used in inlet and Outlet sampling were used.

A mapping system was used to determine the locations of sediment samples and depth to sediment surface measurements. Sample cores and depth to sediment surface measurements were taken at node locations along linear sampling lines (Marsalek *et al.* 1997; Yousef *et al.* 1994). The sample/measurement locations within the pond are shown in Figure 3-14 along with the surveyed pond perimeter and approximate locations of the three inlets (I1, I2, I3) and Outlet (O). The spacing between sample locations varied from approximately 10 to 25 m along the length of a line, where smaller spacing was given for areas thought to have higher solids settling rates (along the flow path near the inlets).

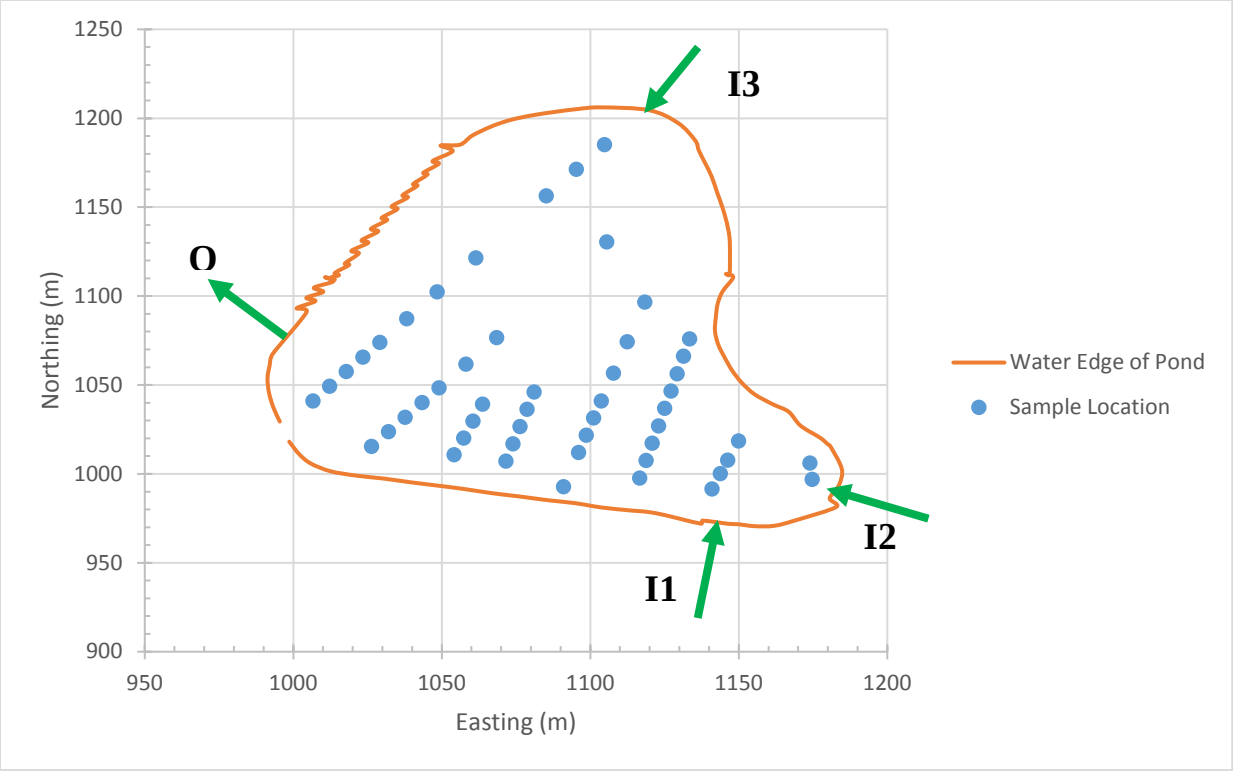

Figure 3-14. Sample/measurement locations within the pond perimeter and locations of the three inlets and Outlet.

To determine the horizontal positioning for sample locations, ASTM Standard D5906 (2013) (*Standard Guide for Measuring Horizontal Positioning during Measurements of Surface Water Depths)* was consulted and the manual measurement method was used. The manual measurement method involves using a taut cable with measured markings along the cable to indicate desired sample locations, where the cable is secured to opposite banks of the water body (Figure 3-15). The markings to indicate the sample locations were measured from the stakes to which the cable was secured at the west bank of the pond. A boat was then used to carry equipment as well as to facilitate taking core samples and depth to sediment surface measurements. For comparison with flow pattern data and the pond perimeter data, the locations where the cable was secured at both banks were then surveyed to determine the ground coordinates. Once sample cores and depth to sediment surface measurements were taken along the cable length, the cable was

moved to the next sampling location along the banks. The locations to place the stakes used to secure the cable were determined using a satellite image of the stormwater pond. The distance between subsequent sample/depth measurement locations along the horizontal length of the cable was generally in the range of 10 to 25 m.

Figure 3-15. Taut cable secured at both banks of the pond (left), where stakes were then surveyed to determine the ground coordinates from which the sample distances from the stakes were measured (right).

Core samples for particle size distribution analysis and depth to sediment surface measurements were taken during dry periods at the beginning (June 23-25, 2014) and end (August 25-29, 2014) of the field sampling season. Sediment core samples were taken from the bottom of the pond to characterize the spatial and particle size distribution variations in sediment. The core samples taken were also to be used as one of two methods to estimate sediment thickness. Some researchers had found that sampling using a simple polyvinyl chloride (PVC) tube sampler induced compaction due to looser surface sediment, which resulted in underestimating the sediment thickness (Yousef *et al.* 1994). For this project, when sampling with a PVC tube sampler was attempted, the pond sediment was too loose to remain in the sampler. Therefore a hand corer was used to collect core samples while minimizing compaction (Marsalek *et al.* 1997; Heal *et al.* 2006). For the hand corer, a Wildco Hand Corer from Hoskin Scientific (Figure 3-16) attached to an

extension pole was used following ASTM D4823-95 (2014) (*Standard Guide for Core Sampling Submerged, Unconsolidated Sediments).* A safety rope was attached to the hand corer and fastened to the boat.

Figure 3-16. Wildco hand corer with extension pole attached, used to take core samples of pond sediment.

To take depth to sediment surface measurements and to collect samples, the boat was rowed along the taut cable until the designated marked sample location was reached. Prior to taking a sample, the depth of water to the sediment surface was measured using a telescopic pole with a foot (Figure 3-17). The telescopic pole with the foot was constructed based on the device detailed in ASTM D5073 (2013) (*Standard Practice for Depth Measurement of Surface Water).* The telescopic pole was gently put into the water at the same location the sample was to be collected, and allowed to sink to the bottom without added force.

Figure 3-17. Telescopic pole with metal foot used to take depth to sediment surface measurements.

To calculate the sediment thickness, only water depth to sediment surface measurements taken using the telescopic pole with the foot were used to compare with the design pond bottom elevation. The alternative method of measuring the length of the core samples from the sediment surface to the pond's clay liner was deemed unreliable for two reasons, the first being that only a few core samples penetrated as deep as the clay liner, the second reason being that water in the sample caused the core sample to break apart or dry with air gaps such that a length measurement could not be taken. Typically, even if the clay liner was contained in a sample, the sample would break apart prior to drying due to the soupy nature, as shown in Figure 3-18. Examples of sediment core samples taken from the bottom of the pond using the hand corer are shown in Figure 3-18. Prior to drying, visible portions of the pond's clay liner that were contained in the sample were removed, as to not affect the particle size distribution. Although the core samples could not be used to measure sediment thickness, visual observations indicated that sediment thicknesses were in the range of that indicated from depth measurements with the telescopic pole with the foot.

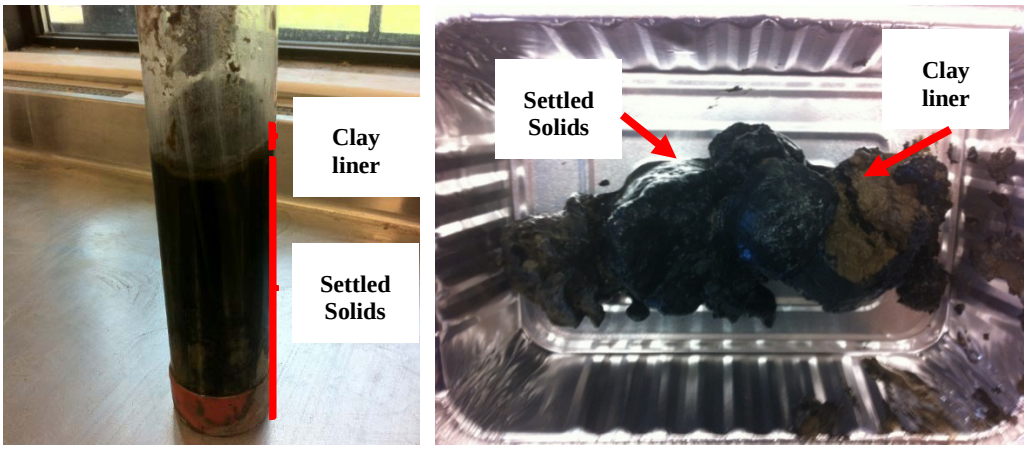

Figure 3-18. Core sample with visible clay liner and water trapped between clay liner and cap (left), along with no longer intact sample prior to drying.

To obtain sediment thickness estimates from the depth to sediment surface measurements, the water surface elevation of the pond was surveyed (Figure 3-19) at the time of sample/measurement collection and was measured to be 500.959 m in June and 500.884 m in late August. For comparison, the normal water level in the pond is 500.86 m, with 2-year and 100-year storm water levels at 501.00 and 501.79 respectively according to hydraulic models (personal communication, H. Azinfar, City of Saskatoon). The design elevation of the bottom of the pond was 499.000 m (personal communication, A. Hildebrandt, City of Saskatoon). The surveyed water surface elevation minus the measured depth to sediment surface elevation was compared to the design bottom elevation of the pond to estimate the sediment thickness because there were no as-constructed drawings.

Figure 3-19. Surveying the water elevation of the pond as part of the sediment depth measurement procedure.

In total, 51 depth measurements and collected samples were performed in June, and then again at the end of August. Once collected, the hand core samples were observed to have sediment stratification and changes in material throughout the core. The samples were analyzed for the particle size distribution, similar to the analysis of the pond inflow and outflow samples, using a hydrometer and mechanical sieve shaker following ASTM D422-63 (1998) (*Standard Test Method for Particle-Size Analysis of Soils).*

The results of the spatial sediment measurements were used to determine dominant areas of the detention basin for the removal of solids of a particular particle size, and the spatial variations in accumulated sediment depth.

3.5 Flow Pattern Investigation

The flow pattern within the stormwater management pond was investigated under a range of wind speeds, wind directions, and inlet flow conditions. Stormwater pond flow patterns were investigated using a combination of drogue tracking by surveying and techniques from LSPTV due to the limitations involved with surveying a large number of drogues.

Drogue designs in the literature vary, and typically consist of a visible, clearly marked float, a variable length line, fin(s), and a weight. The drogue design chosen was based on a design similar to Fyfe *et al.* (2007) and Myers *et al.* (1982), and consisted of a float to maximize visibility while minimizing wind influence, a line to two interlocking rectangular fins (30 cm x 40 cm), and a weight (metal brackets) to ensure the fins remained vertical. Twelve cost-effective drogues were constructed using netting around the ball so it could be secured to a line, cord for the line, brackets for the weights, brightly colored balls for the floats, and coroplast for the fins as shown in Figure 3-20. Once constructed, they were tested in a swimming pool, which had jets to create flow in the pool, to ensure the weight on the drogue fins was sufficient to keep the drogue fins vertical with the float.

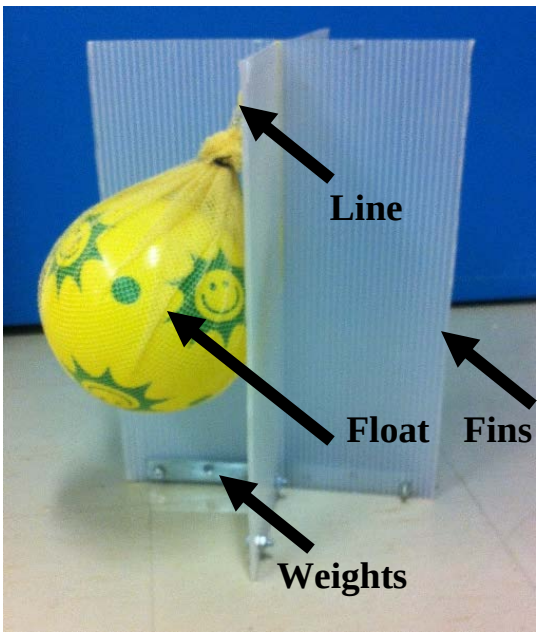

Figure 3-20. Example of a drogue that was constructed

To investigate the velocity at different depths in the pond, drogues with a cord (line) cut at different lengths were used so the fins of the drogues would be at varying depths. When placed in the flow at the same locations, the drogues with fins at varying depths would then give an indication of the vertical velocity profile of the flow. The depth of each drogue was measured from the bottom of the float to the bottom of the fin, and the depth was visually indicated by the color of the float. Initially, the drogue with the blue float had a depth of 1.3 m, the green float drogue had a depth of 1.0 m, the orange float drogue had a depth of 0.7 m, and the yellow float drogue had a depth of 0.40 m. Following a trial run in the stormwater pond it was noted that often the blue drogue would become grounded on the bottom of the pond. Therefore, the fins were cut off and the blue float was used as a visual indicator of wind direction in addition to wind measurements taken using the hand-held Kestrel® 4500 Pocket Weather Tracker.

An additional drogue was constructed to house the prism used for surveying with a Leica robotic total station. The float for the prism-attached drogue was constructed out of Styrofoam and

had a weighted bottom. A 3-dimensional prism (Figure 3-21) was then attached to the top of the drogue float for automatic tracking and surveying with the Leica robotic total station (Figure 3-21).

Figure 3-21. Three-dimensional prism (left) and Leica robotic total station (right) used to track the prism-attached drogue.

For recording the position of the drogues with time, a remote for the Leica robotic total station was used to log the surveyed coordinates of the prism-attached drogue a few times per minute. Since the coordinates surveyed by the robotic total station were time-stamped, the velocity of the prism-attached drogue could be calculated using the survey data. Drogue tracking using surveying was limited to one drogue since there was only access to one Leica robotic total station. To track the additional drogues simultaneously with the robotic total station measurement, techniques from LSPTV were used.

For the LSPTV measurements of the movements of the drogues with the flow, a Nikon D5300, 24.2 Megapixel camera with a wide angle (18 mm) lens was set up on a telescopic metal

pole to view the pond (Figure 3-22) to minimize non-ideal lighting conditions, as recommended by Muste *et al.* (2008). This Nikon camera was chosen due to its high resolution, since the floats of the drogues had to be seen clearly in the image from far distances. The location of the camera was surveyed each time it was in the field to be in the same location for each drogue tracking event. The camera height was also measured and was typically around 3.85 m above the ground surface (approximately 6 m above the pond's surface). Images from the camera were set to be captured every 15 seconds during drogue tracking. A field computer was connected to the camera to enable the operator to view the camera's field of view to ensure the camera lens was focused on the desired area of the stormwater pond.

Figure 3-22. Camera set up at an oblique angle overlooking the stormwater pond with the drogues in the flow.

For each test where the drogues were used to track the flow pattern in the pond, the coordinates of the camera stand and height of the camera were surveyed in order to allow for later LSPTV calculations of the drogue velocities. When tracking the drogues, they were initially placed near the inlet(s) of the stormwater management pond by the small zodiac row boat, and then left undisturbed to be carried by the flow in the pond (Myers *et al.* 1982). During drogue tracking, the wind direction and wind speed were recorded at the same location each time.

For the large scale particle tracking velocimetry, PTVlab open source software could not be used due to reflections from the clouds over the pond. Therefore, an alternative method of data processing was used. Erdbrink (2007) detailed an 8-parameter transformation for tracking particles in a shallow mixing layer using a two dimensional axis since the camera could be set-up directly above the water surface for a top-down view. The transformation is needed to correlate pixel (x, y) coordinates in the camera image of the pond to the real-world coordinate system (u, v) and to undistort the image. This is done using survey of the real-world locations as calibration or reference points in the images. Due to the relatively large size of the stormwater pond at John Avant Park, a top-down view of the pond was not possible. Therefore, the camera was placed at an oblique angle to the pond such that a 3-dimensional axis was needed to obtain spatial information for elevation (z). To include height/depth information an 11-parameter transformation was needed due to the additional z axis. For the 11 parameter transformation, 11 coefficients (A_1, A_2, A_3, A_4, B_1, B_2, B_3, B_4, C_1, C_2, and C_3) are solved for in the collinearity equations (Thomson n.d):

$$x = \frac{A_1u+A_2v+A_3z+A_4}{C_1u+C_2v+C_3+1} \quad [3\text{-}1]$$

$$y = \frac{B_1u+B_2v+B_3z+B_4}{C_1u+C_2v+C_3+1} \quad [3\text{-}2]$$

The coefficients of the collinearity formulas can be thought of as calibrating the system so the formulas can be used to find the real world locations of any pixel coordinate. The formulas also undistort images where image distortion can be caused from use of a wide angle lens.

For data processing using the collinearity equations to define the coefficients in Equation 3-1 and 3-2, the survey coordinates (u, v, z) of at least 6 reference points within an image need to be known, where increased reference points lead to a greater accuracy. For this work, 34 reference points of stationary objects (trees, posts, bench legs, *etc.*) seen in the images of the pond were surveyed to obtain the coordinates (u, v, z) corresponding to pixel coordinates (x, y) for LSPTV calculations (Muste *et al.* 2008). The pixel coordinates were found using Adobe Photoshop software, where the origin (0,0) of pixel coordinates is translated to the center of the image and not the default upper left corner.

Since the surveyed reference points are based on an arbitrary easting (u) and northing (v) reference point, the surveyed reference points needed to be translated from the perspective of the total station surveying instrument to the perspective of the camera used for LSPTV where (z) is the elevation so the (*v*) and (*y*), as well as the (*u*) and (*x*) line up in the image. This translation allows the surveyed coordinate system and the pixel coordinate system to be comparable. Additionally, the surveyed coordinate axis needs to be rotated to the camera axis based on the center point of the image using the following equations, where theta is the angle of rotation and u_{new} and v_{new} are the new rotated easting and northings to align with the camera axis as in (Stewart 2013)

$$u_{new} = u\cos\theta + v\sin\theta \qquad [3\text{-}3]$$

$$v_{new} = -u\sin\theta + v\cos\theta \qquad [3\text{-}4]$$

Once the corrected survey points were calculated, MathCad was used to solve for the unknown calibration coefficients A_1 through to A_4, B_1 through to B_4, and C_1 through to C_3 using a direct linear transformation (Thomson n.d).

Chapter 4

ANALYSIS, RESULTS, AND DISCUSSION

Fourteen rain events were recorded over the three months of data collection from the first week of July to the last week of September in 2014. During each rain event, precipitation amounts were collected from the rain gauge located near the site. Solids concentration samples, water level measurements, and water velocity measurements were also collected during the rain events from the ISCO samplers. Pond sediment samples and depth to sediment surface measurements were taken twice over the summer during dry periods to determine the spatial distribution of sediment. The first round of pond sediment samples were taken from June 23 to 25, 2014 and the second round of pond sediment samples were taken from August 25 to 26, 2014. Drogue tracking took place on five separate occasions over the summer period. The results and analysis of these activities are discussed herein.

4.1 Analysis of Rainfall Events

There were 14 major rain events recorded by the tipping bucket rain gauge from July 9, 2014 to September 30, 2014, with a total rainfall over that period of 82 mm. The number of rain events was determined using the inter-event time definition (IETD), which is defined as the "minimum temporal spacing required between rainfall events to consider the events as separate" (Papa and Adams 1996). To find the IETD, varying inter-event times are plotted to evaluate the corresponding number of rain events over a season. Using this plot, the IETD is considered the time for which the curve begins to plateau (McLeod 2007).

For the determination of the IETD, inter-event durations ranging from 1 to 24 hours were tested for the measurement period to determine the number of rain events that would be established

based on a particular duration. The results are shown in Figure 4-1. In Figure 4-1 it was determined that the inter-event time for the three month sampling season was approximately 13 hours, where the data is seen to plateau, which results in 14 rain events. This IETD is longer than the IETD found for Saskatoon of five hours by McLeod in 2007. The differences in the estimated values of IETD herein and by McLeod (2007) may be due to several reasons. First, Joo *et al.* (2014) suggest that IETD calculations may actually require more sophisticated modelling of the basin. Further, the measurements herein were taken in months that tend to be drier than the period studied by McLeod (2007). Finally, McLeod's tipping bucket rain gauge tipped at increments of 0.2 mm rather than at 0.254 mm, which would mean that it was slightly more sensitive than the one used for work herein. The IETD however, is simply used to define events for solids removal efficiency calculations.

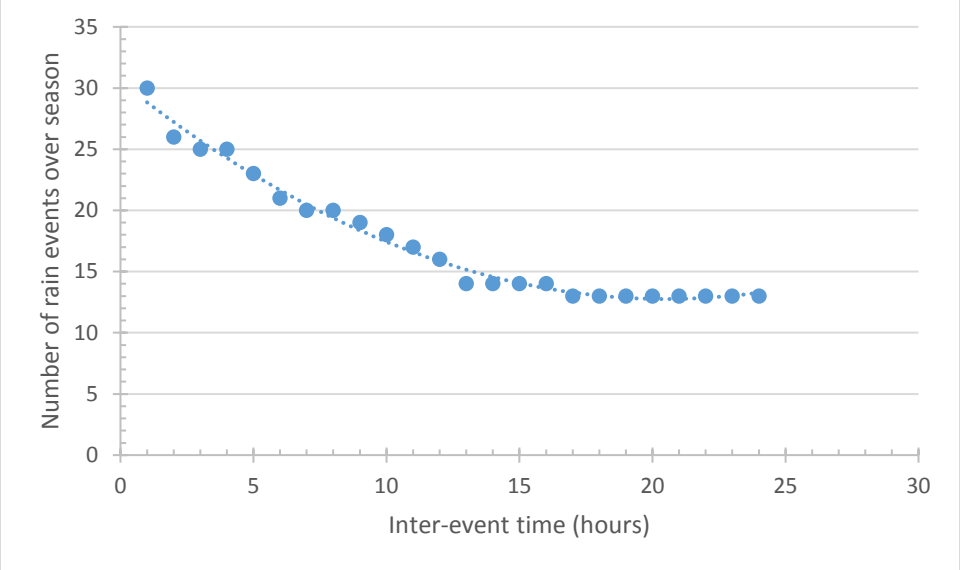

Figure 4-1. Inter-event time plot to determine the number of rain events over the season and the time separating rain events.

Each of the 14 rain events, their corresponding times, and measured rainfall from the tipping bucket rain gauge are shown in Table 4-1. As noted above, there was 82 mm of rainfall

recorded over the 3 month data collection period. The tipping bucket rain gauge used for this research tipped in intervals of 0.254 mm of precipitation. If the tipping bucket did not fill enough to trigger tipping, it is possible that rain collected may have not been recorded and may have evaporated during the time between rain events. Alternatively, this rain may have not completely evaporated and may have then been accounted for in a subsequent rain event, resulting in over or under estimates of rainfall for each individual rain event. Error resulting from tipping bucket rain gauges have also been reported from wind, splashing, spilling, and evaporation (Marsalek 1981; Lanza and Stagi n.d).

Although 14 rain events were measured during the three month sampling season, the presence of rainfall did not necessarily mean that there was sufficient runoff such that all three inlet pipes or the Outlet experienced flow, or that the water level in the inlet pipes or Outlet was sufficient to trigger the sampling routine. In some cases, the water level in an inlet or the Outlet pipe was very low with a corresponding velocity measurement of zero, shown as “NQ-L” (no flow, with measured water level) in Table 4-1; this likely indicated standing water in the inlet pipes or Outlet. For the case where there was both an adequate flow rate and water level for successful measurements during the rain event, this is shown as “YQ-L” (flow, with measured water level) in Table 4-1. The case where there was flow in the inlet pipes or Outlet during a rain event, but the level of water in the pipes was not necessarily sufficient to trigger the sampler is indicated by “S” in Table 4-1. In the instances where a battery had died or a sampler was out of service this is indicated as “Out of Service” in Table 4-1.

Table 4-1. Rain events recorded by the tipping bucket rain gauge and the status of Inlet 1, 2, and 3 (I1, I2, I3 respectively) and Outlet sampler measurements during, and following these rain events.

Start Rain Date, Time End Rain Date, Time	Length of Rain Event (hours)	Antecedent dry period	Cumulative Rainfall (mm)	Status of I1 sampler	Status of I2 sampler	Status of I3 sampler	Status of Outlet sampler
July 9, 11:00 to July 10, 5:15	18.25	0	1.016	NQ-L	YQ-L	YQ-L	YQ-L
July 17, 19:15 to July 18, 9:15	14.00	7 days	12.700	YQ-L S	YQ-L S	YQ-L S	YQ-L S
July 24, 8:40 to July 24, 20:22	11.70	6 days	8.382	YQ-L S	YQ-L S	YQ-L S	YQ-L S
July 25, 12:00 to July 27, 3:43	39.72	<1 day	19.304	YQ-L S	YQ-L S	YQ-L S	YQ-L S
August 8, 22:44 to August 8, 23:24	40.00	11 days	0.508	NQ-L	NQ-L	YQ-L	YQ-L
August 17, 3:38 to August 17, 5:09	1.52	9 days	7.366	O	YQ-L S	YQ-L	YQ-L S
August 20, 3:47 to August 20, 14:40	10.88	3 days	9.398	YQ-L	YQ-L S	YQ-L	YQ-L S
August 24, 10:50 to August 24, 21:28	10.63	4 days	7.620	YQ-L	YQ-L	YQ-L S	YQ-L
August 30, 5:47 to August 30, 6:46	0.98	6 days	3.556	O	YQ-L S	YQ-L	YQ-L
August 31, 14:18 to August 31, 15:45	1.45	1 day	1.778	O	YQ-L	YQ-L	YQ-L
September 1, 20:23 to September 1, 20:24	0.02	1 day	0.254	O	NQ-L	YQ-L	YQ-L
September 2, 19:21 to September 3, 0:29	5.13	1 day	1.524	O	NQ-L	O	YQ-L
September 8, 1:01 to September 8, 21:56	20.92	5 days	8.128	YQ-L	YQ-L S	YQ-L	YQ-L
September 13, 5:57 to September 13, 10:40	9.72	5 days	0.508	NQ-L	NQ-L	YQ-L	NQ-L

YQ-L – Velocity was measured in the inlet or Outlet pipe during the rain event for flow measurements, there was a non-zero measurement for pipe water level.
NQ-L – No velocity measured in the inlet or Outlet pipe during the rain event, there was a non-zero measurement for pipe water level.
S – Sampling was triggered and samples were taken during the rain event.
O – The sampler was out of service during the rain event, generally due to battery issues.

Of the 14 rain events on record for the sampling season, only three of these rain events resulted in water levels that were sufficient to trigger sampling in all three inlet pipes, and all three of these rain events occurred in July. During equipment testing in June, it was determined that had the trigger water level for sampling been adjusted to a lower water level, samples would have consisted of mostly air. Throughout the three month sampling period, which started in July, the longest antecedent period between rain events was 11 days, with the majority of rainfall occurring in July. The single rain event with the largest amount of precipitation occurred on July 25 with 19.3 mm of rainfall. In contrast, the least amount of precipitation in a rain event occurred on September 1st, with approximately 0.3 mm of rainfall. The precipitation amounts for the 14 rain events are shown in Figure 4-2.

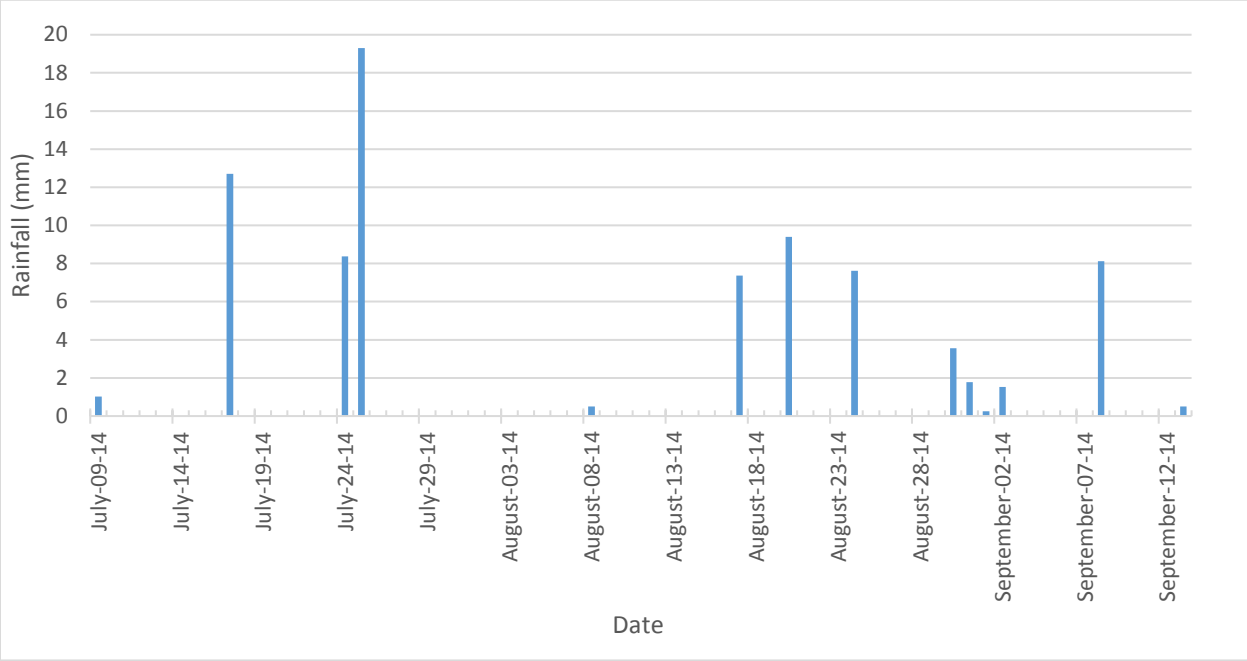

Figure 4-2. Recorded precipitation from the first rainfall to the last rainfall over the measurement period.

Over the season for which rainfall data was recorded, no two rain events were similar in nature in terms of their rainfall intensity (mm/hour) over the entire rainfall event. The hyetographs

for rain events that were longer than two hours in duration, measured using the tipping bucket rain gauge, can be found in Appendix A.

As shown in Table 4-1, Inlet 2, with a catchment area of 21.40 ha (personal communication H. Azinfar, City of Saskatoon), was the most reliable inlet for triggering the sampling routine and measuring flow. Inlet 3, with a catchment area of 71.99 ha (personal communication H. Azinfar, City of Saskatoon), was completely submerged, as the top of the inlet was located at an elevation lower than the water surface of the pond. Varying water flows into and out of the pond, along with changes in flow direction in Inlet 3, likely resulted in sampler triggering at times that did not necessarily correspond with a rain event. The catchment area of 9.67 ha (personal communication H. Azinfar, City of Saskatoon) for Inlet 1 was the smallest of the three inlets, such that there was not as much flow or sample triggering as the other two inlets.

4.2 Pond Inflows and Outflows

For each of the inlets, the average velocity and water level were measured using the ISCO 750 area velocity modules, which were then used to calculate the flow rate (discharge) through the pipes. Measurements of the water level immediately upstream of the broad-crested weir at the Outlet were used to calculate the flow rate through the Outlet pipe of the pond. The flow rates in each of the inlets and Outlet pipes over the measurement period were then used to determine the total loading of solids and the solids removal efficiency of the stormwater management pond.

First, for the calculation of the flow rate through Inlet 1 and 2, the water depth in the pipe (y) and the pipe diameter (d) were used to calculate the cross sectional flow area (A):

$$A = (\theta - sin\theta)\frac{d^2}{8} \quad [4\text{-}1]$$

$$\theta = 2cos^{-1}(1 - 2\frac{y}{d}) \quad [4\text{-}2]$$

as given in (Sturm, 2010), where θ is an angle used to help define the water level in the development of these formulas. The measured average velocity (*U*), from the ISCO 750 Area Velocity Modules, was then multiplied by the cross sectional flow area (*A*) to determine the flow rate (*Q*) in the inlet pipes:

$$Q = UA \qquad [4\text{-}3]$$

The flow rate through Inlet 3 was calculated differently. Inlet 3 was completely submerged, with at least 16.5 cm of water over the crown of the inlet pipe. Therefore, it was assumed that the Inlet 3 pipe flowed full when calculating the flow rate.

To determine the flow rate over the crested weir at the Outlet, an equation for a rectangular finite-crested weir was used (Sturm 2010) with the dimensions of the weir defined in Figure 4-3:

$$Q = C_d C_v \frac{2}{3}\left(\frac{2g}{3}\right)^{0.5} b{h_1}^{1.5} \qquad [4\text{-}4]$$

where C_v is the approach velocity correction coefficient, C_d is the discharge coefficient, g is the acceleration due to gravity (9.81 m/s^2), b is the weir width (2.413 m), and h_1 is the level of water upstream of the weir relative to the weir crest (as measured by the ISCO 750 area velocity flow module). The value of C_v was calculated from (Bos 1989):

$$C_v = \left(\frac{H_1}{h_1}\right)^{1.5} \qquad [4\text{-}5]$$

$$H_1 = h_1 + \frac{\alpha {U_1}^2}{2g} \qquad [4\text{-}6]$$

where H_1 is the total energy head above the weir, α is the kinetic energy correction coefficient (assumed to be 1.0), and U_1 is the average velocity of the flow upstream of the weir where h_1 is measured. The total depth of flow at that location is y_1. Therefore:

$$U_1 = \frac{Q}{(y_1 b)} \qquad [4\text{-}7]$$

The height of the weir was estimated to be approximately 1.0 m based on the height of the subcontractor, but was not measured due to safety concerns given the violent nature of the water in the area.

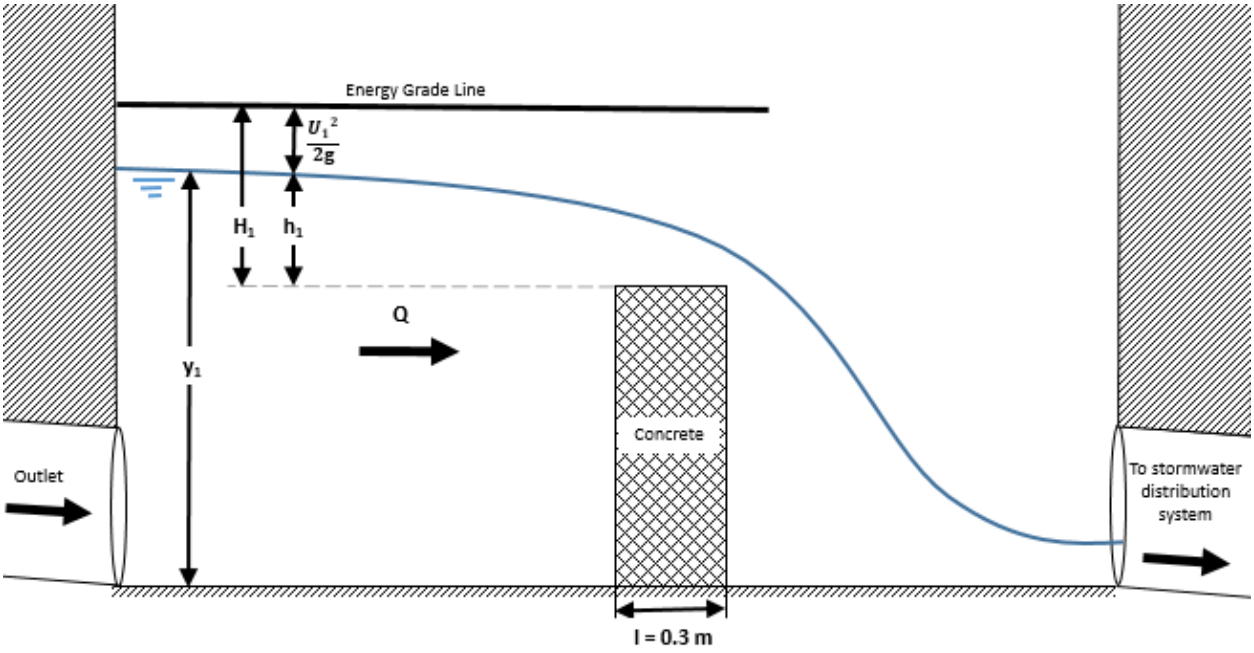

Figure 4-3. Definition sketch for the finite crested-weir located at the Outlet, with the Outlet from the pond (left), and the Outlet to the storm sewer distribution system (right).

To calculate C_v, an iterative approach was used by first assuming C_v = 1.0 and calculating Q, then adjusting the velocity head accordingly until minimal changes in the value of Q were observed. To determine C_d it must be determined whether the weir can be treated as a broad-, short-, or sharp-crested (Sturm, 2010). This is determined from the ratio H_1/l, where l is the length of the weir in the direction of flow. The length of the weir in the direction of flow (l) was estimated to be 0.3 m, based on visual observations taken at the time of the ISCO 750 Area Velocity Module installation (direct measurements could not be taken for safety reasons). For 0.33 > H_1/l the weir

should be treated as broad-crested, for $0.33 < H_1/l < 1.5$ the weir should be treated as short-crested, and for $H_1/l > 1.5$ the weir should be treated as sharp-crested (Sturm 2010). For the current work, based on the value of H_1/l, the Outlet weir could be treated as broad-crested. Therefore, a C_d value of 0.848 was used (Sturm 2010).

The inlet pipe inner diameters along with the maximum water levels, velocities, and flow rates over the season are shown in Table 4-2.

Table 4-2. Maximum water levels, velocities, and flow rates for the three inlet pipes over the data collection season.

Inlet	Pipe Inner Diameter (m)	Maximum level y (m)	Minimum level y (m)	Maximum average velocity U (m/s)	Maximum flow rate Q (m^3/s)
Inlet 1	0.525	0.236	0	1.668	0.157
Inlet 2	0.750	0.648	0	1.617	0.612
Inlet 3	1.050	1.796	1.215	3.859	3.342

The water level in Inlet 1 was typically the shallowest of the three inlets throughout each rain event, ranging from a minimum of 0 m to a maximum of 0.24 m. The maximum average velocity observed in Inlet 1 was 1.67 m/s. The water level in Inlet 2 also had a minimum water level of 0 m, as there was typically no standing water in the pipe at the measurement location during dry periods. The maximum water level and velocity in Inlet 2 were 0.65 m and 1.62 m/s respectively. Inlet 3 was always completely submerged, with a minimum water level of 1.22 m (0.17 m over the top of the inlet pipe) and a maximum water level of 1.80 m, 0.75 m over the crown of the inlet pipe at its entrance within the manhole. The maximum average velocity measured in Inlet 3 was substantially higher than the other inlet pipes at 3.86 m/s, as might be

expected from its larger catchment area. The flow rate in the inlets and Outlet was found to fluctuate with rainfall intensity as shown in Figures 4-4 to 4-6.

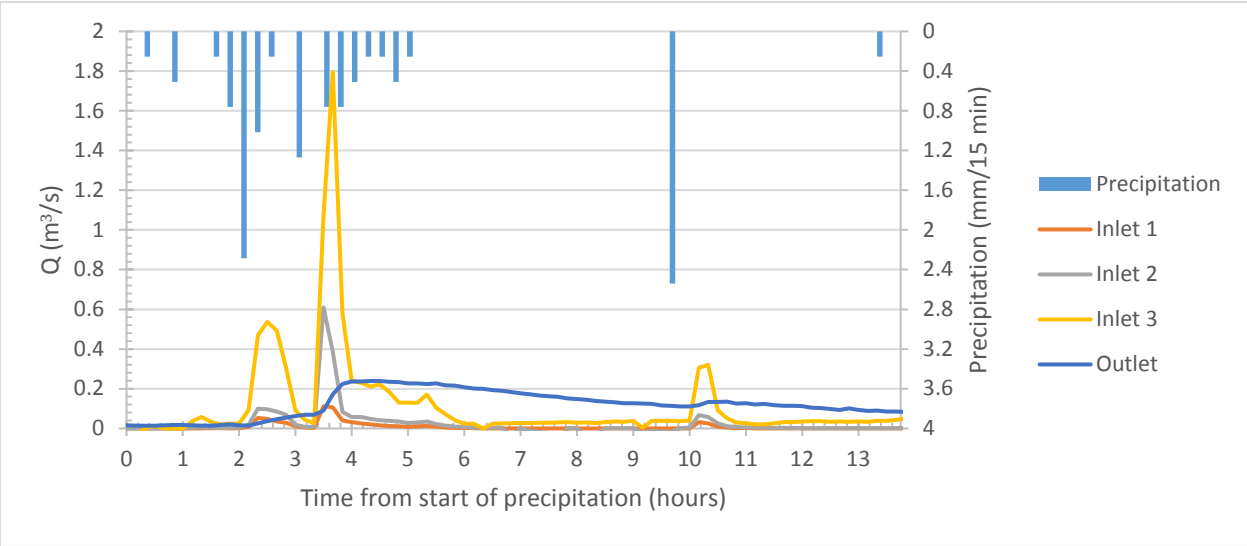

Figure 4-4. Inlet and Outlet pipe flow rate and measured precipitation amounts for the July 17 to 18, 2014 rain event, where flow in the inlets reached a maximum approximately 3.75 hours after the start of precipitation, as determined by the first tip of the tipping bucket rain gauge.

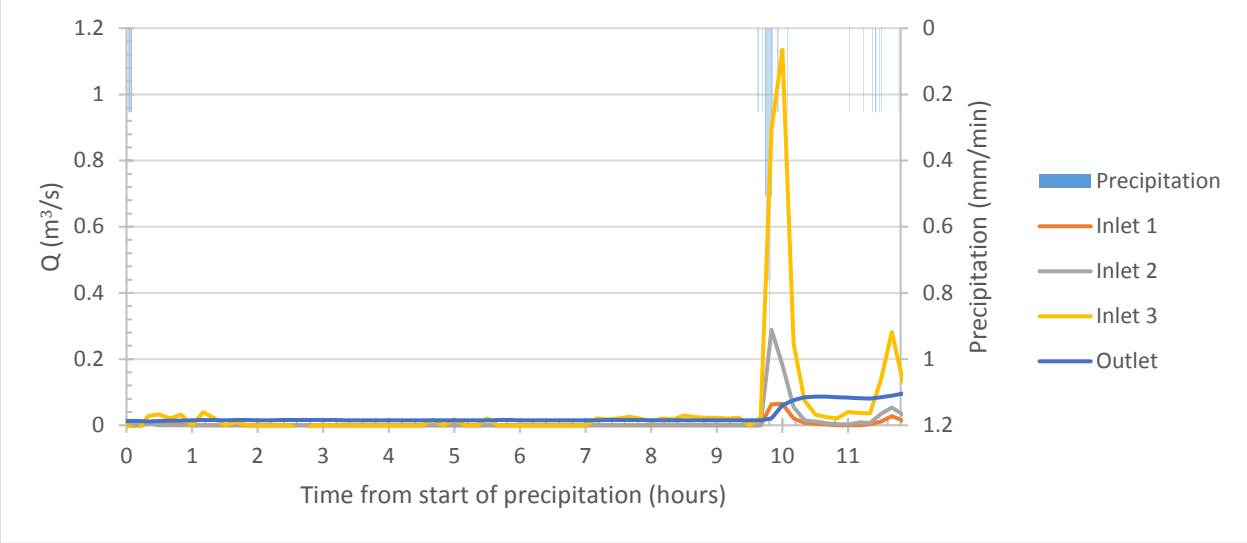

Figure 4-5. Inlet and Outlet pipe flow rate and measured precipitation amounts for the July 24, 2014 rain event, where flow in the inlets reached a maximum approximately 10 hours after the start of precipitation, as determined by the first tip of the tipping bucket rain gauge. Rainfall after this period was considered part of the July 25 rain event.

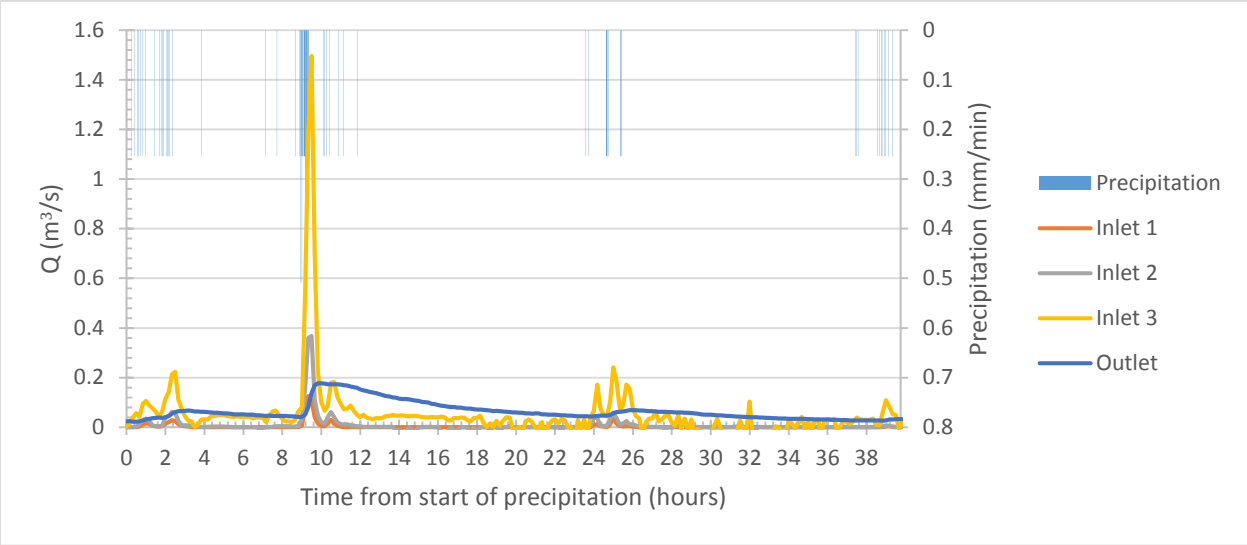

Figure 4-6. Inlet and Outlet pipe flow rate and measured precipitation amounts for the July 25-27, 2014 rain event, where flow in the inlets reached a maximum approximately 9.75 hours after the start of precipitation, as determined by the first tip of the tipping bucket rain gauge.

As shown in Figures 4-4 to 4-6, there was typically a small lag (less than 30 minutes) from a peak in rainfall intensity to the corresponding peak in an inlet flow rate, suggesting there was a time period for rainfall infiltration before there was substantial runoff. There was a slightly greater lag (an additional 15 to 30 minutes) to a maximum flow in the pond Outlet, where the Outlet flow would peak and then steadily decline, likely due pond storage. Additionally, in some cases flow within the inlet pipes preceded the tipping bucket rain gauge's precipitation measurements likely due to precipitation variability within the pond's catchment area.

The total water volume into the pond over the entire sampling season (not just during rain events) from the three inlets is estimated as 67,100 m^3, whereas the total volume out of the pond through the Outlet is estimated as 154,200 m^3. Therefore, 87,100 m^3 or approximately 56% of the flow through the Outlet was not measured or accounted for as incoming flow through the inlet pipes. This could be due to groundwater infiltration or seepage into the stormwater pond that is extraneous to rain events that would have not been accounted for in the flow through the inlets.

Although the pond has a clay liner, groundwater can move into the pond above the liner, through cracks in the liner, or along the inlet pipes. Second, the height and length of the weir crest were based on visual approximations, which may have contributed to error for the total water volume as calculated from the Outlet. Third, there would have been unaccounted for rainfall over the surface area of the pond itself of approximately 29,400 m^2, which was found from survey data and a Google Earth image of the site. Additionally, there is a pond/park catchment area of 11.56 ha for which runoff flows directly to the pond and not to the inlet pipes. The total volume of water contribution from the pond/park catchment area was calculated to see if it could account for the discrepancy between the inflow and outflow volumes. If all of the precipitation over the season did not infiltrate into the soil and was therefore runoff to the pond, this would have accounted for a volume of approximately 9,500 m^3.

It is also important to note that during the 2014 summer season, the water table in the area was high. Many homes in the neighborhood around John Avant Park were often running their sump pumps throughout the summer season. It was observed that some of these homes would also discharge the water from their sump pumps onto the street, which would have been conveyed to the pond inlet pipes, accounting for some of the additional water volume outside of rain events. It is thought that the majority of the discrepancy between the water volume into the pond and the water volume out of the pond was likely due to groundwater inflow into the pond, especially considering that there was outflow from the pond throughout the summer period when there was no flow measured in the inlet pipes. Though there would have been expected evaporation from the pond during the summer months, the evaporation did not appear to affect outflow from the pond during dry periods.

Figure 4-7 can be used to estimate what might be considered baseflow conditions in the Outlet, where baseflow is the outflow from the pond during periods of no precipitation. The baseflow was estimated to be 0.015 m^3/s from June 18, 2014 (test period for samplers) to August 22, 2014. After August 22nd, 2014 the Outlet baseflow diminished to approximately 0.005 m^3/s until the near end of the summer, when there was no baseflow observed from the Outlet after September 9th, 2014. The baseflow accounts for 92,000 m^3 from the Outlet. Considering the volume of flow from the Outlet was 87,000 m^3 above that from the inlets, it is seen that the baseflow accounts for this extra volume of flow when considering there is also additional precipitation to the pond unaccounted for by the inlets. Others have also found that baseflow typically accounts for a high outflow percentage of a stormwater pond. Anderson *et al.* (2013) found that the baseflow, depending on the year, accounted for 66% to 72% of the outflow from a two-stage dry and wet detention pond in the Kingston Township of Ontario. Therefore, the event flow only accounted for 34% and 28% of the total pond outflow respectively.

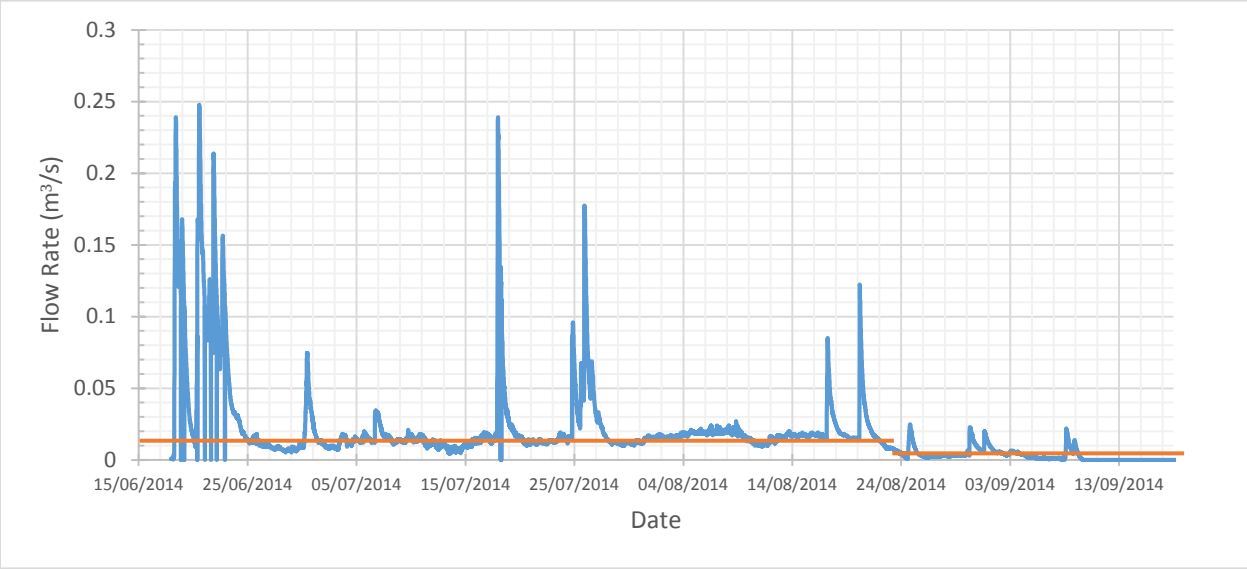

Figure 4-7. Determination of baseflow from the Outlet.

4.3 Total Solids Analysis for Flow in Inlets and Outlet

The total solids mass loading and removal efficiency of the pond was calculated using the event mean concentration (EMC), which is the mean total solids concentration during a single rain event, and the site mean concentration (SMC), which is the total solids concentration for a number of rain events (Kantrowitz and Woodham 1995; Pettersson and Lavieille 2007; McLeod 2007). The EMC (Table 4-3) was calculated by dividing the total mass load of total solids during the rain event by the total discharge volume of water during the rain event (McLeod 2007):

$$EMC = \frac{\sum_{i=1}^{n} C_i V_i}{\sum_{i=1}^{m} V_i} \qquad [4\text{-}8]$$

where C_i is the sample concentration of total solids representing time interval i and V_i is the total volume of water discharged over time interval i. Ideally, the number of time intervals sampled (n for number of actual sampled intervals and m for number of intervals with a measured flow) are identical; however, the automated samplers only hold 24 bottles and were set to discretely sample at either 10 minute (first 12 bottles) or 30 minute (remaining 12 bottles) time intervals as programmed as the sampling routine in the sampler.

The site mean concentration (SMC) (Table 4-3) of total solids for each of the inlets and Outlet was determined for the entire sampling season using the geometric mean of the EMCs to measure the log normal distribution of the EMC's central tendency (McLeod, 2007). To determine the total SMC for all of the inlets (SMC_{in}) combined, a weighted average was used, considering the total discharge volume for each of the inlets:

$$SMC_{in} = \frac{(SMC_1 V_{T1} + SMC_2 V_{T2} + SMC_3 V_{T3})}{(V_{T1} + V_{T2} + V_{T3})} \qquad [4\text{-}9]$$

From this calculation, the SMC_{in} was determined to be 0.150 kg/m^3. The site mean concentration from the Outlet (SMC_{out}) was determined to be 0.251 kg/m^3 as shown in Table 4-3. The mass loading (L) of total solids over the entire sampling season was then calculated using the SMC and the total volume (V_T) of water discharged from the inlet and Outlet pipes over the season (Table 4-3):

$$L = SMC \cdot V_T \qquad [4\text{-}10]$$

Table 4-3. Event mean concentrations (EMCs) and total discharge volume (V_T) for the inlets and Outlet, used to determine the site mean concentration (SMC), load of total solids (L), and the total removal efficiency of the pond.

Start Rain Date, Time End Rain Date, Time	Inlet 1 EMC (kg/m^3)	Inlet 2 EMC (kg/m^3)	Inlet 3 EMC (kg/m^3)	Outlet EMC (kg/m^3)
July 9, 11:00 July 10, 5:15	N/A	N/A	N/A	N/A
July 17, 19:15 July 18, 9:15	0.142	0.138	0.332	0.225
July 24, 8:40 July 24, 20:22	0.116	0.231	0.189	0.265
July 25, 12:00 July 27, 3:43	0.032	0.040	0.061	0.132
August 8, 22:44 August 8, 23:24	N/A	N/A	N/A	N/A
August 17, 3:38 August 17, 5:09	Out of Service	0.156	N/A	0.467
August 20, 3:47 August 20, 14:40	N/A	0.396	N/A	0.269
August 24, 10:50 August 24, 21:28	N/A	N/A	0.071	N/A
August 30, 5:47 August 30, 6:46	Out of Service	0.253	N/A	N/A
August 31, 14:18 August 31, 15:45	Out of Service	N/A	N/A	N/A
September 1, 20:23 September 1, 20:24	Out of Service	N/A	N/A	N/A
September 2, 19:21 September 3, 0:29	Out of Service	N/A	N/A	N/A
September 8, 1:01 September 8, 21:56	N/A	0.138	N/A	N/A
September 13, 5:57 September 13, 10:40	N/A	N/A	N/A	N/A
SMC (kg/m^3)	0.081	0.254	0.128	0.251
V_T (m^3)	3,900	12,900	50,300	154,200
L (kg)	300	3,300	6,400	38,700

For some rain events, sampling did not trigger due to insufficient water levels within the inlet pipe or Outlet to obtain a water sample. In some instances, there may have been no sampling if a particular ISCO sampler was out of order. Since there was no data for these rain events, they were not able to be included in calculations to determine the removal efficiency or loading.

As shown in Table 4-3, the SMCs for the inlets and Outlet ranged from 0.081 to 0.254 kg/m^3. The total solids loads calculated from the SMCs of total solids and the total discharged volume of water were 300 kg for Inlet 1, 3,300 kg for Inlet 2, 6,400 kg for Inlet 3, and 38,700 kg for the Outlet. Therefore, a greater mass of total solids was estimated to be leaving the pond than entering. To determine if this was the case, the removal efficiency of total solids was calculated using the SMCs by the following equation (Pettersson and Lavieille 2007):

$$R(\%) = \frac{(SMC_{in} - SMC_{out})}{SMC_{in}} * 100\% \qquad [4\text{-}11]$$

where *R%* is the removal efficiency and SMC_{in} and SMC_{out} represent inflow and outflow site mean total solids concentrations by volume respectively.

The removal efficiency calculation indicated that over the summer season the stormwater retention pond actually had an estimated negative removal efficiency of -67% for total solids. The mass loading of total solids into the pond for all three of the inlets was determined to be 10,000 kg, whereas the mass loading of the pond's outflow was 38,700 kg for a net difference of 28,700 kg. Considering a range of bulk densities from 1300 kg/m^3 to 2000 kg/m^3, typical for clay to sand sized particles, and a pond area of 29,400 m^2, the net difference is equivalent to 1 mm or less of sediment depth. This negative removal efficiency indicates that there could be possible resuspension of sediment or short-circuiting with too high velocities and not enough time for solids to settle. The pond/park catchment area and the Outlet catchment area would have contributed to the negative removal efficiency.

Negative removal efficiencies for individual rain events or seasons are not uncommon in stormwater pond systems, and removal efficiencies are highly variable. Anderson *et al.* (2013) found that the removal efficiency of total suspended and total dissolved solids varied from when

there was just baseflow to when there was additional flow due to a rain event. They found that during a rain event the removal efficiency of total suspended solids was 42%, whereas there was a negative removal efficiency for total dissolved solids of -11% (Anderson *et al.* 2013). During baseflow, however, there was a negative removal efficiency for total suspended solids of -55% and a near-zero removal efficiency for total dissolved solids of 4% (Anderson *et al.* 2013). It was thought that the negative and near-zero removal efficiencies during baseflow were due to resuspension of fine particles (clay and silt) caused by the operation of a fountain during baseflow conditions (Anderson *et al.* 2013). Others have found negative removal efficiencies to be not as common. Greb and Bannerman examined 16 rain events over a season and found that the removal efficiency of a stormwater pond varied between 66% and 97% by mass, and the pond was less effective at removing smaller particle sizes.

At the John Avant Park stormwater management pond investigated in this study, the aeration fountain was non-operational during the 2014 season, so it would have not contributed to resuspension. Although resuspension would not have been caused by the fountain during this particular field season, it is worth noting due to its implications in years when the fountain is operational. Although the fountain was not operational during the 2014 season, water from the pond was pumped to the start of a man-made stream for some aeration. It is therefore possible that this pumping, along with wind, may have resulted in resuspension of pond sediment. Additionally, surface runoff reporting to the man-made stream that was part of the pond/park catchment area could have contributed to total solids within the pond. There was also a contributing catchment area entering the Outlet directly that did not flow into the pond for settling; this could have resulted in increased total solids loads in the Outlet samples.

The relationship between the total solids concentrations and the flow rate in Inlet 2 is shown in Figure 4-8, and Appendix B for the other inlets and the Outlet. There was no apparent relationship between the flow rate during the time the sample was taken and the concentration of total solids within that sample. However, higher concentrations of total solids were generally associated with the first peak in the flow seen in the inlet and Outlet pipes near the beginning of a rain event, as seen in Figure 4-9. These higher concentrations towards the beginning of a rain event were thought to be representative of the first flush, where total solids are transported along with overland flow. If there was very little precipitation at the beginning of a rain event, there may not have been enough runoff to generate high flows in the inlet and Outlet pipes. For this case, the first flush was typically seen later on in the rain event along with the first larger peak in inlet and Outlet flows, as shown in Figure 4-10.

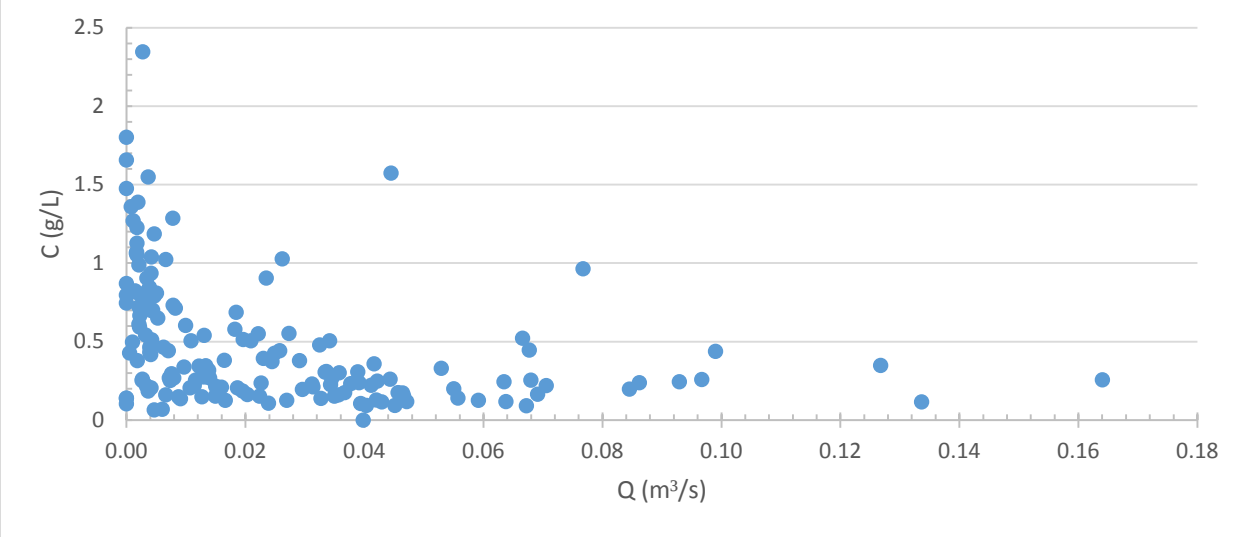

Figure 4-8. The variation of total solids concentrations with flow rate for Inlet 2 over all rain events.

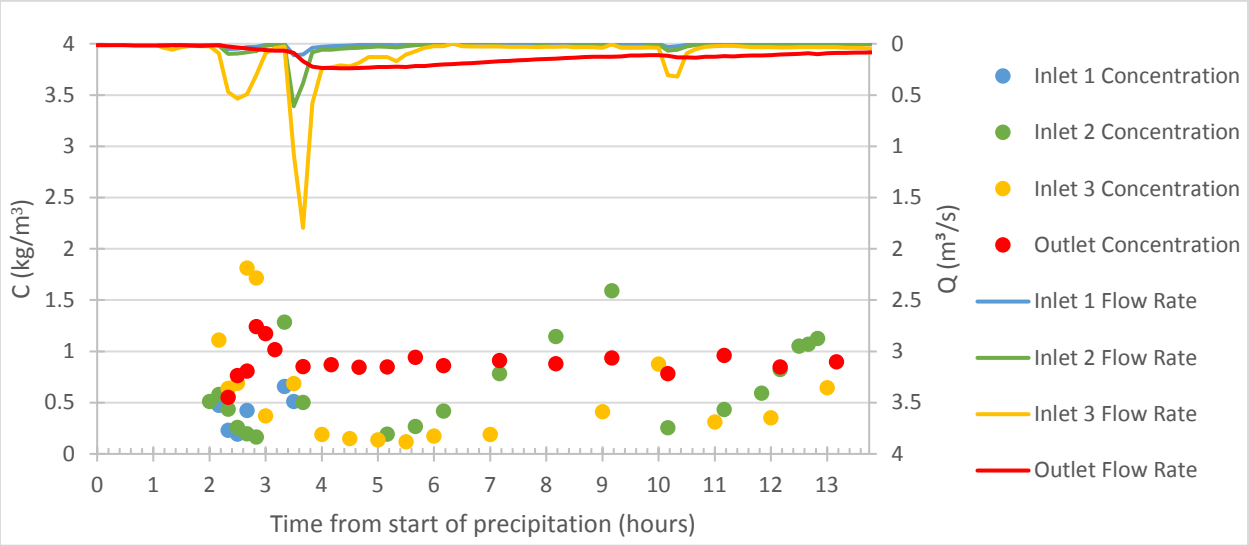

Figure 4-9. Total solids concentration and flow rate with the time from the start of precipitation for the July 17-18, 2014 rain event.

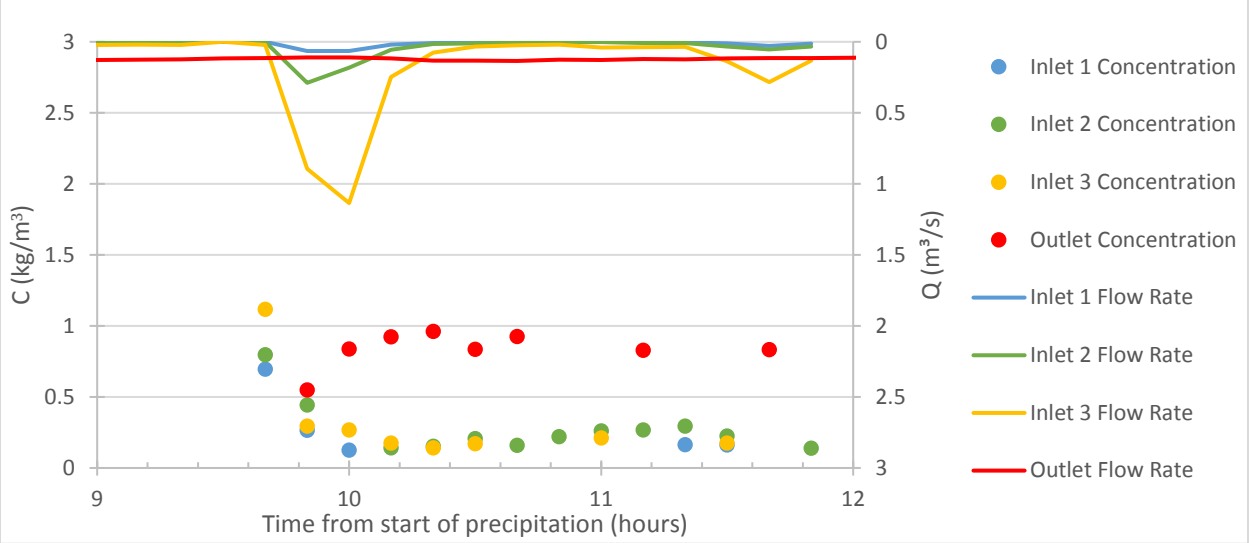

Figure 4-10. Total solids concentration and flow rate with the time from the start of precipitation for the July 24, 2014 rain event.

The particle size distributions of total solids contained in the flows through the inlets and Outlet were also assessed. It was not possible to determine particle size distributions for each rain event, as the sample size of total solids for each rain event was typically a few grams; this is much less than the sample size required by the ASTM standard used to analyze these distributions

(ASTM D422-63 1998). Therefore, the particle size distributions were determined for the entire sampling period.

The different inlets and Outlet showed varying particle size distributions. In general, Inlet 3 samples were associated with the greatest fraction of larger diameter particles, with only 27.6% of particles by mass finer than 0.009 mm, as opposed to 52.4% and 42.4% for Inlet 1 and Inlet 2 respectively. For all three of the inlets, 100% of the particles were smaller than 4.75 mm by mass. The sampled total solids from Inlet 1, Inlet 2, and Inlet 3 had 76.1%, 85.8%, and 85.0% of the particles that were finer than 0.05 mm by mass respectively. For the Outlet, 92.0% of the particles by mass were finer than 0.05 mm. For the Outlet the particle size distribution generally consisted of smaller particles than the inlets, where 100% of the particles were finer than 1.18 mm by mass. This suggests that the John Avant Park stormwater pond was more effective at removing larger size particles. The particle size distributions of solids sampled from all three inlets and the Outlet are shown in Figure 4-11. As shown in Figure 4-11, there were very fine clay particles contained in the sample that were smaller than the size range investigated by hydrometer analysis. The particle size distribution data for the inlets and Outlet is given in Appendix C.

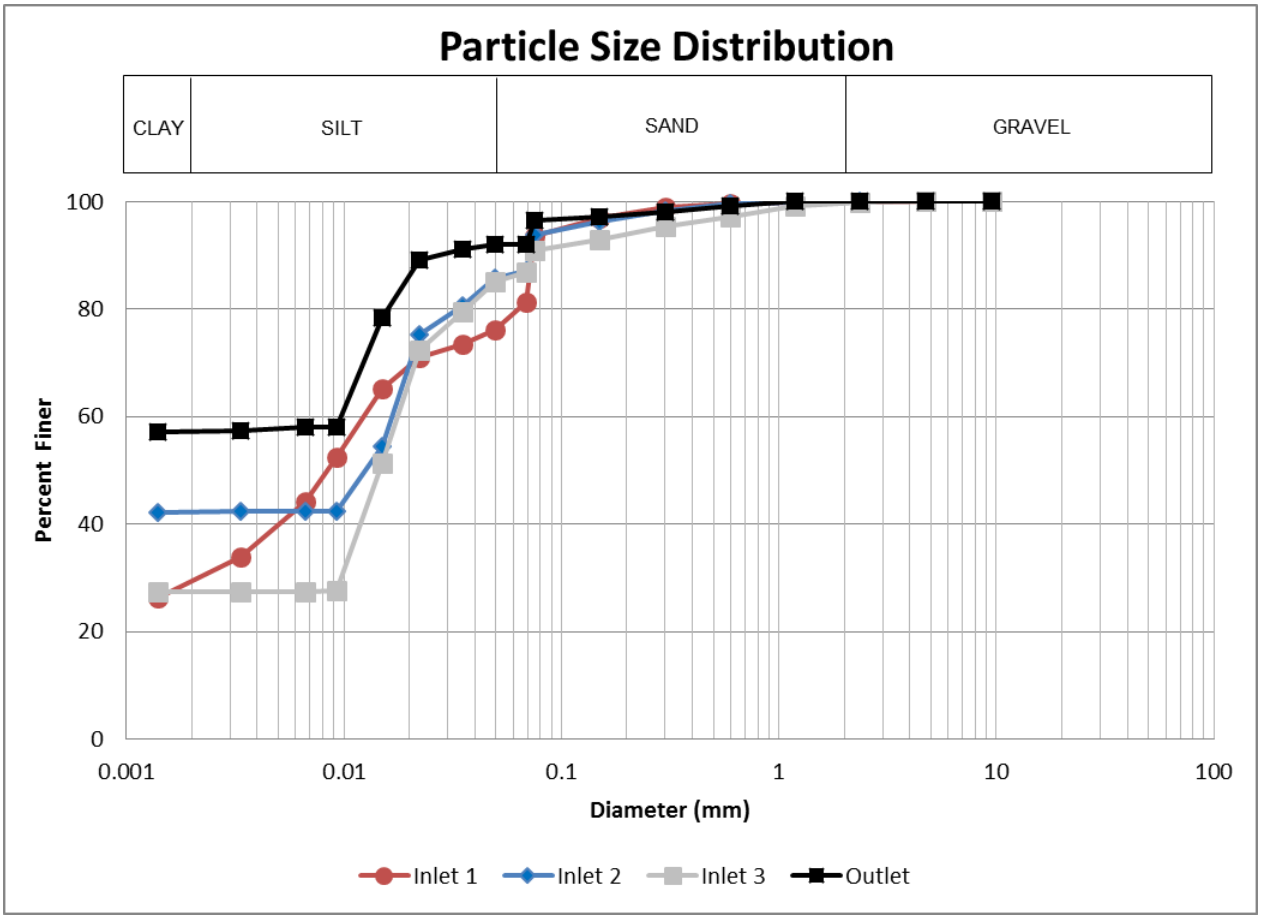

Figure 4-11. Particle size distribution of solids in the inlets and Outlet of the John Avant Park stormwater pond.

The high percentage of silt and clay entrained in inlet stormwater is similar to findings by others. Selbig *et al.* (2013) found that urban concentrations of silt for stormwater suspended solids samples were greater than sand by 44% by mass. Greb and Bannerman (1997) also found that the median particle size of solids from influent samples of a wet stormwater management pond was close to the 0.002 mm particle size range (clay size). They determined that 50.5% and 40.2% by mass of influent solids were in the clay and silt size range, respectively, and that the remainder of the solids in the samples were within the sand size range (Greb and Bannerman 1997). Others have found over several rain events that 65% to 99% of particulates by mass were finer than 0.075 mm (Kim and Sansalone 2008), which is similar to findings at the John Avant Park stormwater pond

where 90% to 93% of inflow solids were finer than 0.075 mm. Similarly, Kayhanian *et al.* (2012) found 67.4% by mass of suspended sediment in stormwater runoff was finer than 0.038 mm.

4.4 Settled Solids Investigation within the Pond

The pond sediment was also investigated as an indicator of total solids from the inlets that had settled in the pond over the years the John Avant Park pond had been in operation, as the pond had never been dredged. Sediment samples and measurements were collected at the beginning (late June) and end (late August) of the summer to observe if there was sediment redistribution occurring.

From the water depth to sediment surface measurements, it was determined that the average sediment thickness throughout the pond from the sampling events was 0.29 m for the June measurements and 0.32 m for the August measurements. Therefore, over approximately 25 years the pond has been in service, it has accumulated somewhere within the range of 25 cm to 32 cm of settled solids (approximately 1 cm/year). This accumulation of sediment per year is not uncommon in stormwater management ponds. Marsalek *et al.* (1997) collected core samples and found the equivalent sediment depths of the cores with no porosity and estimated a sediment accumulation of 2 cm/year.

Uncertainty in the estimate of sediment bed level increase is associated with the telescopic pole since when the foot of the telescopic pole is lowered into the water. It is possible that the foot either compacts the sediment, or the turbulence caused by lowering it to the sediment re-suspends fine particles in the immediate area. Further, there was uncertainty in the location of the samples and measurements between June and August. The uncertainty in the location of samples was caused from wind which would blow the inflatable zodiac and taught sampling lines (that had

markers for sampling locations) while a sample and measurement was being collected. Additionally, when the relatively heavy core sampler was lowered into the pond, it would cause the boat to move. It is therefore estimated that a sample collection and depth measurement location was within +/- 2 m of the intended location. With respect to the calculation of sediment thicknesses, the design pond depth was used instead of an as-constructed depth since it was not available. There were also uncertainties introduced, particularly for the measurements in August, due to increasing vegetation later in the summer. For example, vegetation decay or growth could have interfered with the foot of the telescopic pole. An uncertainty of +/- 10 cm is estimated for the reported sediment depths, due to the considerations noted above.

The measured sediment thicknesses at particular locations can be found in Appendix D for both the June and August, 2014 measurements. The surface elevation of the sediment was plotted using both Matlab (Delaunay triangulation) and AutoCAD Civil3D to visualize where the majority of solids were settling, as shown in Figure 4-12 and Figure 4-13 for June and Figure 4-14 and Figure 4-15 for August. The approximate locations of the inlets and Outlet are shown on each of the figures. As shown in Figure 4-12 to Figure 4-15, the expected flow path from Inlet 2 to the Outlet and Inlet 3 to the Outlet are associated with a higher measured pond bottom elevation than other areas of the pond. Assuming the pond bottom was effectively graded and levelled during construction, higher pond bottom elevations would indicate areas of increased sediment deposition. Between the June and August measurements, the areas directly in front of the Outlet and the area near Inlet 3 had slightly lower sediment surface elevations than the majority of the pond. Over the season general observations were made as to the presence and increase in vegetation later in the summer. As noted, there was always flow out of the pond through the Outlet so that sediment near the Outlet may have eroded. Backflow to Inlet 3 during high water surface

elevations or the high flow rates of water through Inlet 3 may have led to this pattern of erosion near this inlet. There were also some negative depths that were noted when compared to the design depth of the pond.

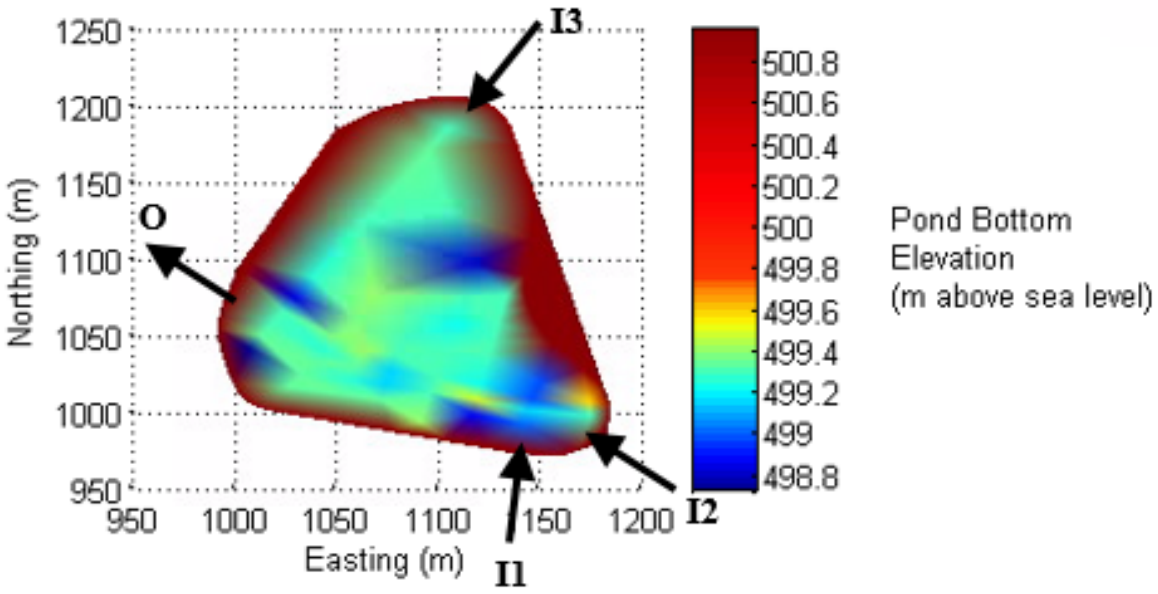

Figure 4-12. Measured in June existing pond bottom elevation, which indicates the distribution of sediment over the pond, where the design pond bottom elevation was 499.0 m.

Figure 4-13. Measured in June existing pond bottom elevation with a 20 cm contour interval, where the design pond bottom elevation was 499.0 m.

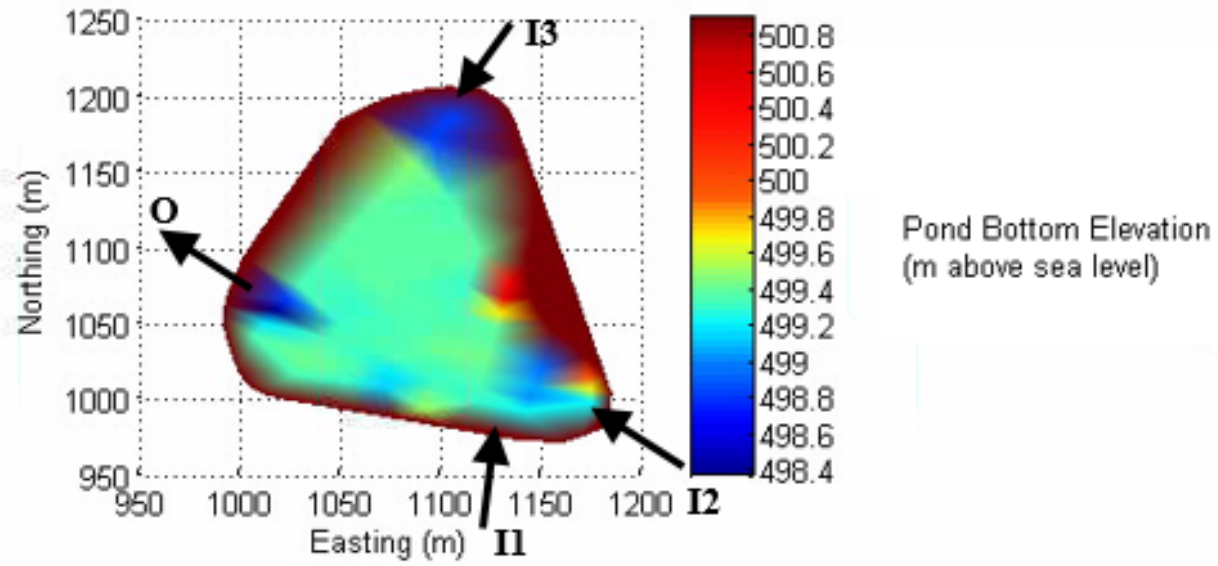

Figure 4-14. Measured in August existing pond bottom elevation, which indicates the distribution of sediment over the pond, where the design pond bottom elevation was 499.0 m.

Figure 4-15. Measured in August existing pond bottom elevations with a 20 cm contour interval, where the design pond bottom elevation was 499.0 m.

The spatial distribution of sediment particle sizes was also assessed. To visualize the particle size distribution of sediment within the pond, particle sizes were classified and plotted based on four categories: gravel (2.0 to 76.0 mm), sand (0.05 to 2.0 mm), silt (0.002 to 0.05 mm), or clay (less than 0.002 mm). The particle size spatial distribution within the pond was also compared between the June and August sampling events, as shown in Figures 4-16 to Figure 4-20. The samples of the bed material showed that the majority of sample mass was made up of sand for both the June and August measurements. The majority of solids appeared to settle in front of the inlets for both the June and August sampling events. There also appeared to be some redistribution

of sediment between June and August as seen in Figures 4-16 to Figure 4-20; however, as previously discussed, this apparent redistribution may be caused by uncertainty in measurement and sampling locations. From Figures 4-16 to Figure 4-20 there does not appear to be any apparent trend in the redistribution or mass percentages of coarser particles (gravel, sand); however, the contour intervals do show slight differences between the June and August sampling events. It is observed that core samples collected in August, generally had lower mass percentages of finer particles (clay, silt) than core samples collected in June. Perhaps during larger rain events throughout the summer months, these finer particles were resuspended or redistributed evenly throughout the pond.

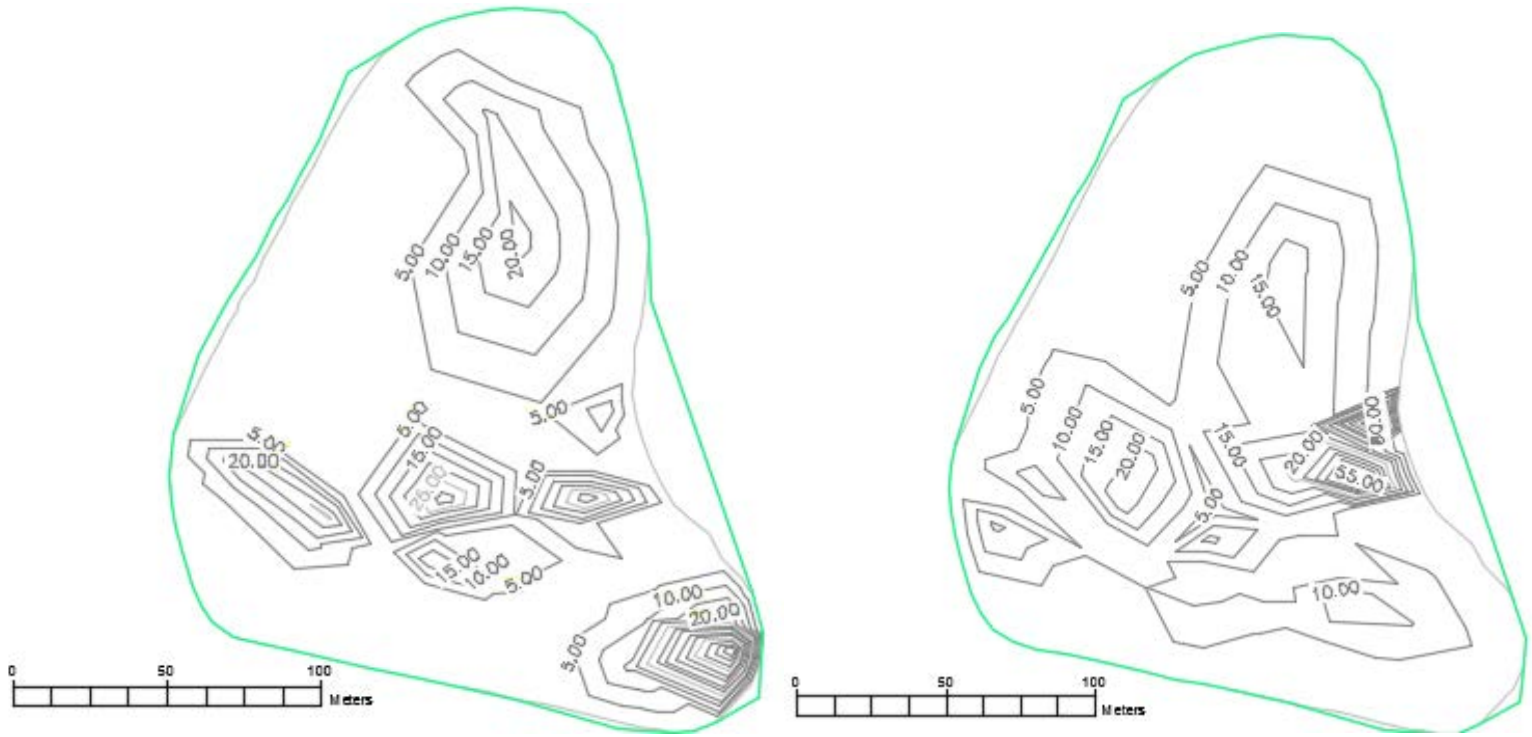

Figure 4-16. Percentage of gravel by mass throughout the pond, from June (left) and August (right) measurements (5% contour intervals)

Figure 4-17. Percentage of sand by mass throughout the pond, from June (left) and August (right) measurements (10% contour intervals)

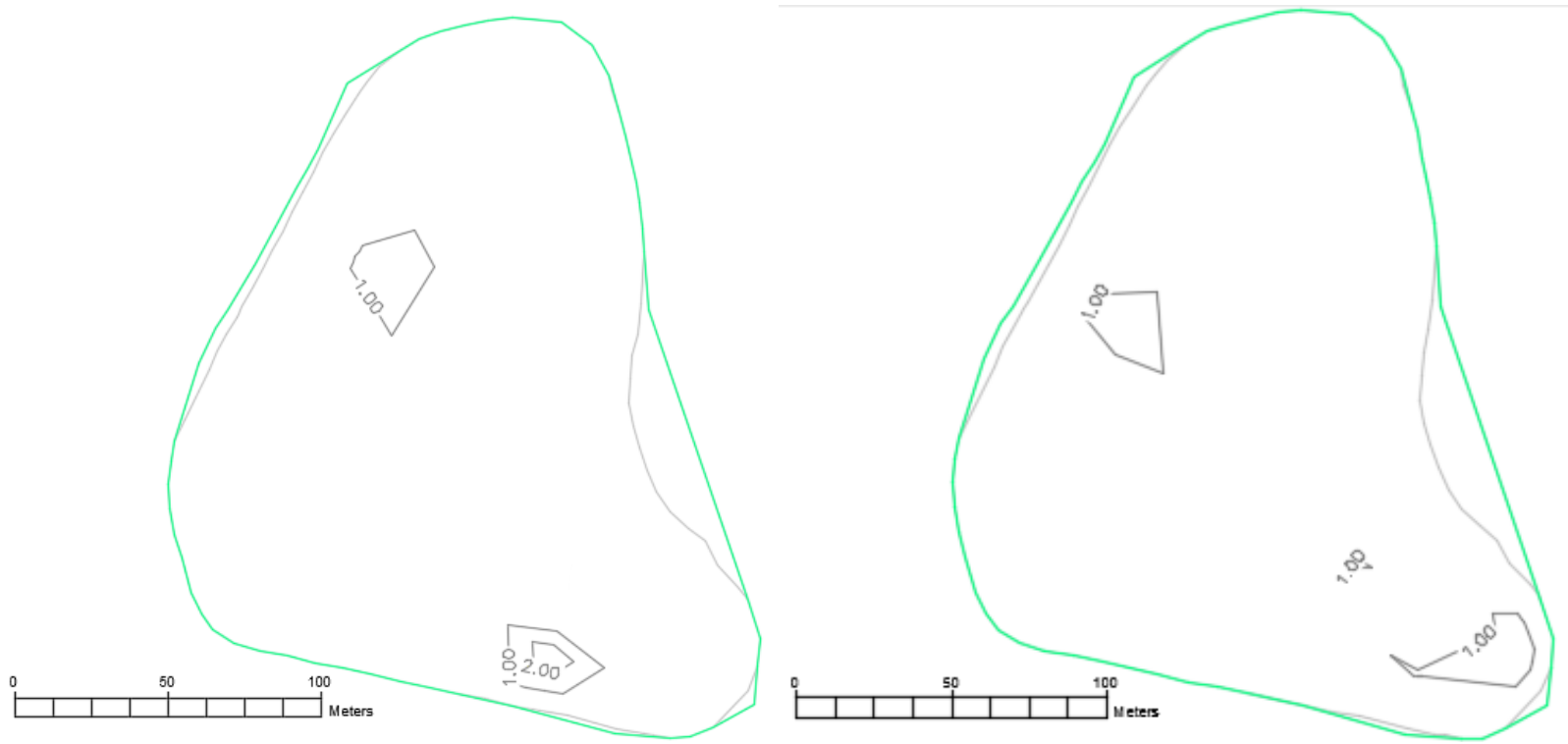

Figure 4-18. Percentage of silt by mass throughout the pond, from June (left) to August (right) measurements (1% contour interval)

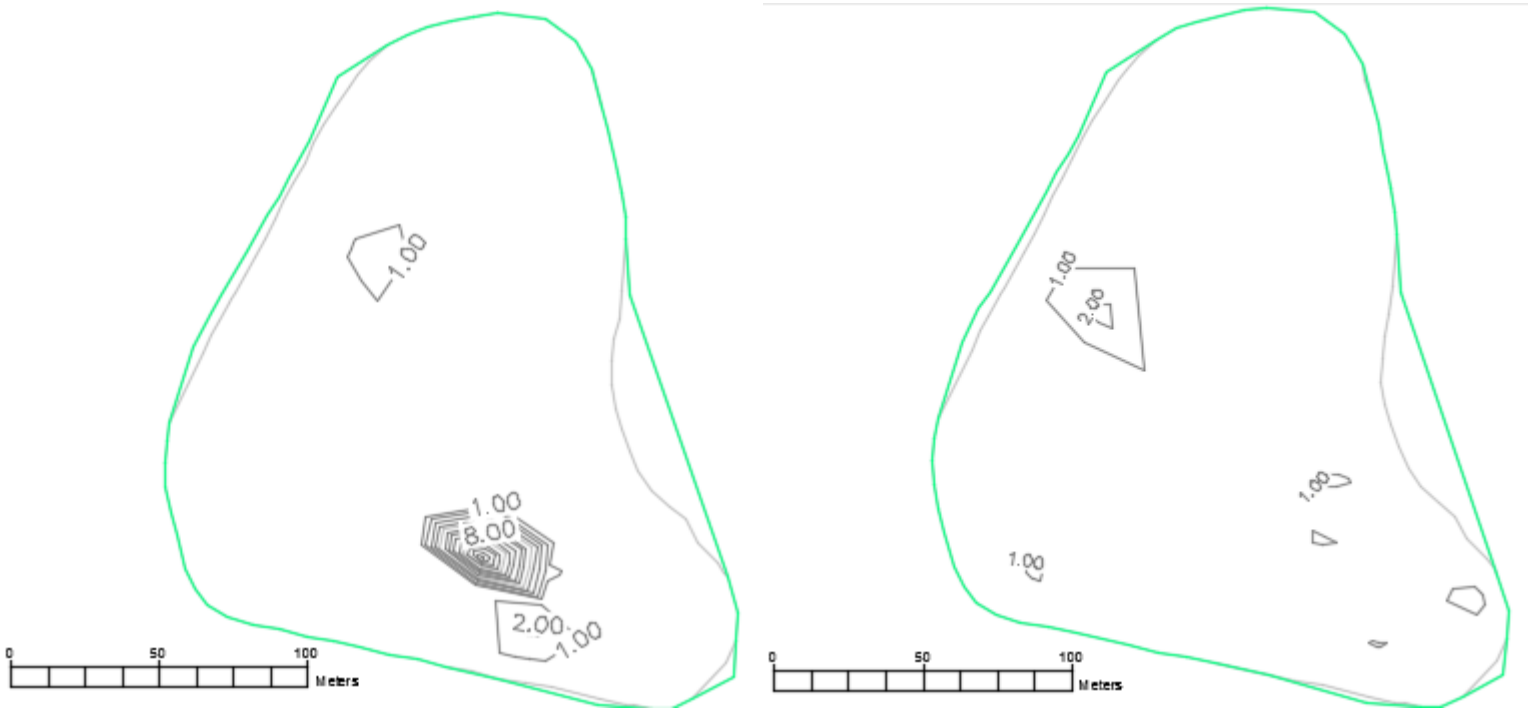

Figure 4-19. Percentage of clay by mass throughout the pond, from June (left) to August (right) measurements (1% contour intervals)

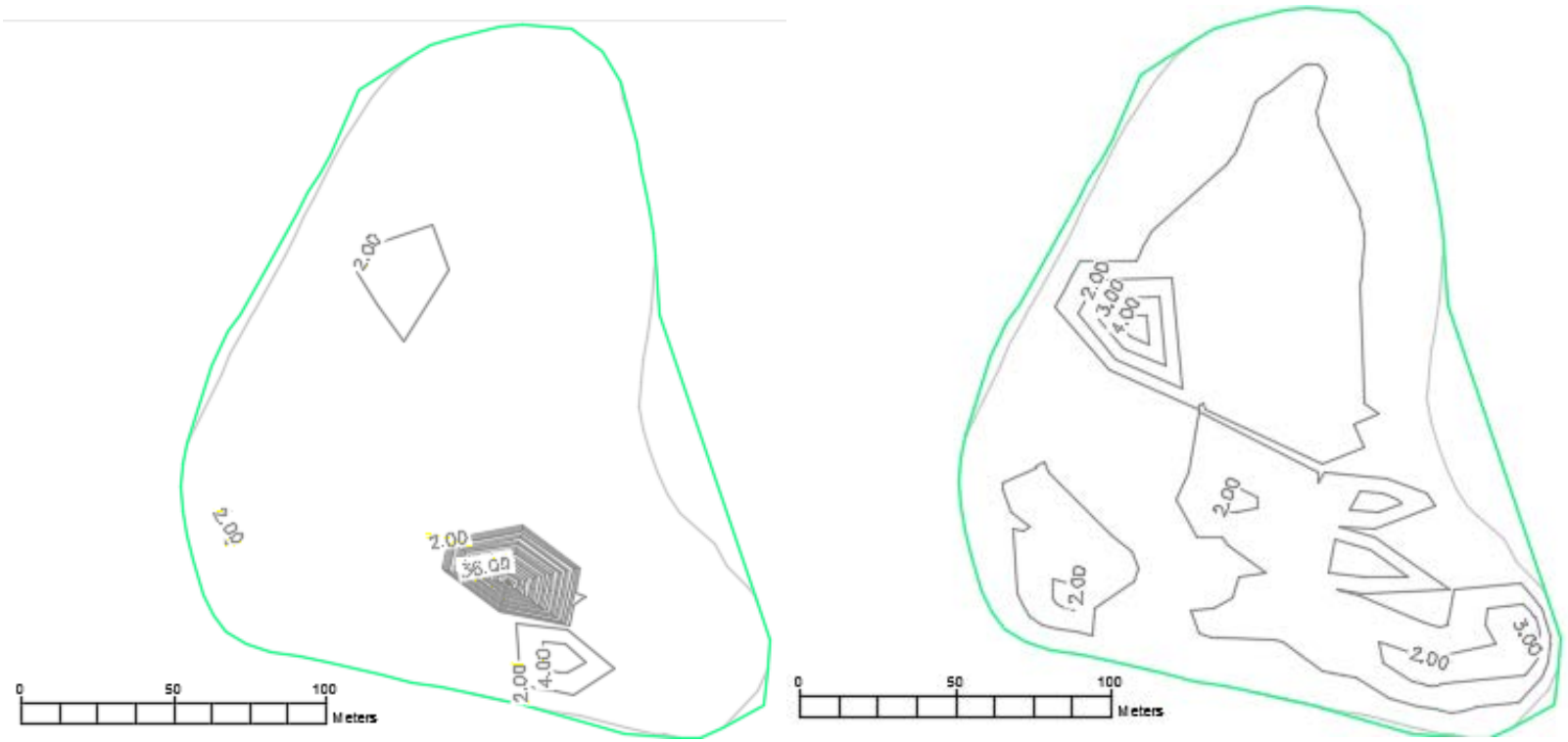

Figure 4-20. Percentage of sediment mass less than 50 microns throughout the pond, from June (left) to August (right) measurements (2% contour interval)

It is also seen in Figures 4-16 to 4-20 that there were higher percentages of sand and gravel near the inlets to the pond along what one might intuitively consider as the pathway to the Outlet. An exception would be where core samples were taken close to the edge of the pond, gravel was placed along the banks during the pond's construction. Silt and clay sized particles were distributed further away from the inlets of the pond toward the center. Marsalek *et al.* (1997) similarly found silt and clay to be more prevalent towards the center of a stormwater pond, typically accounting for approximately 95% of the sediment mass in the pond's central area (41% silt, 54% clay). Near the inlet, Marsalek *et al.* (1997) found that gravel and sand accounted for approximately 99.5% of the sample mass (70.6% sand and 29% gravel). Also, in a stormwater detention basin, Kayhanian *et al.* (2012) found that particle sizes near the inlets of a stormwater pond tended to be larger than particle sizes in the center of the basin, suggesting that larger particle sizes tend to settle out close to the inlets.

4.5 Investigation of the Flow Pattern in the Pond

The flow conditions within the John Avant Park stormwater pond were examined using a combination of concepts from LSPTV, robotic surveying using a Leica 3-dimensional prism to track a drogue, and visual observations. In total, drogue tracking took place on five separate occasions: July 17, August 20, September 3, September 19, and September 29, 2014. The major challenge with tracking the drogues in the stormwater pond was determining when there would be flow in the inlet pipes, as for each drogue tracking event, the robotic total station needed to be rented in advance and the camera equipment set up. Over the sampling season, rain events would often happen overnight or at times where the robotic total station could not be rented. This resulted in drogue tracking taking place, for the most part, when there was little flow from the inlet pipes. Ideally, the drogue tracking would have taken place under conditions of high flow from the inlet

pipes, as the higher flows should have the largest impact on the flow pattern within the stormwater pond. However, the application of LSPTV to measuring the flow field in a stormwater management pond was new, and it was felt that it was important to attempt to evaluate whether the method could be successfully used in this application.

To determine drogue flow paths and velocities using concepts from the LSPTV measurements, MathCad was used to obtain the coefficients for the collinearity formulas (Equations 3-1 and 3-2) to determine the real-world location (u,v,z) from the pixel coordinates (x,y) in the camera images. An example solution for movement of the drogues within the pond, from the September 19, 2014 drogue tracking event is shown in Figure 4-22. For this conversion, there were 11 calibration points (posts, bench legs, tree stumps, *etc.*) used in the direct linear transformation. The translated calibration points are denoted as (u0 to u10), (v0 to v10), and (z0 to z10) and their pixel image coordinates as (x0 to x10) and (y0 to y10). Matrix Q is the solution of coefficients for the collinearity formulas from top to bottom A_1, A_2, A_3, A_4, B_1, B_2, B_3, B_4, C_1, C_2, and C_3.

$$
\begin{array}{lllll}
u0 := -88.104 & v0 := 201.634 & z0 := -5.158 & x0 := -2115 & y0 := 1167 \\
u1 := -85.629 & v1 := 222.978 & z1 := -2.031 & x1 := -1875 & y1 := 1252 \\
u2 := -35.195 & v2 := 210.458 & z2 := -2.311 & x2 := -835 & y2 := 1273 \\
u3 := -29.442 & v3 := 210.981 & z3 := -2.081 & x3 := -705 & y3 := 1281 \\
u4 := 24.321 & v4 := 200.021 & z4 := -2.286 & x4 := 576 & y4 := 1294 \\
u5 := 86.869 & v5 := 202.383 & z5 := -1.762 & x5 := 2035 & y5 := 1307 \\
u6 := -1.651 & v6 := 11.880 & z6 := -5.7599 & x6 := -725 & y6 := -904 \\
u7 := 0.000 & v7 := 12.550 & z7 := -5.7599 & x7 := 0 & y7 := -838 \\
u8 := 92.972 & v8 := 188.401 & z8 := -3.042 & x8 := 2329 & y8 := 1272 \\
u9 := 60.250 & v9 := 185.330 & z9 := -4.593 & x9 := 1546 & y9 := 1233 \\
u10 := 81.788 & v10 := 191.676 & z10 := -3.278 & x10 := 2021 & y10 := 1268
\end{array}
$$

$$
M := \begin{bmatrix}
u0 & v0 & z0 & 1 & 0 & 0 & 0 & 0 & -u0 \cdot x0 & -v0 \cdot x0 & -z0 \cdot x0 \\
0 & 0 & 0 & 0 & u0 & v0 & z0 & 1 & -u0 \cdot y0 & -v0 \cdot y0 & -z0 \cdot y0 \\
u1 & v1 & z1 & 1 & 0 & 0 & 0 & 0 & -u1 \cdot x1 & -v1 \cdot x1 & -z1 \cdot x1 \\
0 & 0 & 0 & 0 & u1 & v1 & z1 & 1 & -u1 \cdot y1 & -v1 \cdot y1 & -z1 \cdot y1 \\
u2 & v2 & z2 & 1 & 0 & 0 & 0 & 0 & -u2 \cdot x2 & -v2 \cdot x2 & -z2 \cdot x2 \\
0 & 0 & 0 & 0 & u2 & v2 & z2 & 1 & -u2 \cdot y2 & -v2 \cdot y2 & -z2 \cdot y2 \\
u3 & v3 & z3 & 1 & 0 & 0 & 0 & 0 & -u3 \cdot x3 & -v3 \cdot x3 & -z3 \cdot x3 \\
0 & 0 & 0 & 0 & u3 & v3 & z3 & 1 & -u3 \cdot y3 & -v3 \cdot y3 & -z3 \cdot y3 \\
u4 & v4 & z4 & 1 & 0 & 0 & 0 & 0 & -u4 \cdot x4 & -v4 \cdot x4 & -z4 \cdot x4 \\
0 & 0 & 0 & 0 & u4 & v4 & z4 & 1 & -u4 \cdot y4 & -v4 \cdot y4 & -z4 \cdot y4 \\
u5 & v5 & z5 & 1 & 0 & 0 & 0 & 0 & -u5 \cdot x5 & -v5 \cdot x5 & -z5 \cdot x5 \\
0 & 0 & 0 & 0 & u5 & v5 & z5 & 1 & -u5 \cdot y5 & -v5 \cdot y5 & -z5 \cdot y5 \\
u6 & v6 & z6 & 1 & 0 & 0 & 0 & 0 & -u6 \cdot x6 & -v6 \cdot x6 & -z6 \cdot x6 \\
0 & 0 & 0 & 0 & u6 & v6 & z6 & 1 & -u6 \cdot y6 & -v6 \cdot y6 & -z6 \cdot y6 \\
u7 & v7 & z7 & 1 & 0 & 0 & 0 & 0 & -u7 \cdot x7 & -v7 \cdot x7 & -z7 \cdot x7 \\
0 & 0 & 0 & 0 & u7 & v7 & z7 & 1 & -u7 \cdot y7 & -v7 \cdot y7 & -z7 \cdot y7 \\
u8 & v8 & z8 & 1 & 0 & 0 & 0 & 0 & -u8 \cdot x8 & -v8 \cdot x8 & -z8 \cdot x8 \\
0 & 0 & 0 & 0 & u8 & v8 & z8 & 1 & -u8 \cdot y8 & -v8 \cdot y8 & -z8 \cdot y8 \\
u9 & v9 & z9 & 1 & 0 & 0 & 0 & 0 & -u9 \cdot x9 & -v9 \cdot x9 & -z9 \cdot x9 \\
0 & 0 & 0 & 0 & u9 & v9 & z9 & 1 & -u9 \cdot y9 & -v9 \cdot y9 & -z9 \cdot y9 \\
u10 & v10 & z10 & 1 & 0 & 0 & 0 & 0 & -u10 \cdot x10 & -v10 \cdot x10 & -z10 \cdot x10 \\
0 & 0 & 0 & 0 & u10 & v10 & z10 & 1 & -u10 \cdot y10 & -v10 \cdot y10 & -z10 \cdot y10
\end{bmatrix}
\qquad
XY := \begin{bmatrix}
x0 \\ y0 \\ x1 \\ y1 \\ x2 \\ y2 \\ x3 \\ y3 \\ x4 \\ y4 \\ x5 \\ y5 \\ x6 \\ y6 \\ x7 \\ y7 \\ x8 \\ y8 \\ x9 \\ y9 \\ x10 \\ y10
\end{bmatrix}
$$

$$
M^{\mathrm{T}} = \begin{bmatrix}
-88.104 & 0 & -85.629 & 0 & -35.195 & 0 & -29.442 & 0 & 24.321 & 0 & 86.869 & 0 \\
201.634 & 0 & 222.978 & 0 & 210.458 & 0 & 210.981 & 0 & 200.021 & 0 & 202.383 & 0 \\
-5.158 & 0 & -2.031 & 0 & -2.311 & 0 & -2.081 & 0 & -2.286 & 0 & -1.762 & 0 \\
1 & 0 & 1 & 0 & 1 & 0 & 1 & 0 & 1 & 0 & 1 & 0 \\
0 & -88.104 & 0 & -85.629 & 0 & -35.195 & 0 & -29.442 & 0 & 24.321 & 0 & 86.869 \\
0 & 201.634 & 0 & 222.978 & 0 & 210.458 & 0 & 210.981 & 0 & 200.021 & 0 & 202.383 \\
0 & -5.158 & 0 & -2.031 & 0 & -2.311 & 0 & -2.081 & 0 & -2.286 & 0 & -1.762 \\
0 & 1 & 0 & 1 & 0 & 1 & 0 & 1 & 0 & 1 & 0 & 1 \\
-1.863 \cdot 10^5 & 1.028 \cdot 10^5 & -1.606 \cdot 10^5 & 1.072 \cdot 10^5 & -2.939 \cdot 10^4 & 4.48 \cdot 10^4 & -2.076 \cdot 10^4 & 3.772 \cdot 10^4 & -1.401 \cdot 10^4 & -3.147 \cdot 10^4 & -1.768 \cdot 10^5 & -1.135 \cdot 10^5 \\
4.265 \cdot 10^5 & -2.353 \cdot 10^5 & 4.181 \cdot 10^5 & -2.792 \cdot 10^5 & 1.757 \cdot 10^5 & -2.679 \cdot 10^5 & 1.487 \cdot 10^5 & -2.703 \cdot 10^5 & -1.152 \cdot 10^5 & -2.588 \cdot 10^5 & -4.118 \cdot 10^5 & -2.645 \cdot 10^5 \\
-1.091 \cdot 10^4 & 6.019 \cdot 10^3 & -3.808 \cdot 10^3 & 2.543 \cdot 10^3 & -1.93 \cdot 10^3 & 2.942 \cdot 10^3 & -1.467 \cdot 10^3 & 2.666 \cdot 10^3 & 1.317 \cdot 10^3 & 2.958 \cdot 10^3 & 3.586 \cdot 10^3 & 2.303 \cdot 10^3
\end{bmatrix} \ldots
$$

$$
x := \left(M^{\mathrm{T}} \cdot M\right)^{-1}
$$

$$
Q := x \cdot M^{\mathrm{T}} \cdot XY \qquad Q = \begin{bmatrix}
-67.536 \\ 1.256 \\ -0.362 \\ -233.467 \\ -1.177 \\ -16.05 \\ -47.15 \\ -457.096 \\ -0.001 \\ -0.018 \\ 0.06
\end{bmatrix}
$$

Figure 4-21. MathCad example of finding collinearity equation camera calibration coefficients, shown as matrix (Q), from the September 19, 2014 drogue tracking session.

Once the calibration coefficients were found, Goal seek in Excel was used by equating the two collinearity equations to determine *z* (height) as shown in Table 4-4. An example solution where the solved collinearity formula coefficients were used to calculate the corresponding real-world coordinates (u, v, z) of the pixel coordinates (x, y) for surveyed points is shown in Table 4-4. As shown in Table 4-4, typically once the calibration coefficients were solved for, there was a difference ranging from 0.0 m to 7.1 m between the calculated (u) and (v) and the real-world surveyed (u) and (v). When the calibration coefficients were then used to determine the location of the tracking drogue for comparison with surveying by the 3D robotic total station, the calculated location of the tracking drogue was often outside of the perimeter of the pond indicating that the accuracy of the collinearity equation solution was insufficient.

Table 4-4. Using collinearity equation calibration coefficients to back calculate calibration points to test the accuracy of the method.

n	X (pixel)	x (pixel)	Y (pixel)	y (pixel)	u (meters)	v (meters)	z (meters)	v difference	u difference
0	885	-2115	833	1167	-88.104	201.634	-5.158	5.0	-3.3
1	1125	-1875	748	1252	-85.629	222.978	-2.031	4.0	-0.2
2	2165	-835	727	1273	-35.195	210.458	-2.311	0.8	-0.2
3	2295	-705	719	1281	-29.442	210.981	-2.081	0.9	-0.4
4	3576	576	706	1294	24.321	200.021	-2.286	1.8	-0.2
5	5035	2035	693	1307	86.869	202.383	-1.762	1.7	0.0
6	2275	-725	2904	-904	-1.651	11.880	-5.7599	0.6	3.1
7	3000	0	2838	-838	0.000	12.550	-5.7599	-0.7	-3.2
8	5329	2329	728	1272	92.972	188.401	-3.042	7.1	3.9
9	4546	1546	767	1233	60.250	185.330	-4.593	-1.9	0.2
10	5021	2021	732	1268	81.788	191.676	-3.278	1.5	1.0

It is believed the reason for this lack of accuracy may have been due to the locations of the selected calibration points. The camera was set up overlooking the pond, with no stationary calibration points in near-view. Nearly all of the calibration points used were on the other side of the pond where there were many stationary calibration points (posts, trees, lights, *etc.*) as shown in Figure 4-22. Not having calibration points nearer to the camera may have not given enough spatial information related to elevation for the assessment of the collinearity coefficients. Although others have used calibration points in field applications that were on the other side of the camera from the water, the locations were well-distributed throughout the image, as the water body was typically smaller, with calibration points staked on both sides of the water's edge (Daigle *et al.*, 2013). After it was discovered that more calibration points near the camera were needed, the real-world location (x, y, z) of one calibration point (scum on gravel) near the camera was approximated after-the-fact, but it did not appear to improve the results as there was only the one extra point. Therefore, other calibration points within this area were estimated for their x, y, z coordinates, but the estimations did not reduce uncertainty in the drogue position enough to be reliable. It was therefore concluded that LSPTV might be used for tracking drogues to determine flow patterns in stormwater management ponds, but camera imagery must have known control points (known coordinates) throughout the image in order to have reliable results. For example, future work using camera imagery could use surveyed colorful posts installed throughout the pond as calibration points. Note however that the John Avant Park stormwater pond is used recreationally by the public for kayaking, canoeing, boating lessons, dog swimming, and playing with remote controlled watercraft, so posts in ponds with extensive recreational use could be problematic.

Figure 4-22. Example of a photo from the camera set up for LSPTV during the September 19, 2014 drogue tracking event.

Despite not being able to collect accurate velocity data from drogue tracking, the camera imagery collected during drogue tracking, intended for LSPTV, was useful for observing flow patterns as indicated by drogue movement. These visual observations were used in conjunction with the survey data from surveying the tracking drogue with the robotic total station to assess flow patterns within the pond. For the five drogue tracking events over the summer using the robotic total station, there were two drogue tracking events with sufficient camera imagery and survey data (September 3 and September 19) that could be used to determine both the flow path and velocity of the drogues. The setup of the robotic total station during the July and August drogue tracking events were not referenced properly to effectively orient the measurements within the pond. The tracking drogue speeds and general direction for the improperly referenced events could,

however, be determined based on the difference between the surveyed points and the photography for LSPTV.

It should be noted that for the July 17, 2014 event, the Leica 3-dimensional prism and robotic total station was rented for the day as precipitation was forecasted to begin in early morning. However, precipitation on that day did not start until late evening (closest rain event to this drogue tracking session was on July 10, 2014). Although there was no precipitation logged by the tipping bucket rain gauge during the time of drogue tracking, there was a small flow in the inlet and Outlet pipes, as shown in Table 4-5. For the July 17, 2014 drogue tracking event, the wind speed ranged from 2.8 to 3.1 m/s in the northwesterly to westerly direction. The average drogue speed during the first tracking event was 0.009 m/s; however, the drogue seemed to be stuck in place during this time. Once the drogue was moved to a different location the velocity was closer to 0.034 m/s and in the northwest direction as observed in the field and through camera imagery comparisons, similar to the wind direction.

Table 4-5. Tracking drogue velocity, inlet flows, and Outlet flow for the July 17, 2014 drogue tracking event.

July 17 Drogue Tracking Event	Track 1 (15:42 to 16:03)	Track 2 (16:06 to 16:11)
Average Drogue Velocity	0.009 m/s	0.034 m/s
Average I1 flow rate	0.000 m^3/s	0.000 m^3/s
Average I2 flow rate	0.005 m^3/s	0.004 m^3/s
Average I3 flow rate	0.004 m^3/s	0.000 m^3/s
Average Outlet flow rate	0.014 m^3/s	0.015 m^3/s

For the August 20, 2014 drogue tracking event, there had been approximately 9 mm of rainfall in the early morning hours, ending at 4:00. Therefore, flow was expected in the inlet and Outlet pipes and was indeed observed during drogue tracking as shown in Table 4-6. As observed

from camera imagery, the direction of the tracking drogue was to the southeast direction. The wind direction was also towards the southeast with gusts ranging from 0.6 m/s to 2.0 m/s. Therefore, it appeared that the drogue followed the wind direction with a velocity of 0.019 m/s for the first drogue track, and 0.036 m/s for the second drogue track, thought to be due to changes in wind speed.

Table 4-6. Tracking drogue velocity, inlet flows, and Outlet flow for the August 20, 2014 drogue tracking event.

August 20 Drogue Tracking Event	Track 1 (13:35 to 13:46)	Track 2 (13:55 to 13:58)
Average Drogue Velocity	0.019 m/s	0.036 m/s
Average I1 flow rate	0.000 m^3/s	0.000 m^3/s
Average I2 flow rate	0.003 m^3/s	0.003 m^3/s
Average I3 flow rate	0.047 m^3/s	0.036 m^3/s
Average Outlet flow rate	0.043 m^3/s	0.043 m^3/s

For the September 3 drogue tracking event, the instantaneous wind direction was easterly to northeasterly with gusts ranging from 1.1 to 2.7 m/s. As shown in Figure 4-23, the tracking drogue generally followed the direction of the wind during the three different times it was tracked. For the three different drogue tracking periods during the September 3 test, drogues were placed at different starting locations within the pond. These locations were chosen based on where there was likely to be no interference from weeds. The different color lines within the pond (Figure 4-23) show the movement of the drogues with the associated drogue tracking times, velocity, and flow through the inlets and Outlet which are given in Table 4-7. For this drogue tracking event it was expected that there would be flow in the inlet pipes, as there was precipitation in the late hours of September 2, 2014 and early hours of September 3, 2014. However, as shown in Table 4-7 this

rain event was not sufficient to produce flow in the pipes at the time the drogue tracking was performed. During this time the data logger for the Inlet 1 sampler was not functioning, and the Inlet 3 sampler had a dead battery. Based on the flow data from the most reliable sampler (Inlet 2 sampler), however, it is likely there was not flow in either of those pipes as well. Furthermore, the flow through the Outlet during this time was very low at 0.005 m^3/s. With these low flows from the inlet pipes to the Outlet pipe, the flow pattern within the pond was generally dominated by wind, with drogue velocities ranging from 0.024 m/s to 0.036 m/s.

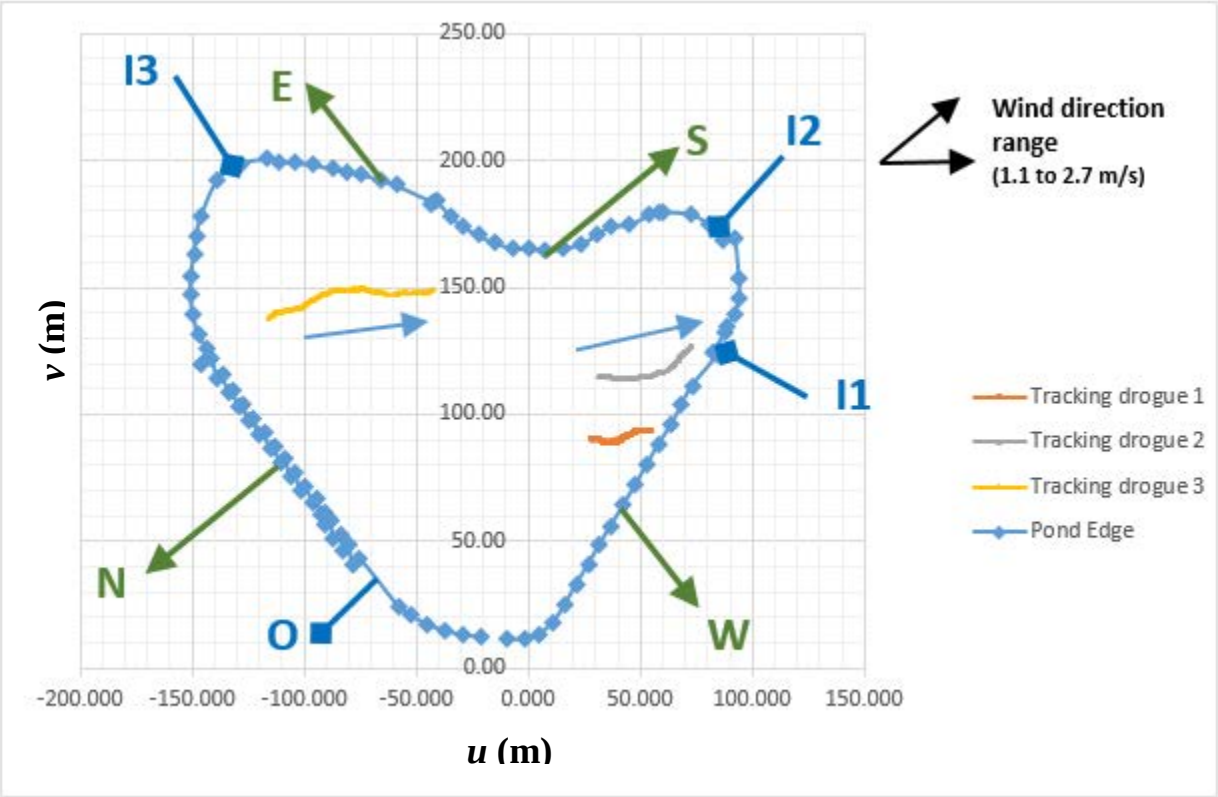

Figure 4-23. September 3, 2014 drogue tracking using the robotic total station and the 3D prism, where arrows near the drogue flow paths indicate direction of drogue movement, and the arrows N, E, S, W indicate north, east, south, and west directions.

Table 4-7. Drogue velocity as well as the inlet and Outlet flows for the September 3, 2014 drogue tracking event.

September 3 Drogue Tracking Event	Track 1 (15:04 to 15:25)	Track 2 (15:27 to 15:51)	Track 3 (15:60 to 16:39)
Average Drogue Velocity	0.024 m/s	0.034 m/s	0.036 m/s
Average I1 flow rate	Not available	Not available	Not available
Average I2 flow rate	0.000 m^3/s	0.000 m^3/s	0.000 m^3/s
Average I3 flow rate	Not available	Not Available	Not Available
Average Outlet flow rate	0.005 m^3/s	0.005 m^3/s	0.005 m^3/s

For the September 19, 2014 drogue tracking event, weeds were predominant within the pond and it was difficult to find a location near Inlet 1 and Inlet 2 that would be suitable for drogue tracking that would not be interfered with by weeds. Therefore, drogue tracking primarily took place in the area between Inlet 3 and the Outlet. For this drogue tracking event, there had not been any rainfall for 6 days, so flow in the inlet pipes was not necessarily expected. There was, however, one instance of flow during the tracking period in Inlet 3. Since there was no rainfall during this time it is undetermined what may have caused this small amount of flow; however, Inlet 3 was always completely submerged and there was signs of muskrats noted during the installation. It is possible that an animal swimming in the pipe may have led to this reading. It is also possible that periodic flushing of fire hydrants or residential sump pumps could have led to this reading as this water would discharge to a storm sewer. The wind direction on September 19, 2014 ranged from 0 to 1.5 m/s in the easterly to southeasterly direction, and the tracking drogue velocity ranged from 0.024 m/s to 0.029 m/s as shown in Figure 4-24 and given in Table 4-8.

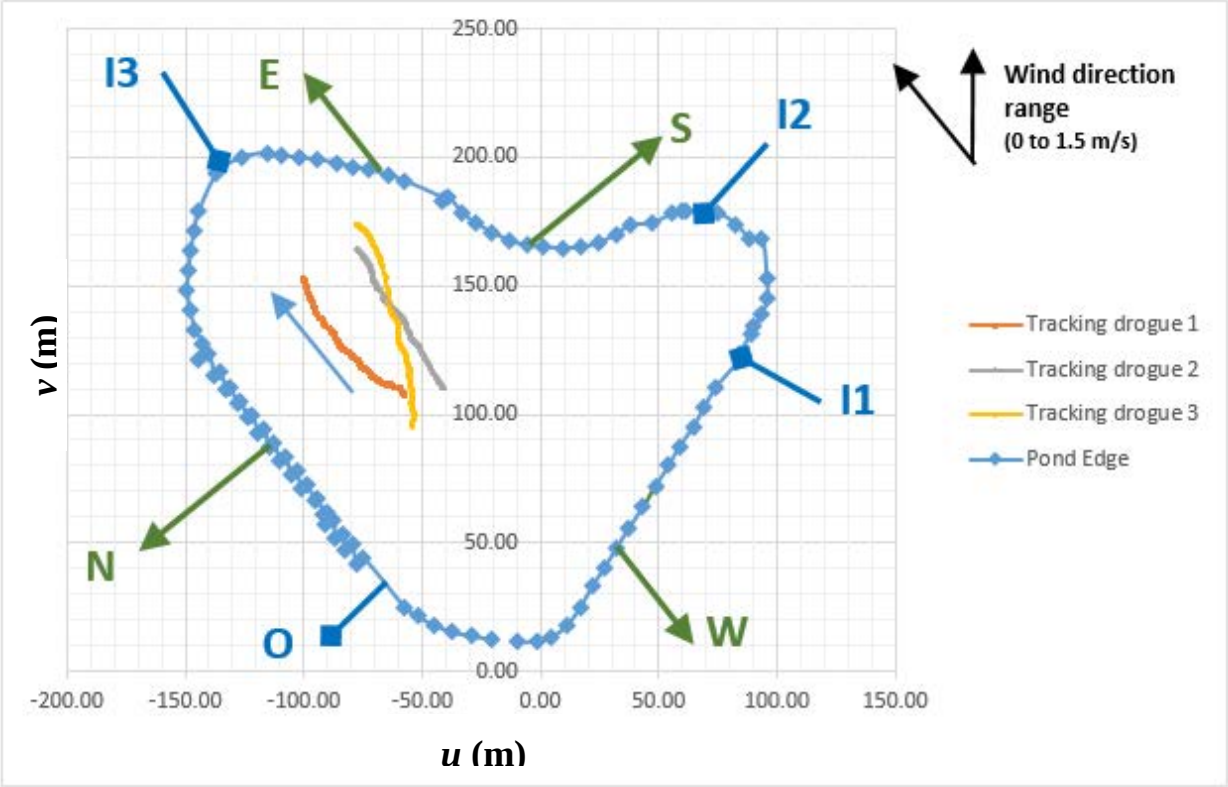

Figure 4-24. September 19th drogue tracking using the robotic total station and the 3D prism, where arrows near the drogue flow paths indicate direction of drogue movement, and the arrows N, E, S, W indicate the north, east, south, and west directions.

Table 4-8. Drogue velocity as well as the inlet and Outlet flows for the September 19, 2014 drogue tracking event.

September 19 Drogue Tracking Event	Track 1 (13:02 to 13:47)	Track 2 (13:50 to 14:37)	Track 3 (14:47 to 15:34)
Average Drogue Velocity	0.024 m/s	0.024 m/s	0.029 m/s
Average I1 flow rate	0.000 m^3/s	0.000 m^3/s	0.000 m^3/s
Average I2 flow rate	0.000 m^3/s	0.000 m^3/s	0.000 m^3/s
Average I3 flow rate	0.000 m^3/s	0.002 m^3/s	0.000 m^3/s
Average Outlet flow rate	0.000 m^3/s	0.000 m^3/s	0.000 m^3/s

For the September 29, 2014 drogue tracking event there was very little movement of the drogues. The little movement was likely a result of low wind speeds and a predominant presence of weeds in the pond. There had also not been precipitation for a couple of weeks so there was no flow in any of the inlet pipes or the Outlet. The only drogue tracking event that was successful that afternoon resulted in a drogue velocity of 0.015 m/s towards the north. During this time the wind was in the southeasterly to easterly direction and the wind speed was 0 to 1.5 m/s. Therefore, the wind did not appear to play a major role in drogue movement. It is possible though that weeds in the area influenced the flow path of the drogues.

Based on the data obtained from the camera images and surveying using the 3-dimensional prism and robotic total station, the flow in the pond was found to be primarily wind dominated in low to zero inflow conditions. The wind on the pond surface generates waves and a surface current, contributing to flow at the depth of the fins. However, it could be questioned whether or not the drogue movement was due to flow patterns generated by the wind, or the wind moving the drogue's float and consequentially the drogue. To assess whether the drogue was moving with the flow in the pond or if its movement was driven by wind, the drag on the drogue's float was compared to the drag on the drogue's fins (from the current).

To investigate the forces on the drogue, the drogue and float dimensions (previously discussed in Chapter 3) were considered. The drogue fin is 0.4 m high and 0.3 m in diameter, where the fin is connected to the drogue float (15.93 cm diameter ball) by a line (string) of varying lengths for free movement and to submerge the drogue fin at the desired depth. In experiments, the float was observed to be floating with half of the ball submerged due to the weight of the fins. The forces on the drogue, as suggested in Krauss *et al.* (1989), are shown in Figure 4-25. In Figure 4-25, the wind velocity at the elevation of the float is shown as *W*, the water velocity at surface

(due to wind) is shown as U_s, the water velocity at fin depth is shown as U_f, the drag force on the unsubmerged top-half of the float (caused by wind flow over the ball) is shown as F_{bu}, the drag force on the submerged bottom-half of the float is shown as F_{bs}, the drag force on the line connecting the float and the fin is shown as *Fs* and is considered negligible, and the drag force on the fin is shown as F_f.

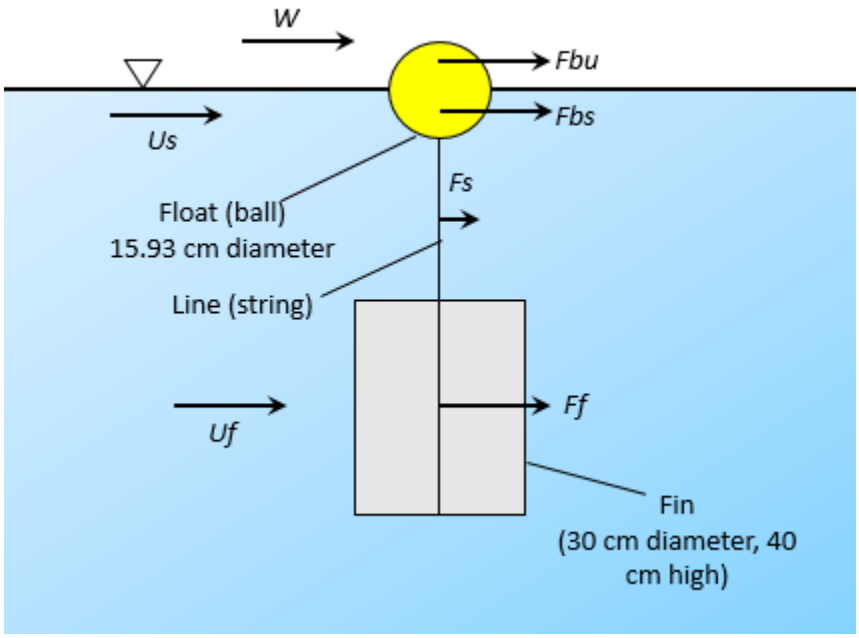

Figure 4-25. Definition of forces on the drogue.

To quantify the relative forces on the drogue, it is first assumed that drogue movement is caused by the force of drag on the fin, and that the drogue is moving at the same velocity as the water (U_f). The drag force on the fin, F_f would then be calculated using the formula for drag on a blunt body (Douglas *et al.* 2005):

$$F_f = \frac{1}{2} C_d \rho {U_f}^2 A \qquad [4\text{-}12]$$

where C_d is the dimensionless drag coefficient of the fin, ρ is the water density (taken as 999.7 kg/m^3 assuming a water temperature of 10°C (Potter *et al.* 2017)), and *A* is the projected area of

the fin to the oncoming flow (diameter x height = 0.12 m^2). Vachon (1973) experimentally determined C_d for a similar drogue fin which consisted of 2 plastic vanes (approximately 25 cm diameter x 25 cm high) on a pendulous string at a steady velocity. In these experiments it was determined that C_d ranged from 1.19 to 1.77 (1.51 average).

The August 20, 2014 drogue tracking event was used as it was considered representative of velocity measurements, where drogue movement was observed to be in the same direction as the wind. For this tracking event, the drogue velocity was U_f = 0.036 m/s with a maximum wind measurement approximately 2 m above the water surface of 2.0 m/s. For this drogue tracking event it was estimated that the drag force on the fin was 0.117 N, given in Table 4-9.

To estimate the drag forces from wind on the unsubmerged top-half of the float, the wind velocity measurement taken at the height of approximately 2 m above the water surface was converted to a wind velocity measurement at the water's surface. The log-law wind velocity profile was used assuming neutral atmospheric stability (Oke 1997):

$$u = \frac{u_*}{\kappa} ln\left(\frac{z}{z_o}\right) \qquad [4\text{-}13]$$

where u is the (time-averaged velocity) above the water surface at elevation z, the shear velocity is u_*, the Von Karman's constant is κ (κ = 0.4), and the roughness height due to waves is z_o. The shear velocity was determined through its relationship with shear stress (τ) on the water-air interface from:

$$\tau = \rho_{air} {u_*}^2 \qquad [4\text{-}14]$$

where ρ_{air} is the air density (kg/m^3). The shear stress was estimated from wind velocity at a 10 m elevation above the water surface (W_{10}) from:

$$\tau = \rho_{air} C_{aw} {W_{10}}^2 \quad [4\text{-}15]$$

where C_{aw} is the drag coefficient (C_{aw} = 0.00166 according to Lick (2008)). The iterative solver (goal seek) in Microsoft Excel was used to solve equations 4-14 and 4-15 simultaneously. It was calculated that z_o = 0.000079 m and u_* = 0.079 m/s. This roughness is outside of what would be expected for a relatively smooth water surface (Hansen 1993). Therefore, the viscous formula for the log-law was assumed (due to its assumption of a smooth boundary) using Garratt (1992) as an alternative:

$$z_o = 0.1\nu/u_* \quad [4\text{-}16]$$

where ν is the kinematic viscosity of the wind (air) (ν = 1.51 x10^{-5} m^2/s). Using Equation 4-13 and Equation 4-16 the shear velocity was recalculated assuming an ambient air temperature of 20°C for the kinematic viscosity, which gave u_* = 0.07 m/s. The wind velocity at the mid height ($z \approx 4$ cm) of the unsubmerged portion of the float was then calculated to be W = 1.32 m/s. Since the wind velocity at the elevation of the float was determined, the wind drag on the top half of the float (F_{bu}) could then be determined from:

$$F_{bu} = \frac{1}{2}\rho_{air} C_{dbu}\left(W - U_f\right)^2 A_{bu} \quad [4\text{-}17]$$

where ρ_{air} is the density of air at 20°C and atmospheric pressure and ρ_{air} = 1.204 kg/m^3, C_{dbu} is the drag coefficient on the top-half of the float, and A_{bu} is the projected area of the top half of the float (A_{bu} = 9.97x10^{-3} m^2). It was assumed that the drag coefficient for the top half unsubmerged portion of the float is the same as a hemisphere attached to a rigid boundary. The drag coefficient typically depends on the Reynolds number ($R = Wd/\nu$), where d is the diameter of the float. However, for a hemisphere attached to a rigid boundary, Nishida *et al.* (1994) found the drag coefficient was somewhat insensitive to the Reynolds number, and was approximately 0.5. Using C_{dbu} the wind

drag force on the unsubmerged top-half of the drogue's float was estimated to be F_{bu} = 0.0049 N, as given in Table 4-9.

The water current as a result of wind must be first determined to estimate the drag on the submerged bottom-half of the drogue's float. For lakes, the ratio of the surface water velocity to the shear velocity due to wind (U_s/u_*) is 12.5 (Hendersen-Sellers 1988). For the August 20, 2014 drogue tracking event (where u_* = 0.070 m/s) this gives a value of U_s = 0.88 m/s. The drag on the submerged bottom-half of the float can then be calculated from:

$$F_{bs} = \frac{1}{2}\rho C_{dbs}\left(U_s - U_f\right)^2 A_{bd} \qquad [4\text{-}18]$$

where C_{dbs} is the drag coefficient and A_{bd} is the projected area for the bottom-half of the float. Both are considered equal to the values of the unsubmerged part of the float to give F_{bs} = 1.8 N. This force is larger than the drag force on the drogue's fin (F_f = 0.117 N) and the wind drag force on the unsubmerged portion of the float (F_{bu} = 0.0049 N). If drogue movement was in fact due to the surface velocity caused by wind, the drogue would have been expected to move closer to a velocity of 0.88 m/s instead of the actual observed drogue velocity of 0.036 m/s. Alternatively, Hendersen-Sellers (1988) suggested that a typical good estimate of water surface velocity is 1.5% of the wind velocity. They did not indicate the elevation used to determine wind velocity, but typically an elevation of 10 m above the water surface is used such that $U_s = 0.015W_{10}$). Using Equations 4-13 and 4-15, W_{10} = 2.28 m/s. As a result the water surface velocity (U_s) is estimated to be 0.034 m/s. The drag on the submerged bottom-half of the float is then estimated to be F_{bu} = 0.00001 N. Due to the high variability in the two methods of calculating the water surface velocity, a third alternative method was used. Smith (1979) suggested the following applies for wind velocities less than 4 m/s:

$$\frac{U_S}{W_{10}} = \frac{6.91}{{W_{10}}^{0.56}}\% \qquad [4\text{-}19]$$

which gives a surface water velocity of U_s = 0.099 m/s and a drag force on the submerged bottom-half of the float of F_{bu} = 0.01 N.

Table 4-9. Summary of forces on the drogue.

Force	Value
Drag force on fin (F_f)	0.117 N
Drag force on unsubmerged portion of float (F_{bu})	0.0049 N
Drag force on submerged portion of float (F_{bs})	0.00001 N to 1.8 N range depending on calculation method

As given in Table 4-9, the wind force on the unsubmerged top-half of the drogue float was less than forces associated with the submerged portions of the drogue, such that it would have had very little of an effect on the drogue's movement. The high variability in the water surface velocity (the surface current) suggests that at the higher magnitude, the surface velocity due to wind could have influenced drogue movement. However, the observed drogue velocities were not consistent with the larger calculated water surface velocity, suggesting that it was more than likely the drag force on the drogue's fin that was responsible for drogue movement.

Others have also found the flow pattern in stormwater ponds to be largely influenced by wind direction. Using drogue tracking and current-metering traverses in an oblong stormwater pond Anderson *et al.* (2013) found a circulation pattern to be predominant in the pond, the orientation of which was dependent on the wind direction. They noted that, due to the wind's

influence on pond flow, the residence time was reduced when compared to modelled non-wind conditions (Anderson *et al.* 2013).

It should be noted when considering the observations of the flow patterns in the pond that the flows recorded in the inlet pipes during each period of drogue tracking were not close to the maximum flows recorded during the sampling season of 0.157 m^3/s for Inlet 1, 0.612 m^3/s for Inlet 2, and 3.342 m^3/s for Inlet 3. Therefore, it is possible at the maximum flows that the flow pattern in the pond may have been more strongly influenced by the inflows than the wind. Drogue data was not obtained during high flow conditions as in the summer months in Saskatchewan rain events are often thunderstorms occurring late at night.

It was also observed that the drogues at different depths travelled at different velocities, which suggests that there was a variation in the vertical velocity profile, as shown in Figure 4-26, where the arrows show the flow path where the shallowest drogue is leading and the deeper drogues are lagging in order of depth. This observation was apparent for all of the drogue tracking events where larger displacements were observed, where drogues with fins of all lengths were placed near each other to start.

Figure 4-26. Drogue tracking showing the leading drogue with the shallowest fin, with drogues with deeper fins lagging in order of depth.

Chapter 5

CONCLUSIONS AND RECOMMENDATIONS

Over the summer season of 2014, field research took place at the John Avant Park stormwater management pond in Saskatoon, Saskatchewan, Canada to investigate the total solids concentrations, particle size distributions, and loading for inflows and outflows, the settling of solids and removal efficiency of the pond, as well as the flow pattern within the pond. This work was conducted through sampling of the flows in the inlet and Outlet pipes, sampling of sediment within the pond, and flow visualization using surveying and LSPTV techniques.

The results of this field research indicate that overall, the John Avant Park stormwater management pond had an estimated removal efficiency of -67% for total solids in 2014. The inlet loading of solids was 26% of the total potential outflow of solids, indicating that substantial resuspension could be occurring. It is important to also note, that a man-made stream for aeration may have also been contributing to the resuspension of sediment within the pond. In addition to inflow through the pond's inlets, other flow would have contributed to this negative removal efficiency, as baseflow (flow from the pond associated with or without precipitation), the park area of the pond, and the area immediately surrounding the Outlet also contributed to the sampled Outlet flow. However, the total solids from the pond catchment area should have settled in the pond if the pond was effective, and the Outlet catchment area total solids contribution would have been expected to be minimal due to the relatively small Outlet catchment area. The negative removal efficiency particularly suggests that, in 2014, resuspension likely occurred in the pond, specifically with finer (silt and clay sized) sediment. It is likely, however, that the removal efficiency of the pond changes from year-to-year and from event-to-event. Years of research, for varying return

period events, would be needed to effectively evaluate the pond's average removal efficiency for solids.

Sediment measurements within the pond suggest that over its lifetime, the stormwater management pond at John Avant Park has accumulated approximately 1 cm/year of solids. The core samples taken were predominately comprised of sand, with coarser particles (sand, gravel) located closer to the inlets or towards the periphery of the pond. Finer particles (silt, clay) were more predominant further away from the inlets. Though the fact that there is deposited material in the ponds seemingly contradicts with the finding of a negative removal efficiency, as noted it is likely that the removal efficiency varies from year to year.

Flow pattern investigations using a combination of surveying a 3-dimensional prism attached to a drogue float with a Leica robotic total station, and concepts from LSPTV, suggest that typical pond flow patterns within the John Avant Park during the 2014 field season were dominated by wind. Therefore, although one may expect the solids to settle out along the flow path, no dominant flow path was found in this research such that no clear relationship between the flow pattern and settling was found. The significance of a wind-dominated flow is that short-circuiting could be occurring when the wind direction is from the inlets to the Outlet. Therefore, there is a need to reduce this short-circuiting. The installation of submerged baffles or altering the pond design to minimize wind influence may mitigate short-circuiting. The growth of weeds in the pond over the summer season may also contribute to low flow dead zones; however, the weeds may have also promoted settling if they break up flow created by wind.

For drogue tracking methodologies used in this field investigation, surveying a 3-dimensional prism with a robotic total station was preferred over using concepts from LSPTV. Although the field surveying of multiple drogues in the field is more labor and equipment intensive

in the field, the time savings in data processing render it more attractive. At the time of this field investigation, to the author's knowledge, there was no commercial software available for analyzing data for LSPTV. The presence of reflections on the pond's surface led open-source LSPTV software to be unusable as reflections were recognized as tracer particles.

Since LSPTV software could not be used, data processing equations typically used to develop LSPTV software were used to develop an alternative manual system for processing data using MathCad and Excel. Although this system was able to correlate real world (x, y, z) locations to camera image (pixel) locations, the lack of calibration reference points throughout the image led to a very large unacceptable error of the solution. One solution to this issue in the future would be to have colorful metal posts within the pond that can be surveyed and not moved over the field season. Due to the fact that the pond was publicly accessible and used recreationally for canoeing, kayaking, dog swims, and playing with remote control boats (all observed during field research), disturbing public use of the pond was not desirable. Alternatively buoys on a rope could be used, but buoys could be moved by the public during drogue tracking events, and it would be very challenging to put the buoy in the exact original spot as surveying with an inflatable zodiac boat proved to be challenging.

It is recommended that future field experiments using drogues should take surface velocity measurements for varying wind velocities at the field site, since it has been shown that equations from the literature used to calculate this velocity tend to produce highly variable results. It is also recommended that similar calculations are performed to ensure drogue movement in ponds and lakes is due to water flow patterns and not wind.

Drogue tracking could potentially be done using an unmanned aerial vehicle (UAV) equipped with a camera. These devices are becoming popular for building three dimensional

models for comparison with photogrammetry applications and are now equipped with stabilizers (personal communication, Golder Associates, Vancouver, September 2016). Although these newer UAV models are equipped with stabilizers, flying them in very windy, stormy, or rainy conditions is not ideal. To operate UAVs for research or commercial purposes in a municipal setting there are also particular permitting and pilot licensing requirements (personal communication, Golder Associates, Vancouver, September 2016), which may in itself be a potential constraint to their use.

The data processing for using camera imagery to determine flow paths and velocities of drogues is currently very labor intensive. At the time of this field research, to the author's knowledge, there was no commercially available LSPTV software available. Therefore, those who had used LSPTV to analyze surface water flows in the field (typically river flows) had done so using open-source software and typically were not using it for larger ponds or lakes, as discussed in Chapter 2. Unfortunately, the open source software is still under development as in some circumstances, it recognizes surface reflections on the water as tracer particles. In the images, the reflection of bright white clouds led to issues in processing the data. Therefore, the data processing system described herein was used as an alternative.

Others have indicated challenges or implementation issues in using large scale particle image velocimetry (LSPIV) in field applications due to reduced visibility during precipitation events, low contrast of images during sunrise and sunset, and the presence of reflections which complicate the recognition of tracer particles from one image to the next (Daigle *et al.* 2013). Muste *et al.* (2011) further describe unfavorable conditions for LSPTV such as that produced when the water surface is mirror-like. Non-ideal lighting conditions make the neon ball floats of the drogues almost unrecognizable in the image. It is not often that field conditions are ideal for software use.

When compared to the LSPTV techniques, drogue tracking using a robotic total station and a three dimensional prism was deemed more desirable. Although more expensive equipment is used in the field for this method, the labor hours saved on the data processing side may be a desirable tradeoff for the more expensive equipment. Surveying is also generally more accurate, where the accuracy is within a couple of millimeters as opposed to several centimeters which could be the case with camera usage using proper calibration points.

There are several recommendations for future work based on the findings of this project as listed below:

- If possible, have the data loggers of automatic samplers connected to a remote site so pond hydraulics are evaluated when there is known high flow through the Inlet pipes. Removing data loggers from the manholes to determine whether or not there was flow took approximately 4 hours and is therefore undesirable as flow conditions would likely change within that time frame.
- Conduct drogue tracking in the spring when weeds are less predominant in the pond, and then compare late summer flow patterns and velocities to the spring when vegetation was not present.
- Conduct measurements over a longer time period (5 years or more) to obtain data for the pond removal efficiency over several different return periods.
- Collect water samples from within the pond during baseflow and rain events as an indicator of possible resuspension.

- Conduct groundwater elevation measurements to determine the water table elevation and confirm that groundwater baseflow accounts for the major discrepancy between the total measured volume in the inlets and the Outlet.
- If possible, install rain gauges in each of the main catchment areas and improve wind measurements such that wind speed monitoring is continuous.
- Place calibration reference points throughout the field of vision when using LSPTV to investigate pond hydraulics, as this will improve the accuracy of coefficients determined for use in the collinearity formulae using a direct linear transformation.
- Investigate the presence of other contaminants such as organics and heavy metals to determine how they relate to the particle size distribution of solids.
- Improve software such that the data processing aspects for LSPTV are less cumbersome following field research. Presentations at the IAHR Congress (2015) in the Hague, Netherlands, suggest some researchers are in the early stages of developing phone apps that will conduct LSPIV or LSPTV for the user.
- Investigate the effect of baffle installation on pond hydraulics, and the effect on short-circuiting, the settling of solids, and settled solids resuspension.
- Investigate the effect of purpose-grown vegetation in the pond to improve settling and direct pond hydraulics.

LIST OF REFERENCES

Admiraal, D. M. Stansbury, J. S., and Haberban, C. J. 2004. Case study: particle velocimetry in a model of Lake Ogalla. Journal of Hydraulic Engineering, **130**(7): 599-607.

Alberta Environmental Protection. 1999. Stormwater management guidelines for the province of Alberta. Municipal Program Development Branch, Environmental Services Division. Available from http://environment.gov.ab.ca/info/library/6786.pdf [cited March 27 2016]

Anderson, B. C., Watt, W. E., Marsalek, J., and Crowder, A. 1996. Integrated urban stormwater quality management: field investigations at a best management facility. Canadian Water Resources Journal, **21**(2): 165-182.

ASTM Standard D422-63, 1998, "Standard Test Method for Particle-Size Analysis of Soils," ASTM International, West Conshohocken, PA, 1998, www.astm.org.

ASTM Standard D5073-02, 2013, "Standard Practice for Depth Measurement of Surface Water," ASTM International, West Conshohocken, PA, 2013, www.astm.org.

ASTM Standard D4823-95, 2014, "Standard Guide for Core Sampling Submerged, Unconsolidated Sediments," ASTM International, West Conshohocken, PA, 2014, www.astm.org.

ASTM Standard D5906-02, 2013, "Standard Guide for Measuring Horizontal Positioning During Measurements of Surface Water Depths," ASTM International, West Conshohocken, PA, 2013, www.astm.org.

Barter, P. J. 2003. Investigation of pond velocities using dye and small drogues: a case study of the Nelson City Waste Stabilization Pond. Water Science and Technology, **48**(2): 145-151.

Birch, G. F., Matthai, C., and Fazeli, M. S. 2006. Efficiency of a retention/detention basin to remove contaminants from urban stormwater. Urban Water Journal, Taylor & Francis, **3**(2): 69-77.

Bos, M. G. 1989. Discharge measurement structures, third revised edition. International Institute for Land Reclamation and Improvement, Wageningen: The Netherlands.

Braskerud, B. C. 2001. The influence of vegetation on sedimentation and resuspension of soil particles in small constructed wetlands. Journal of Environmental Quality, **30**: 1447-1457.

City of Calgary Water Resources. 2011. Stormwater management and design manual. The City of Calgary. Available from http://www.calgary.ca/PDA/pd/Documents/urban_development/bulletins/2011-stormwater-management-and-Design.pdf [cited 28 March 2016]

City of Saskatoon. 2012. City of Saskatoon new neighborhood design and development standards manual: section six, storm water drainage system. City of Saskatoon, Saskatoon, Saskatchewan.

Creutin, J. D., Muste, M., Bradley, A. A., Kim, S. C., and Kruger, A. 2003. River gauging using PIV techniques: a proof of concept experiment on the Iowa River. Journal of Hydrology, **277**: 182-194.

Daigle, A., Bérubé, F., Bergeron, N., and Matte, P. 2013. A methodology based on particle image velocimetry for river ice velocity measurement. Cold Regions Science and Technology, **89**: 36-47.

Dermisis, D. C., and Papanicolaou, A. N. 2005. Determining the 2-D surface velocity field around hydraulic structures with the use of a large scale particle image velocimetry

(LSPIV) technique. Environmental and Water Resources Institute of the American Society of Civil Engineers.

Douglas, J. F., Gasiorek, J. M., Swaffield, J. A., and Jack, L. B. (2005). Fluid Mechanics Fifth Edition. Pearson Education Ltd., England.

Droste, R. L. 1997. Theory and practice of water and wastewater treatment. John Wiley & Sons, Inc, New York, United States of America.

Environmental Protection Agency (EPA). 2012. Total solids. Available from http://water.epa.gov/type/rsl/monitoring/vms58.cfm [cited on 28 March 2016]

Erdbrink, C. 2007. Particle tracking in a shallow mixing layer: a fluid dynamics laboratory in the field. M.Sc. Thesis. Delft University of Technology, Delft, the Netherlands..

Fox, J. F., Patrick, A., and Wood, S. 2006. The use of LSPIV to measure large streamwise vortices. *In* Proceedings of the World Environmental and Water Resource Congress 2006, American Society of Civil Engineers, New York, pp. 1-10.

Fox, J. F., and Patrick, A. 2008. Large-scale eddies measured with large scale particle image velocimetry. Flow Measurement and Instrumentation, **19**: 283-291.

Fujita, I., Aya, S., and Deguchi, T. 1997. Surface velocity measurement of river flow using video images at an oblique angle. *In* Proceedings of the XXVII IAHR Conference, Theme B. Vol 1. San Francisco, pp. 227-232.

Fujita, I., Muste, M., and Kruger, A. 1998. Large-scale particle image velocimetry for flow analysis in hydraulic engineering applications. Journal of Hydraulic Research, **36**(3): 397-414.

Fyfe, J., Smalley, J., Hagare, D., and Sivakumar, M. 2007. Physical and hydrodynamic characteristics of a dairy shed waste stabilization pond system. Water Science & Technology, **55**(11): 11-20.

Garratt, J.R. (1992). The Atmospheric Boundary Layer. Cambridge University Press.

Gettel, M., Gulliver, J. S., Kayhanian, M., DeGroot, G., Brand, J., Mohseni, O., and Erikson, A. J. 2011. Improving suspended sediment measurements by automatic samplers. Journal of Environmental Monitoring, **13**: 2703-2709.

Glenn, J. S., and Bartell, E. M. 2010. Evaluating short-circuiting potential of stormwater ponds. *In* Proceedings of the World Environmental and Water Resources Congress, May 16-20, Providence, Rhode Island, American Society of Civil Engineers, New York, pp. 3942-3951.

Google Maps. 2014. Digital globe, map data. Available from https://www.google.ca/maps/@52.1387031,-106.5665639,244m/data=!3m1!1e3 [cited 16 March 2014]

Greb, S. R., and Bannerman, R. T. 1997. Influence of particle size on wet pond effectiveness. Water Environment Research, **69**(6): 1134-1138.

Hall, N. (2015). Shape effects on drag. National Aeronautics and Space Administration (NASA). Available from https://www.grc.nasa.gov/WWW/K-12/airplane/shaped.html [cited 19 February, 2017]

Hanna, G. L. 1989. An investigation of the flow and retention time in a two-metre deep waste stabilization pond system. Proceedings of the 13th Australian Water and Wastewater Association Federal Convention, 6-10 March, Canberra, Australia, pp. 243-247.

Hansen, F.V. (1993). “Surface roughness lengths.” Army Research Laboratory Report ARL-TR-61, August 1993, Adelphi, Maryland.

Heal, K. V., Hepburn, D. A., and Lunn, R. J. 2006. Sediment management in sustainable urban drainage system ponds. Water Science & Technology, **53**(10): 219-227.

Hendersen-Sellers, B. (1988). “The dependence of surface velocity in water bodies on wind velocity and latitude.” Applied Mathematical Modelling, 12(April), 202-203.

Holland, J. F., Martin, J. F., Granata, T., Bouchard, V., Quigley, M., and Brown, L. 2004. Effects of wetland depth and flow rate on residence time distribution characteristics. Ecological Engineering, **23**(3): 189-203.

Hvitved-Jacobsen, T., Johansen, N. B., and Yousef, Y. A. 1994. Treatment systems for urban and highway run-off in Denmark. The Science of the Total Environment, **146-147**: 499-506.

Jeyapalan, K. 2004. Mobile digital cameras for as-built surveys of roadside features. Photogrammetric Engineering & Remote Sensing, **70**(3): 301-312.

Joo, J., Lee, J., Kim, J. H., and Jo, D. 2014. Inter-event time definition setting procedure for urban drainage systems. Water, **6**(1): 45-58.

Kantoush, S. A., and Schleiss, A. J. 2009. Large-scale PIV surface flow measurements in shallow basins with different geometries. **12**(4): 361-373.

Kantoush, S. A., Schleiss, A. J., Sumi, T., and Murasaki, M. 2011. LSPIV implementation for environmental flow in various laboratory and field cases. Journal of Hydro-environment Research, **5**: 263-276.

Kantrowitz, I. H., and Woodham, W. M. 1995. Efficiency of a stormwater detention pond in reducing loads of chemical and physical constituents in urban streamflow, Pinellas County, Florida. U.S Department of the Interior. Available from http://pubs.usgs.gov/wri/1994/4217/report.pdf [cited 20 March 2016]

Kayhanian, M., McKenzie, E. R., Leatherbarrow, J. E., and Young, T. M. 2012. Characteristics of road sediment fractionated particles captured from paved surfaces, surface run-off and detention basins. Science of the Total Environment, **439**: 172-186.

Kim, J-Y., and Sansalone, J. J. 2008. Event-based size distributions of particulate matter transported during urban rainfall-runoff events. Water Research, **42**: 2756-2768.

Krauss, W., Dengg, J., and Hinrichsen, H. H. 1989. The response of drifting buoys to currents and wind. Journal of Geophysical Research, **94**: 3201-3210.

Lanza, L. G., and Stagi, L. n.d. On the quality of tipping-bucket rain intensity measurements. University of Genova, Department of Environmental Engineering. Available from https://www.wmo.int/pages/prog/www/IMOP/publications/IOM-94-TECO2006/P3(15)_Lanza_Italy.pdf [cited April 22, 2017]

Lick, W. (2008). *Sediment and Contaminant Transport in Surface Waters*. CRC Press, Boca Raton, Florida.

Lodhi, A. R., and Acharya, K. 2014. Detention basins as best management practices for water quality control in an arid region. Water Science and Engineering, **7**(2): 155-167.

Marsalek, J. 1981. Calibration of the tipping-bucket raingage. Journal of Hydrology, **53**: 343-354.

Marsalek, J., Watt, W. E., Anderson, B. C., and Jaskot, C. 1997. Physical and chemical characteristics of sediments from a stormwater management pond. Water Quality Resource Journal Canada, **32**(1).

McLeod, S. 2007. Characterization of the urban runoff quality from the city of Saskatoon to the South Saskatchewan River. M.Sc. Thesis, Department of Civil and Geological Engineering, University of Saskatchewan, Saskatoon, Saskatchewan.

Meselhe, E. A., Peeva, T., and Muste, M. 2004. Large scale particle image velocimetry for low velocity and shallow water flows. Journal of Hydraulic Engineering, **130**(9): 937-940.

Muste, M. Xiong, Z., Bradley, A. and Kruger, A. 2004. Large-scale particle image velocimetry – a reliable tool for physical modelling. Water Resources 2000, American Society of Civil Engineers.

Muste, M., Fujita, I., and Hauet, A. 2008. Large-scale particle image velocimetry for measurements in riverine environments. Water Resources Research, **44**(4): 1-14.

Muste, M., Ho, H-C., and Kim, D. 2011. Considerations on direct stream flow measurements using video imagery: outlook and research needs. Journal of Hydro-environment Research, **5**: 289-300.

Muste, M., Hauet, A., Fujita, I., Legout, C., and Ho, H.-C. 2014. Capabilities of large-scale particle image velocimetry to characterize shallow free-surface flows. Advances in Water Resources, **70**: 160-171.

Myers, E. J., Oldham, R. S., and Ferguson, A. J. D. 1982. Circulation patterns; their investigation and prediction. Hydrobiologia, **88**(1): 67-77.

Nishida, H., Tada, A., Nishihira, F. (1994). “Hydrodynamic forces on bottom-seated hemisphere in waves and currents.” Coastal Engineering ’94, 24th International Conference on Coastal Engineering (ASCE), October 23-28, 1994, Kobe, Japan, 1484-1495.

Oke, T.R. (1997). “Chapter 2: Surface climate processes” in *The Surface Climates of Canada*, *eds.* Bailey, W.E., Oke, T.R., Rouse, W.R., McGill-Queen’s University Press, Montreal, Quebec, 21-43.

Papa, F., and Adams, B. J. 1996. Quality control optimization of extended detention dry ponds. Journal of Water Management Modelling R191-13: 201-222.

Persson, J. 2000. The hydraulic performance of ponds of various layouts. Urban Water **2**(3): 243-250.

Pettersson, T. J. R., German, J., and Svensson, G. 1998. Modelling of flow pattern and particle removal in an open stormwater detention pond. *In* Proceedings of HydraStorm ’98, 27-30 September, Adelaide, Australia, pp. 63-68.

Pettersson, T. J. R. 1999. Stormwater ponds for pollution reduction. Ph.D. Thesis, Department of Sanitary Engineering, Chalmers University of Technology, Göteborg, Sweden.

Pettersson, T. J. R., Lavieille, D. 2007. Evolution on pollutant removal efficiency in storm water ponds due to changes in pond morphology. *In* Proceedings of the 8th Highway and Urban Environment Symposium: 429-439.

Potter, M.C., Wiggert, D.C., Bassem, H.R., Shih, T.I-P. (2017). *Mechanics of Fluids, 5th edition*. Cengage Learning, Boston, Massachusetts, USA.

Selbig, W. R., Bannerman, R., and Corsi, S. R. 2013. From streets to streams: assessing the toxicity potential of urban sediment by particle size. Science of the Total Environment, **444**: 381-391.

Shaw, J. K. E., Watt, W. E., Marsalek, J., Anderson, B. C., and Crowder, A. A. 1997. Flow pattern characterization in an urban stormwater detention pond and implications for water quality. Water Resource Journal of Canada, the Canadian Association on Water Quality (CAWQ), **32**(1): 53-71.

Shilton, A. 2001. Studies into the hydraulics of waste stabilization ponds. Ph.D. Thesis, Department of Environmental Engineering, Massey University. Palmerson North, New Zealand.

Shilton, A., and Bailey, D. 2006. Drogue tracking by image processing for the study of laboratory scale pond hydraulics. Flow Measurement and Instrumentation, **17**: 69-74.

Smith, I.R. (1979). "Hydraulic conditions in isothermal lakes." Freshwater Biology, 9, 119-145.

Spencer, K. L., Droppo, I. G., He, C., Grapentine, L. and Exall, K. 2011. A novel tracer technique for the assessment of fine sediment dynamics in urban water management systems. Water Research, **45**: 2595-2606.

Stewart, J. 2013. Calculus. Rotation of axes. Available from http://www.stewartcalculus.com/data/CALCULUS%20Early%20Vectors/upfiles/RotationofAxes.pdf [cited 20 June 2015]

Sturm, T. W. 2010. Open channel hydraulics. Second Edition. McGraw-Hill International Edition, New York.

Texas Electronics. (n.d). TR-525 series rainfall sensors user's manual. Available from http://texaselectronics.com/media/mconnect_uploadfiles/t/r/tr-525_rainfall_manual_new.pdf [cited 29 January 2017]

Thomson, S. (n.d). Direct linear transformation. Brigham Young University, Mechanical Engineering Elementary Instrumentation Lecture. Available from https://me363.byu.edu/sites/me363.byu.edu/files/userfiles/5/DLTNotes.pdf [cited 20 June 2015]

United States Department of Agriculture (USDA). 1993. Soil survey manual. Soil Conservation Service Handbook 18. Available from http://www.nrcs.usda.gov/wps/portal/nrcs/detail/soils/ref/?cid=nrcs142p2_054253 [cited 17 August 2016]

Vachon, W.A. (1973). *Scale Model Testing of Drogues for Free Drifting Buoys*. Final Report (R-769), The Charles Stark Draper Laboratory Inc., Cambridge, Massachusetts.

Vaze, J., and Chiew, H. S. 2004. Nutrient loads associated with different sediment sizes in urban stormwater and surface pollutants. Journal of Environmental Engineering, **130**: 391-396.

Wakelin, S. C., Elefsiniotis, P., and Wareham, D. G. 2003. Assessment of stormwater retention basin water quality in Winnipeg, Canada. Water Quality Research Journal of Canada, **38**(3): 433-450.

Water Security Agency. 2006. Stormwater Guidelines: EPB 322. Available from http://www.saskh20.ca/DWBinder/epb322.pdf [cited 24 January 2014]

Wolf, P. R., Dewitt, B. A., and Wilkenson, B. E. 2014. Elements of photogrammetry with applications in GIS: 4th edition. Access Engineering.

Yousef, Y. A., Hvitved-Jacobsen, T., Sloat, J., and Lindeman, W. 1994. Sediment accumulation in detention or retention ponds. The Science of the Total Environment, **146/147**: 451-456.

Zhao, H., Li, X., Wang, X., and Tian, D. 2010. Grain size distribution of road-deposited sediment and its contribution to heavy metal pollution in urban runoff in Beijing, China. Journal of Hazardous Materials, **183**: 203-210.

APPENDIX A

RAINFALL HYETOGRAPHS

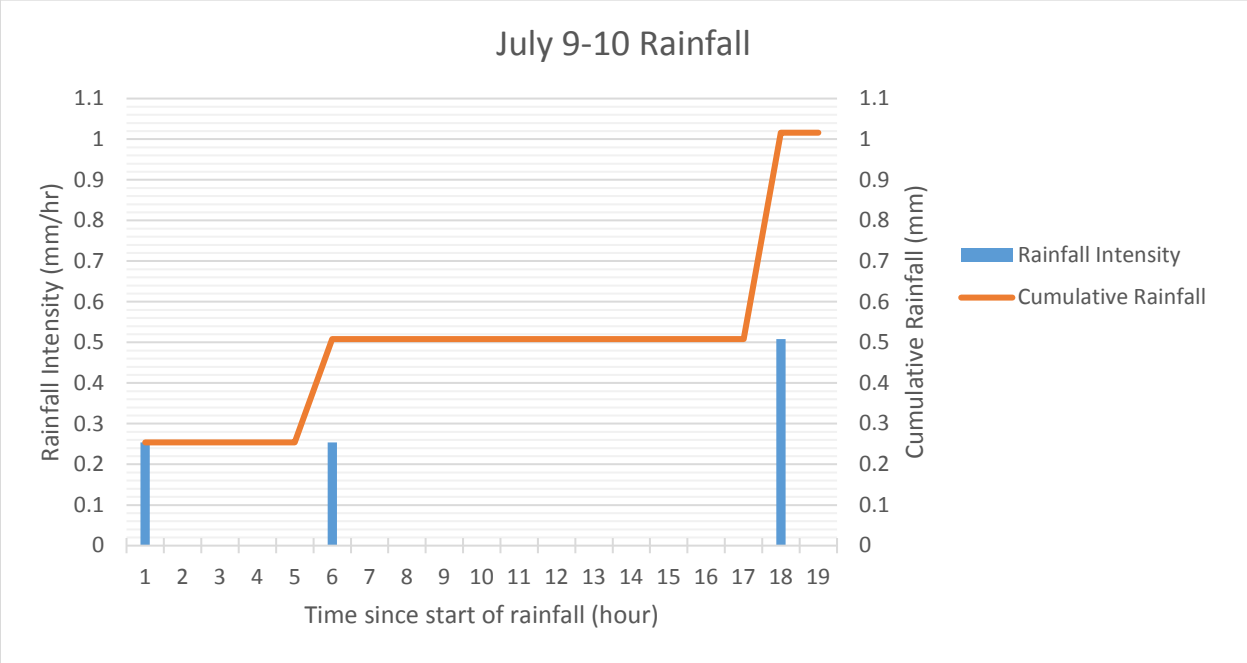

Figure A-1. Hyetograph for the rain event beginning at 11:00 July 9, 2014

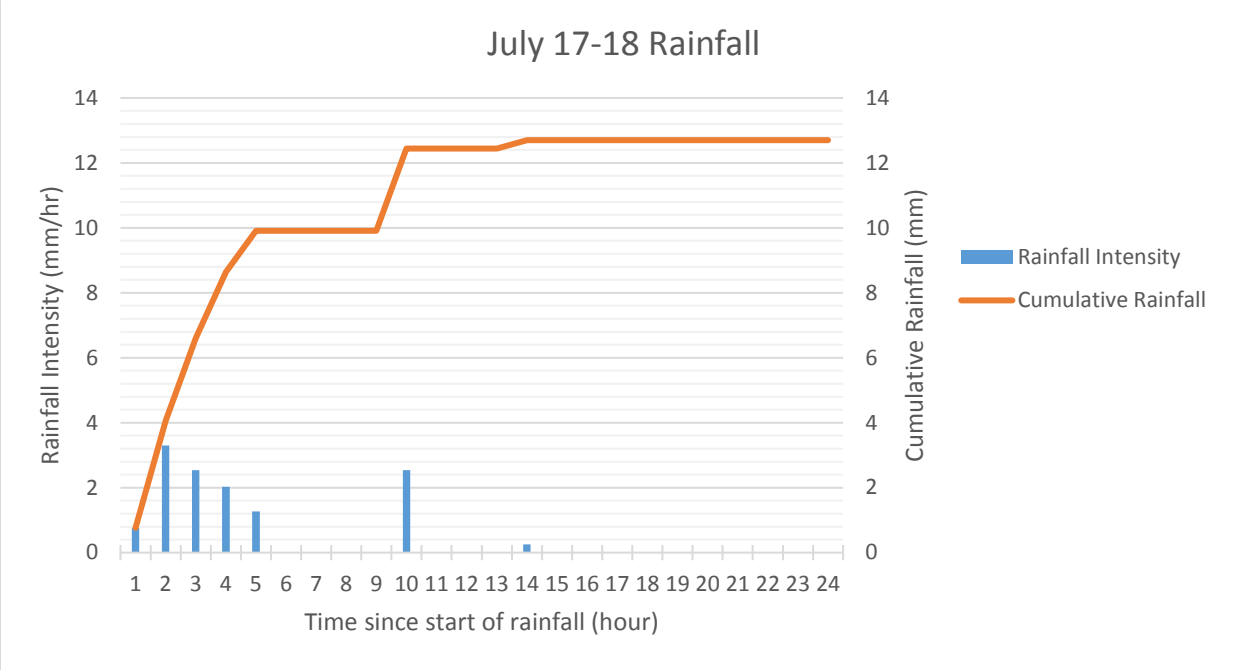

Figure A-2. Hyetograph for the rain event beginning at 19:15 July 17, 2014

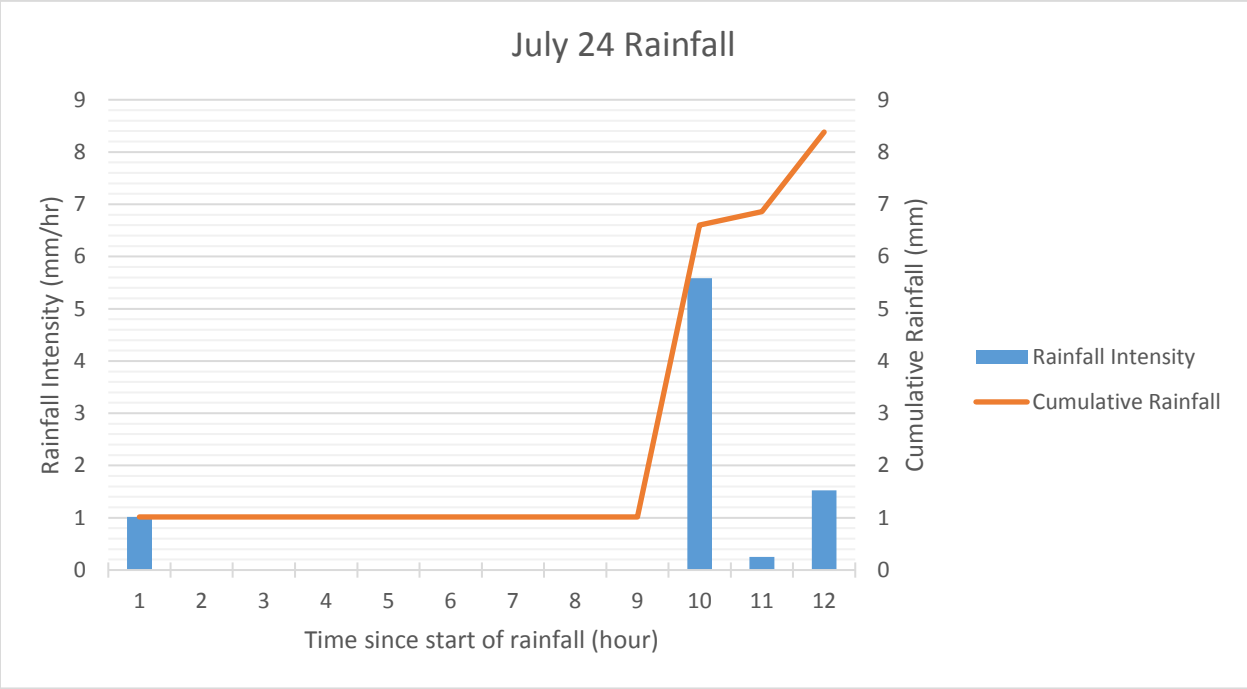

Figure A-3. Hyetograph for the rain event beginning at 8:40 July 24, 2014

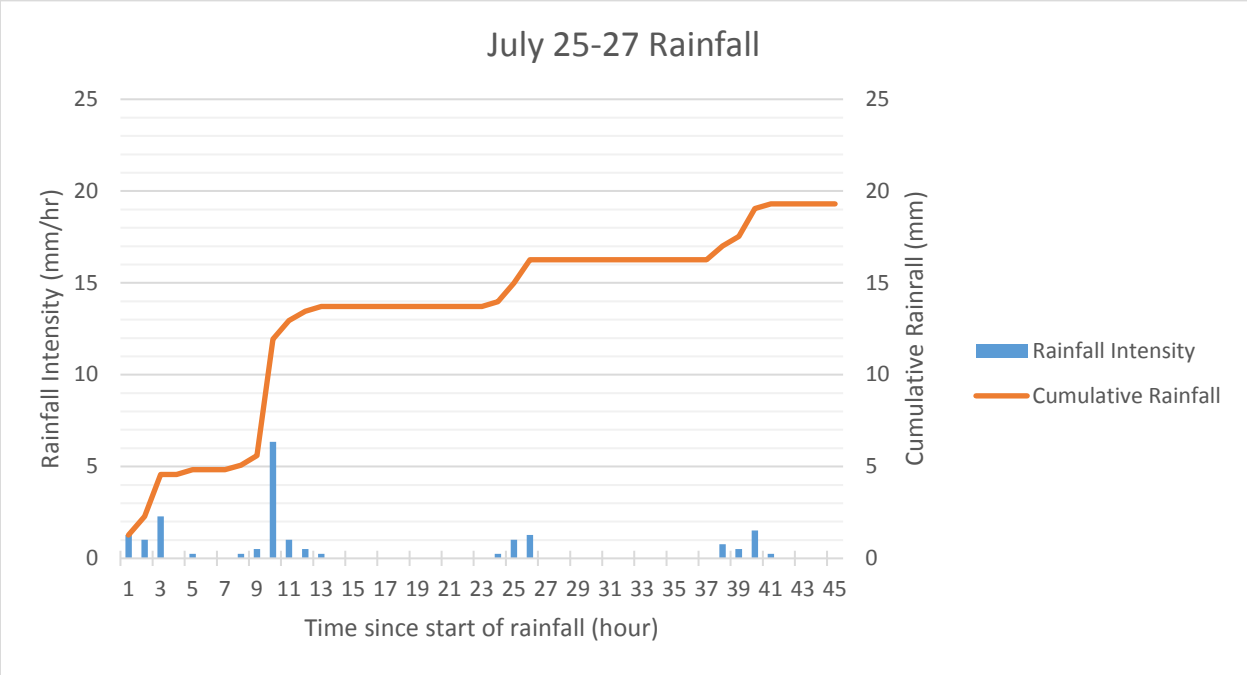

Figure A-4. Hyetograph for the rain event beginning at 12:00 July 25, 2014

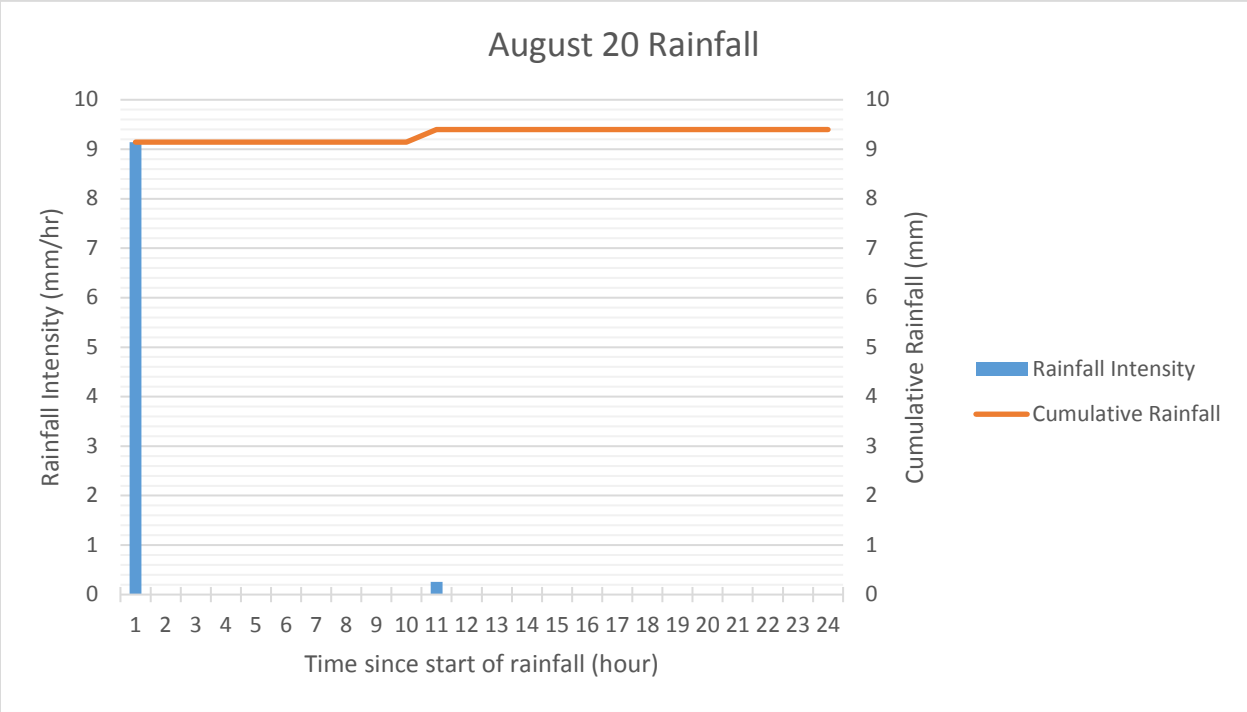

Figure A-5. Hyetograph for the rain event beginning at 3:47 August 20, 2014

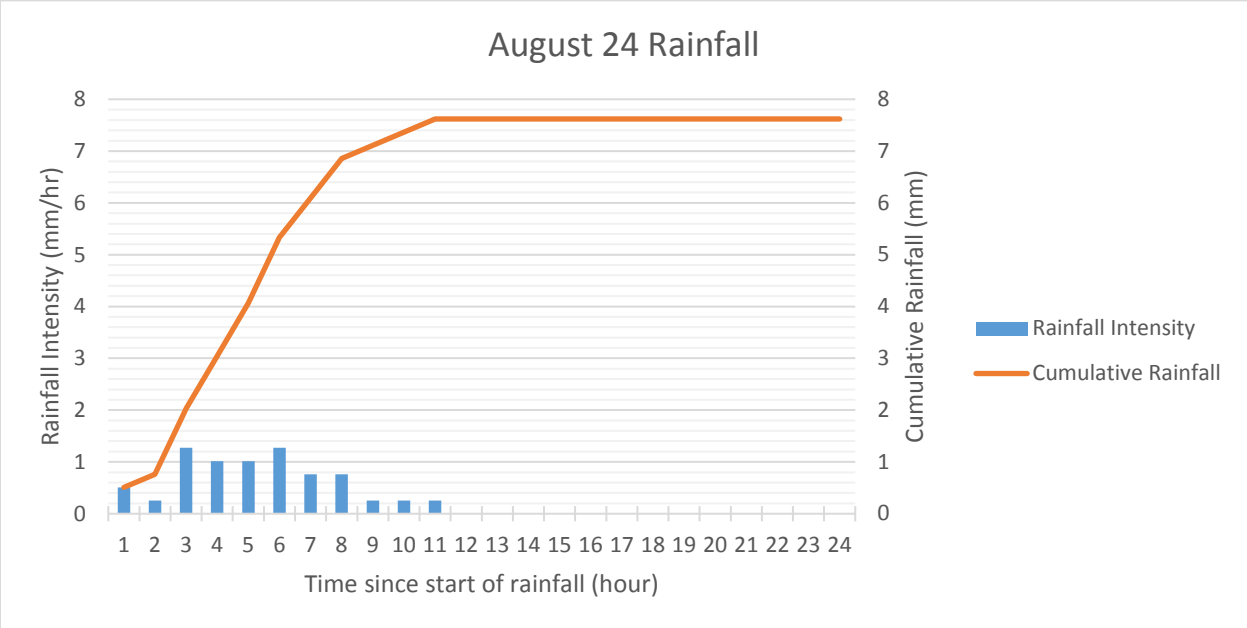

Figure A-6. Hyetograph for the rain event beginning at 10:50 August 24, 2014

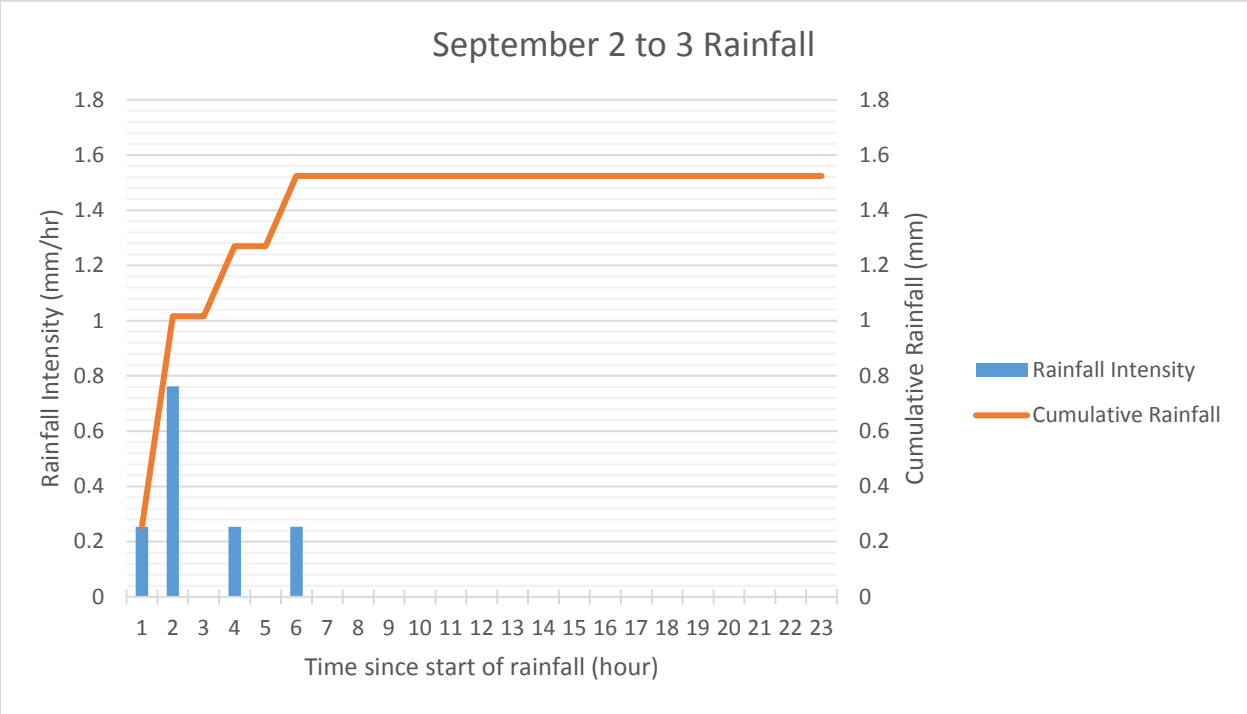

Figure A-7. Hyetograph for the rain event beginning at 19:21 September 2, 2014

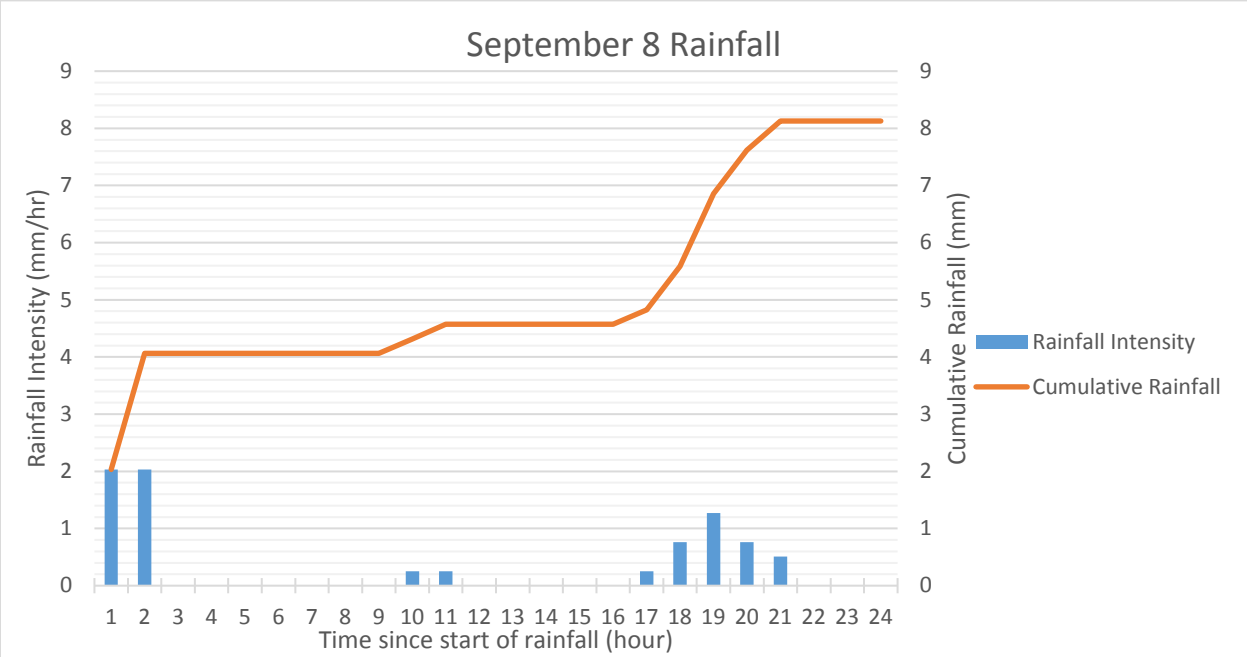

Figure A-8. Hyetograph for the rain event beginning at 1:01 September 8, 2014

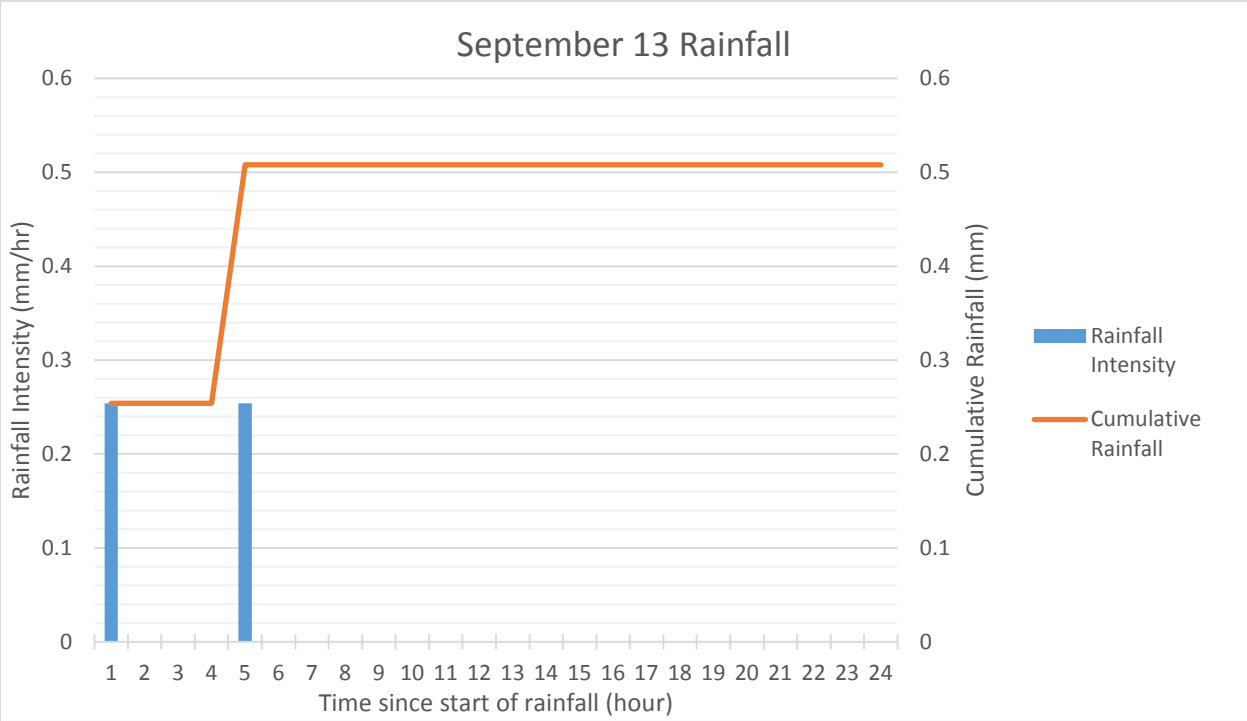

Figure A-9. Hyetograph for the rain event beginning at 5:57 September 13, 2014

APPENDIX B

INLET AND OUTLET TOTAL SOLIDS CONCENTRATION WITH FLOW

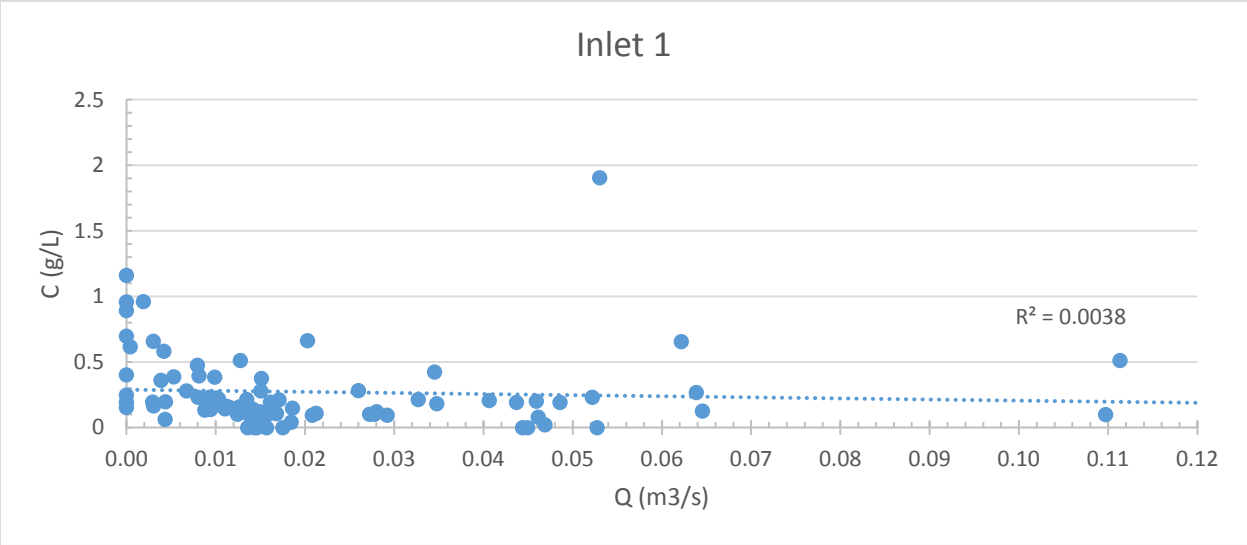

Figure B-1. Relationship of total solids concentration and flow rate in Inlet 1

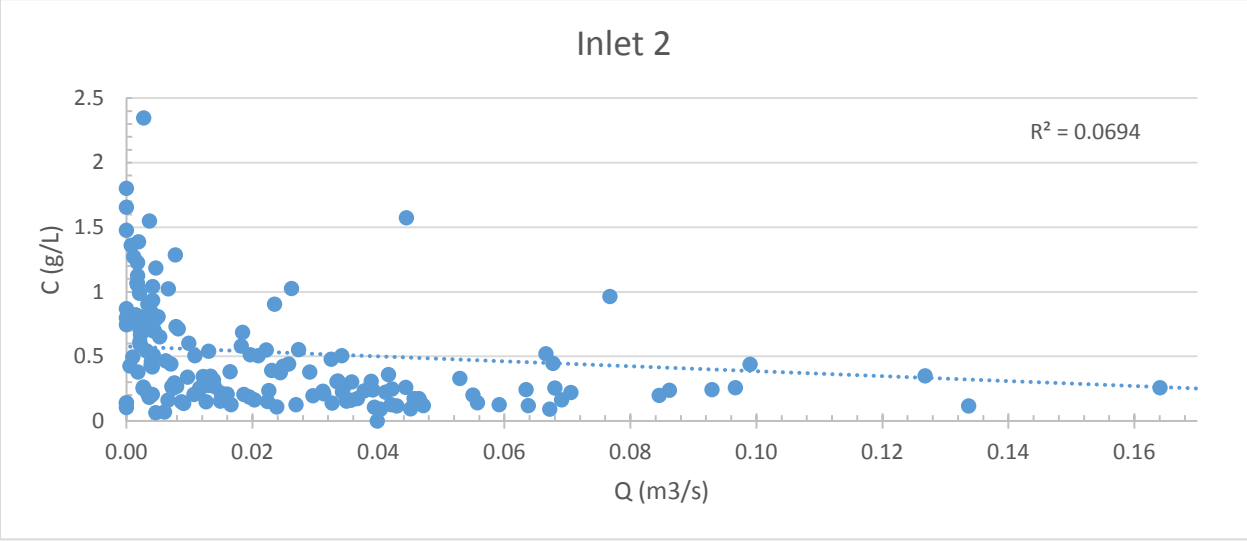

Figure B-2. Relationship of total solids concentration and flow rate in Inlet 2

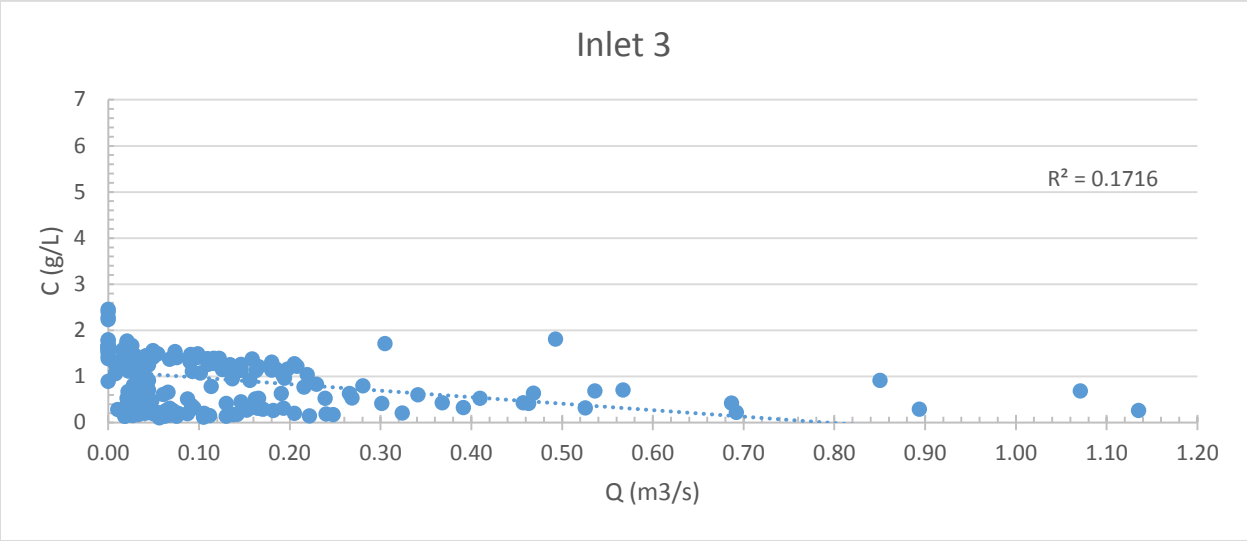

Figure B-3. Relationship of total solids concentration and flow rate in Inlet 3

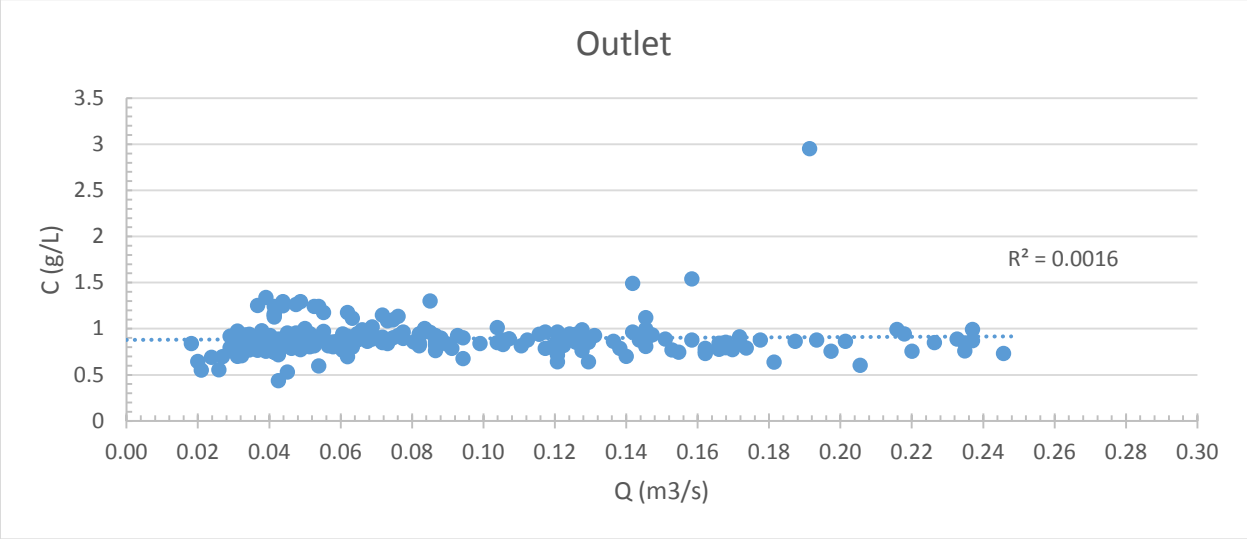

Figure B-4. Relationship of total solids concentration and flow rate in the Outlet

APPENDIX C

PARTICLE SIZE DISTRIBUTION DATA

Table C-1. Particle size distribution of total solids sampled over the summer sampling season in 2014

Nominal Particle Diameter (mm)	Mass percentage of particles finer than			
	Inlet 1	Inlet 2	Inlet 3	Outlet
9.5	100.00	100.00	100.00	100.00
4.75	100.00	100.00	100.00	100.00
2.36	99.91	100.00	99.90	100.00
1.18	99.91	99.95	99.23	100.00
0.6	99.68	99.61	97.18	99.11
0.3	98.89	98.39	95.35	98.06
0.15	96.87	96.33	92.87	97.22
0.075	93.59	93.83	90.83	96.44
0.0691	81.21	87.08	86.84	92.01
0.0492	76.07	85.78	85.02	92.01
0.0351	73.50	80.55	79.57	91.04
0.0222	70.93	75.32	72.30	89.11
0.0150	65.27	54.39	51.41	78.51
0.0093	52.43	42.37	27.61	58.06
0.0066	44.20	42.37	27.43	58.06
0.0033	33.92	42.37	27.43	57.29
0.0014	26.21	42.10	27.43	57.10

APPENDIX D

POND SEDIMENT THICKNESS MEASUREMENTS (JUNE, AUGUST)

Table D-1. June 2014 sediment depth measurements along with the corresponding northing and easting survey coordinates

Northing (m)	Easting (m)	Pond bottom elevation with sediment (m)	Sediment thickness (m)
997	1175	499.279	0.279
1006	1174	499.569	0.569
991	1141	499.000	0.000
1000	1144	499.169	0.169
1008	1146	498.969	-0.031
1018	1150	498.979	-0.021
998	1117	498.861	-0.139
1007	1119	499.479	0.479
1017	1121	499.229	0.229
1027	1123	499.259	0.259
1037	1125	499.299	0.299
1047	1127	499.289	0.289
1056	1129	499.309	0.309
1066	1131	499.309	0.309
1076	1133	499.299	0.299
993	1091	499.399	0.399
1012	1096	499.289	0.289
1022	1099	499.289	0.289
1031	1101	499.289	0.289
1041	1104	499.279	0.279
1057	1108	499.239	0.239
1074	1112	499.289	0.289
1007	1072	499.339	0.339
1017	1074	499.139	0.139
1027	1076	499.149	0.149
1036	1079	499.289	0.289
1046	1081	499.299	0.299
1011	1054	499.339	0.339
1020	1057	499.259	0.259
1030	1061	499.339	0.339
1039	1064	499.399	0.399
1015	1026	499.319	0.319
1024	1032	499.329	0.329
1032	1038	499.319	0.319
1040	1043	499.269	0.269
1048	1049	499.359	0.359
1062	1058	499.379	0.379
1077	1068	499.419	0.419
1097	1118	498.809	-0.191
1130	1106	499.289	0.289
1041	1007	498.719	-0.281
1049	1012	499.339	0.339
1057	1018	499.289	0.289
1066	1023	499.289	0.289
1074	1029	498.859	-0.141
1087	1038	499.249	0.249
1102	1048	499.259	0.259
1121	1061	499.289	0.289
1156	1085	499.329	0.329
1171	1095	499.339	0.339
1185	1105	499.289	0.289

Table D-2. August 2014 sediment depth measurements with the corresponding northing and easting survey coordinates.

Northing (m)	Easting (m)	Pond bottom elevation with sediment (m)	Sediment thickness (m)
997	1175	499.209	0.209
1006	1174	499.629	0.629
1014	1173	499.969	0.969
992	1141	499.219	0.219
1000	1144	499.029	0.029
1008	1146	499.049	0.049
1019	1150	498.939	-0.061
998	1117	499.289	0.289
1007	1119	499.329	0.329
1017	1121	499.359	0.359
1027	1123	499.389	0.389
1037	1125	499.359	0.359
1046	1127	499.369	0.369
1056	1129	499.689	0.689
1066	1131	500.509	1.509
1076	1133	500.379	1.379
993	1091	499.489	0.489
1012	1096	499.269	0.269
1022	1099	499.329	0.329
1031	1101	499.389	0.389
1041	1104	499.359	0.359
1057	1108	499.319	0.319
1074	1112	499.279	0.279
1007	1072	499.129	0.129
1017	1074	499.179	0.179
1026	1076	499.339	0.339
1036	1079	499.339	0.339
1046	1081	499.339	0.339
1011	1054	499.289	0.289
1020	1057	499.309	0.309
1030	1061	499.289	0.289
1039	1064	499.339	0.339
1015	1026	499.329	0.329
1024	1032	499.389	0.389
1032	1038	499.349	0.349
1040	1043	499.319	0.319
1048	1049	499.269	0.269
1062	1058	499.279	0.279
1077	1068	499.349	0.349
1097	1118	499.359	0.359
1130	1105	499.319	0.319
1041	1007	499.329	0.329
1049	1012	499.159	0.159
1058	1018	498.359	-0.641
1066	1023	498.819	-0.181
1074	1029	499.309	0.309
1087	1038	499.329	0.329
1102	1048	499.349	0.349
1122	1061	499.359	0.359
1156	1085	499.429	0.429
1171	1095	498.799	-0.201
1185	1105	498.799	-0.201

APPENDIX E

POND SEDIMENT PARTICLE SIZE DISTRIBUTION (JUNE, AUGUST)

Table E-1. June stormwater pond sediment particle size distribution

Northing (m)	Easting (m)	% of gravel	% of sand	% finer than 50 microns	silt	clay
996.96	1174.68	69.59	19.57	0.21	0.09	0.09
1006.12	1173.91	24.59	71.45	1.26	0.49	0.60
991.50	1140.93	15.87	65.07	0.42	0.23	0.11
1007.68	1146.30	9.31	75.15	0.46	0.25	0.13
1018.50	1149.89	4.06	84.80	0.90	0.50	0.23
997.68	1116.68	1.37	92.12	5.59	2.76	2.29
1007.46	1118.78	0.09	98.33	1.56	0.61	0.73
1017.24	1120.88	0.00	97.83	2.15	0.76	1.13
1027.01	1122.97	4.42	78.16	1.09	0.40	0.53
1036.79	1125.07	6.13	72.17	0.43	0.15	0.22
1046.57	1127.17	33.52	52.56	0.59	0.17	0.31
1056.35	1129.27	1.19	86.27	0.30	0.11	0.14
1066.12	1131.37	9.34	60.79	0.26	0.07	0.14
1075.90	1133.46	12.80	64.38	0.88	0.29	0.44
1012.06	1096.07	3.40	75.44	0.65	0.23	0.33
1021.73	1098.62	7.84	24.30	56.11	24.42	14.22
1041.07	1103.71	4.39	85.78	0.58	0.24	0.26
1056.64	1107.81	0.72	92.85	0.63	0.24	0.32
1074.24	1112.44	4.03	81.11	1.20	0.41	0.63
1007.17	1071.63	2.92	81.71	0.62	0.26	0.25
1016.88	1074.00	0.59	96.02	1.40	0.56	0.60
1026.60	1076.36	19.70	52.42	0.10	0.04	0.04
1036.32	1078.73	4.60	85.34	1.03	0.41	0.46
1046.03	1081.09	33.06	46.17	0.16	0.05	0.09
1020.21	1057.36	0.74	95.35	1.59	0.53	0.81
1029.69	1060.54	0.00	97.40	0.15	0.02	0.10
1015.42	1026.35	0.89	93.45	0.82	0.29	0.42
1023.65	1032.02	4.89	81.61	0.41	0.16	0.19
1031.89	1037.69	11.55	68.49	1.04	0.36	0.54
1040.13	1043.36	25.69	65.17	0.25	0.15	0.06
1048.36	1049.03	1.04	92.11	0.71	0.27	0.32
1061.62	1058.16	0.67	96.12	1.41	0.69	0.53
1076.61	1068.49	0.38	97.94	0.68	0.43	0.17
1130.40	1105.52	21.79	71.98	0.48	0.29	0.12
1040.95	1006.60	0.74	92.25	2.03	0.71	0.99
1049.22	1012.23	9.30	66.87	0.75	0.26	0.38
1057.48	1017.86	22.82	67.66	0.63	0.27	0.26
1065.75	1023.48	3.72	81.63	0.12	0.02	0.06
1074.02	1029.11	4.64	90.10	0.38	0.19	0.16
1087.32	1038.17	0.33	99.00	0.64	0.28	0.30
1102.37	1048.41	3.26	79.66	0.53	0.20	0.25
1121.46	1061.41	1.19	92.75	3.06	1.43	1.32
1156.35	1085.16	1.88	87.12	1.05	0.43	0.47
1171.23	1095.29	15.91	69.48	1.09	0.43	0.51
1185.11	1104.75	2.40	80.62	0.41	0.15	0.16

Table E-2. August stormwater pond sediment particle size distribution

Northing (m)	Easting (m)	% of gravel	% of sand	% finer than 50 microns	silt	clay
996.92	1174.67	2.86	87.83	2.74	1.66	0.65
1006.09	1173.92	2.39	89.41	3.12	1.3	1.34
991.56	1140.91	3.14	88.44	2.49	1.05	1.03
1007.73	1146.30	10.2	72.83	0.84	0.3	0.39
1018.55	1149.90	6.96	71.86	0.96	0.5	0.32
997.56	1116.55	2	82.04	1.61	0.54	0.8
1007.33	1118.65	9.77	76.5	1.74	0.92	0.6
1017.11	1120.75	12.19	76.83	0.93	0.34	0.42
1026.89	1122.85	0.54	94.1	2.97	1.07	1.11
1036.66	1124.95	4.74	76.7	0.78	0.38	0.18
1046.44	1127.05	4.38	82.6	2.59	0.99	1.2
1056.22	1129.15	55.56	41.57	0.66	0.17	0.33
1066.00	1131.25	18.06	74.06	0.08	0.04	0.03
1075.77	1133.36	64.67	31.1	0.8	0.23	0.43
1012.15	1096.07	6.92	78.4	1.56	0.76	0.6
1021.82	1098.61	1.02	92.06	1.12	0.58	0.38
1041.16	1103.71	6.55	75.97	1.2	0.41	0.59
1056.73	1107.81	26.62	52.07	0.94	0.35	0.26
1074.33	1112.44	13.59	66.17	1.42	0.52	0.67
1007.05	1071.54	7.63	71.97	1.24	0.51	0.51
1016.76	1073.91	3.76	83.09	0.83	0.39	0.29
1026.48	1076.28	1.94	83.37	0.81	0.43	0.29
1036.19	1078.65	16.37	69.44	1.12	0.38	0.57
1045.91	1081.02	2.76	85.58	2.32	0.98	0.94
1020.19	1057.37	5.01	80.27	0.61	0.25	0.25
1029.66	1060.55	6.12	76.3	0.22	0.09	0.11
1015.42	1026.31	2.33	82.05	2.41	0.83	1.13
1023.65	1031.98	1.9	89.35	1.65	0.54	0.82
1031.89	1037.66	5.43	83.13	1.57	0.56	0.76
1040.13	1043.33	8.14	74.67	0.41	0.15	0.18
1048.36	1049.00	23.37	57.23	0.16	0.04	0.09
1061.62	1058.13	22.86	59.39	0.38	0.14	0.17
1076.61	1068.46	5.87	77.24	0.98	0.34	0.44
1130.39	1105.50	17.66	58.79	1.64	0.55	0.83
1041.09	1006.55	16.17	71.41	0.82	0.27	0.39
1049.35	1012.18	0.26	97.11	1.49	0.52	0.55
1057.61	1017.82	11.69	70.86	1.06	0.33	0.52
1065.87	1023.45	7.32	78.94	0.8	0.35	0.29
1074.13	1029.08	9.14	78.54	0.92	0.33	0.42
1087.44	1038.15	10.33	70.47	0.47	0.23	0.18
1102.47	1048.41	0.72	89.93	4.74	1.75	2.34
1121.56	1061.42	0.1	91.95	1.56	0.61	0.73
1156.42	1085.20	1.43	96.07	1.18	0.58	0.33
1171.29	1095.34	1.39	92.84	1.33	0.72	0.36
1185.17	1104.80	2.57	83.69	1.15	0.49	0.44

Table E-3. Individual sample data from particle size distribution analysis for June and August samples of 2014.

Sample number	Nominal % Passing in Millimeters																		
	Gravel					very coarse sand	coarse sand	medium sand	fine sand	very fine sand		% finer than 50 microns	Silt						Clay
	37.5	19	9.5	4.75	2.36	1.18	0.6	0.3	0.15	0.075	0.0691	0.0492	0.0351	0.0222	0.0150	0.0093	0.0066	0.0033	0.0014
02-Jun	100.00	100.00	76.80	53.86	30.41	19.79	10.87	7.00	3.91	0.40	0.22	0.21	0.20	0.18	0.18	0.17	0.16	0.13	0.09
03-Jun	100.00	100.00	79.20	79.20	75.41	72.78	68.29	62.18	40.84	1.39	1.33	1.26	1.21	1.13	1.09	0.96	0.88	0.77	0.60
04-Jun	100.00	100.00	97.46	95.87	84.13	65.50	34.50	18.49	7.84	0.60	0.43	0.42	0.41	0.38	0.36	0.29	0.25	0.19	0.11
05-Jun	100.00	100.00	100.00	100.00	99.81	99.07	71.76	45.23	21.48	1.96	1.42	1.40	1.35	1.26	1.07	0.88	0.76	0.50	0.31
5.5 June	100.00	100.00	100.00	99.62	90.69	75.63	47.42	29.65	13.66	0.73	0.47	0.46	0.42	0.40	0.38	0.33	0.29	0.21	0.13
06-Jun	100.00	100.00	100.00	98.82	95.94	85.72	43.86	23.86	11.18	1.18	0.92	0.90	0.87	0.79	0.75	0.64	0.55	0.40	0.23
07-Jun	100.00	100.00	100.00	100.00	98.63	97.95	92.86	80.82	50.20	7.73	5.82	5.59	4.96	4.35	4.11	3.55	3.22	2.83	2.29
8 June	100.00	100.00	100.00	100.00	99.91	99.91	99.68	98.89	96.87	93.59	1.57	1.56	1.52	1.50	1.43	1.26	1.18	0.95	0.73
09-Jun	100.00	100.00	100.00	100.00	100.00	100.00	77.16	44.62	20.77	2.54	2.17	2.15	2.10	2.05	1.98	1.82	1.70	1.39	1.13
10-Jun	100.00	100.00	100.00	100.00	95.58	79.27	49.20	31.84	15.38	1.14	1.11	1.09	1.08	1.06	1.02	0.88	0.85	0.69	0.53
11-Jun	100.00	100.00	100.00	99.47	93.87	72.61	35.82	16.99	6.00	0.43	0.44	0.43	0.42	0.42	0.40	0.36	0.34	0.28	0.22
12-Jun	100.00	100.00	100.00	95.29	66.48	53.16	32.10	18.55	6.73	0.59	0.59	0.59	0.57	0.57	0.55	0.52	0.50	0.41	0.31
13-Jun	100.00	100.00	100.00	100.00	98.81	86.58	42.97	20.65	7.88	0.36	0.30	0.30	0.28	0.28	0.28	0.25	0.24	0.19	0.14
14-Jun	100.00	100.00	100.00	100.00	90.66	61.05	29.62	13.08	3.96	0.29	0.26	0.26	0.26	0.26	0.25	0.23	0.22	0.19	0.14
14.5/15 June	100.00	100.00	100.00	98.77	87.20	65.27	37.66	21.06	8.64	0.91	0.89	0.88	0.87	0.85	0.81	0.75	0.71	0.59	0.44
15-Jun	100.00	100.00	100.00	99.73	90.08	70.52	39.65	21.01	7.90	0.57	0.53	0.52	0.51	0.49	0.47	0.43	0.39	0.32	0.20
16-Jun	100.00	100.00	100.00	100.00	96.60	76.10	36.58	18.61	6.83	0.68	0.66	0.65	0.64	0.63	0.60	0.59	0.51	0.42	0.33
17-Jun	100.00	100.00	100.00	100.00	92.16	80.95	67.02	59.84	54.89	54.27	56.66	56.11	53.94	49.60	45.80	40.92	37.55	31.69	14.22
18-Jun	100.00	100.00	100.00	99.06	93.55	83.22	50.24	27.84	10.38	0.79	0.81	0.81	0.78	0.74	0.70	0.63	0.58	0.49	0.39
19-Jun	100.00	100.00	100.00	99.79	95.61	86.38	53.38	30.39	11.69	1.85	0.60	0.58	0.58	0.54	0.51	0.45	0.40	0.34	0.26
20-Jun	100.00	100.00	100.00	100.00	99.28	93.48	58.13	30.64	11.49	0.62	0.63	0.63	0.60	0.57	0.55	0.50	0.46	0.38	0.32
21-Jun	100.00	100.00	100.00	100.00	95.97	82.32	57.80	33.80	12.68	1.31	1.20	1.20	1.19	1.16	1.12	1.00	0.94	0.79	0.63
22-Jun	100.00	100.00	100.00	100.00	97.08	82.33	38.41	18.09	6.41	0.66	0.63	0.62	0.60	0.56	0.52	0.47	0.42	0.35	0.25
23-Jun	100.00	100.00	100.00	100.00	99.41	97.43	60.63	31.11	12.11	1.46	1.41	1.40	1.37	1.28	1.22	1.10	1.03	0.84	0.60
24-Jun	100.00	100.00	100.00	100.00	80.30	52.52	22.64	9.04	2.38	0.10	0.10	0.10	0.09	0.09	0.09	0.08	0.07	0.06	0.04

Table E-3 Continued. Individual sample data from particle size distribution analysis for June and August samples of 2014.

25-Jun	100.00	100.00	100.00	99.60	95.40	86.38	47.95	22.92	8.15	1.14	1.03	1.03	1.02	0.97	0.92	0.80	0.75	0.62	0.46
26-Jun	100.00	100.00	100.00	100.00	66.94	46.33	23.35	10.89	3.71	0.16	0.16	0.16	0.16	0.16	0.16	0.15	0.15	0.12	0.09
28-Jun	100.00	100.00	100.00	100.00	99.26	96.96	71.00	38.60	16.36	2.29	1.61	1.59	1.56	1.49	1.45	1.36	1.27	1.05	0.81
29-Jun	100.00	100.00	100.00	100.00	100.00	97.56	53.35	17.68	4.27	0.30	0.16	0.15	0.15	0.15	0.15	0.17	0.10	0.13	0.10
29.5 June	100.00	100.00	100.00	100.00	98.37	92.75	56.55	32.41	13.16	0.59	0.20	0.19	0.19	0.18	0.17	0.15	0.13	0.10	0.08
30-Jun	100.00	100.00	100.00	100.00	99.11	94.29	53.18	27.17	10.76	0.89	0.84	0.82	0.81	0.78	0.76	0.71	0.67	0.53	0.42
31 June	100.00	100.00	100.00	99.13	95.11	82.02	37.78	17.36	5.41	0.44	0.41	0.41	0.40	0.38	0.35	0.32	0.29	0.25	0.19
32 June	100.00	100.00	100.00	100.00	88.45	69.56	39.75	22.61	9.21	1.19	1.07	1.04	1.04	1.04	0.99	0.89	0.84	0.68	0.54
33 June	100.00	100.00	87.62	84.01	74.31	65.44	34.46	16.17	6.29	0.41	0.26	0.25	0.23	0.21	0.20	0.17	0.10	0.10	0.06
34 June	100.00	100.00	100.00	100.00	98.96	92.83	66.87	47.71	24.38	0.86	0.71	0.71	0.71	0.70	0.67	0.62	0.56	0.45	0.32
35 June	100.00	100.00	100.00	99.52	99.33	97.65	90.37	75.17	33.72	3.10	1.53	1.41	1.31	1.22	1.13	0.97	0.85	0.72	0.53
36 June	100.00	100.00	100.00	100.00	99.62	98.66	89.64	60.09	19.43	1.04	0.71	0.68	0.68	0.57	0.52	0.40	0.35	0.25	0.17
37 June	100.00	100.00	100.00	100.00	91.91	81.21	51.83	28.06	10.12	1.12	1.15	1.14	1.09	1.08	1.05	0.99	0.95	0.81	0.66
37.5 June	100.00	100.00	95.17	87.08	78.21	72.48	57.59	32.81	10.65	0.64	0.49	0.48	0.47	0.41	0.38	0.31	0.27	0.20	0.12
38 June	100.00	100.00	100.00	100.00	99.26	94.30	55.52	33.15	14.62	2.27	2.06	2.03	2.01	1.97	1.90	1.69	1.67	1.32	0.99
39 June	100.00	100.00	100.00	98.90	90.70	67.63	39.67	22.03	7.94	0.86	0.75	0.75	0.74	0.70	0.68	0.62	0.58	0.48	0.38
40 June	100.00	100.00	78.10	78.10	77.18	68.30	36.98	19.28	8.03	0.74	0.64	0.63	0.60	0.55	0.52	0.47	0.43	0.36	0.26
41 June	100.00	100.00	100.00	99.69	96.28	81.75	35.75	14.60	4.19	0.27	0.12	0.12	0.11	0.12	0.14	0.14	0.12	0.10	0.06
42 June	100.00	100.00	100.00	97.90	95.36	90.50	61.19	35.86	14.03	0.47	0.40	0.38	0.37	0.34	0.31	0.26	0.24	0.19	0.16
43 June	100.00	100.00	100.00	100.00	99.67	99.64	63.04	30.28	8.42	0.77	0.64	0.64	0.63	0.62	0.59	0.50	0.46	0.37	0.30
44 June	100.00	100.00	100.00	100.00	96.74	80.20	41.61	22.85	9.07	0.56	0.54	0.53	0.52	0.50	0.47	0.43	0.40	0.33	0.25
45 June	100.00	100.00	100.00	100.00	98.81	95.86	83.55	49.33	19.85	3.32	3.10	3.06	3.03	2.73	2.54	2.32	2.00	1.63	1.32
46 June	100.00	100.00	100.00	100.00	98.12	88.19	47.63	25.60	10.91	1.19	1.07	1.05	1.04	0.95	0.92	0.82	0.74	0.63	0.47
47 June	100.00	100.00	100.00	97.26	84.09	70.59	37.95	20.67	9.24	1.25	1.10	1.09	1.09	1.03	0.98	0.88	0.78	0.66	0.51
48 June	100.00	100.00	100.00	100.00	97.60	81.04	43.40	22.58	9.28	0.64	0.42	0.41	0.46	0.43	0.41	0.35	0.31	0.26	0.16
01-Aug	100.00	100.00	94.76	61.93	40.81	35.86	30.94	25.01	14.14	1.29	1.23	1.19	1.16	1.09	1.01	0.83	0.74	0.58	0.44
02-Aug	100.00	100.00	100.00	99.68	97.14	90.61	76.68	53.71	26.20	3.69	2.78	2.74	2.52	2.19	1.97	1.60	1.42	1.08	0.65
03-Aug	100.00	100.00	100.00	100.00	97.61	92.60	83.53	71.84	39.86	3.82	3.19	3.12	2.89	2.77	2.66	2.39	2.12	1.82	1.34
3.5 Aug	100.00	89.37	82.37	54.17	28.97	24.96	21.35	16.74	8.67	0.57	0.53	0.52	0.50	0.48	0.46	0.43	0.40	0.35	0.26

Table E-3 Continued. Individual sample data from particle size distribution analysis for June and August samples of 2014.

04-Aug	100.00	100.00	100.00	99.62	96.86	90.96	74.42	50.23	22.81	3.29	2.52	2.49	2.42	2.39	2.26	1.96	1.76	1.44	1.03
5.5 Aug	100.00	100.00	100.00	98.03	89.80	73.69	49.57	30.79	14.36	1.14	0.86	0.84	0.83	0.81	0.77	0.70	0.64	0.54	0.39
6 Aug	100.00	100.00	100.00	98.47	93.04	72.84	42.31	22.94	10.29	1.07	0.98	0.96	0.94	0.85	0.75	0.67	0.59	0.46	0.32
7 Aug	100.00	100.00	100.00	100.00	98.00	83.67	57.76	35.77	14.80	1.73	1.63	1.61	1.60	1.54	1.49	1.39	1.30	1.08	0.80
8 Aug	100.00	100.00	100.00	97.32	90.23	78.26	51.54	30.95	15.93	1.61	1.76	1.74	1.72	1.66	1.20	1.12	1.02	0.82	0.60
9 Aug	100.00	100.00	100.00	98.27	87.81	77.78	51.87	32.63	16.96	1.05	0.94	0.93	0.92	0.87	0.85	0.77	0.71	0.60	0.42
10 Aug	100.00	100.00	100.00	100.00	99.46	97.10	86.82	59.21	28.63	3.44	3.00	2.97	2.94	2.80	2.66	2.53	2.32	1.90	1.11
11 Aug	100.00	100.00	100.00	100.00	95.26	77.50	49.85	29.17	13.21	0.87	0.79	0.78	0.76	0.71	0.67	0.59	0.52	0.40	0.18
12 Aug	100.00	100.00	100.00	100.00	95.62	85.22	63.47	40.20	17.46	2.90	2.62	2.59	2.56	2.47	2.39	2.18	2.01	1.60	1.20
13 Aug	100.00	100.00	71.98	49.90	44.44	42.26	36.88	28.77	15.13	0.68	0.69	0.66	0.64	0.62	0.61	0.58	0.54	0.49	0.33
14 Aug	100.00	100.00	82.08	82.08	81.94	74.14	54.49	35.86	15.34	0.10	0.08	0.08	0.08	0.07	0.07	0.06	0.05	0.04	0.03
14.5 Aug	100.00	100.00	73.84	49.77	35.33	31.91	27.17	20.89	10.25	0.78	0.81	0.80	0.79	0.78	0.76	0.72	0.66	0.57	0.43
16 Aug	100.00	100.00	100.00	100.00	93.08	79.97	50.34	28.45	12.51	1.61	1.57	1.56	1.52	1.47	1.38	1.19	1.05	0.80	0.60
17 Aug	100.00	100.00	100.00	100.00	98.98	93.19	54.32	29.61	12.89	1.21	1.13	1.12	1.11	0.94	0.86	0.78	0.67	0.54	0.38
19 Aug	100.00	100.00	100.00	100.00	93.45	77.19	52.57	32.65	12.66	1.18	1.22	1.20	1.18	1.13	1.10	1.01	0.94	0.79	0.59
20 Aug	100.00	100.00	100.00	96.60	73.38	53.02	31.23	17.23	7.32	0.99	0.95	0.94	0.92	0.91	0.84	0.75	0.72	0.59	0.26
21 Aug	100.00	100.00	100.00	99.06	86.41	67.60	41.59	22.96	8.97	1.45	1.43	1.42	1.41	1.33	1.24	1.13	1.05	0.90	0.67
22 Aug	100.00	100.00	100.00	98.54	92.37	73.23	45.13	24.82	10.30	1.30	1.25	1.24	1.23	1.14	1.09	0.98	0.92	0.73	0.51
23 Aug	100.00	100.00	100.00	100.00	96.24	83.93	49.42	26.51	10.46	0.88	0.84	0.83	0.82	0.75	0.68	0.60	0.54	0.44	0.29
Aug 24	100.00	100.00	100.00	100.00	98.06	84.18	52.87	28.23	11.37	0.85	0.81	0.81	0.79	0.75	0.70	0.57	0.49	0.38	0.29
24.5 Aug	100.00	100.00	100.00	100.00	99.80	97.52	74.18	47.28	20.12	3.15	3.08	3.05	2.95	2.79	2.54	2.22	2.00	1.78	1.24
25 Aug	100.00	100.00	100.00	96.95	83.63	70.58	46.52	24.96	9.66	1.16	1.13	1.12	1.11	1.05	1.00	0.91	0.84	0.74	0.57
26 Aug	100.00	100.00	100.00	100.00	97.24	87.92	65.76	39.95	17.07	2.34	2.34	2.32	2.25	2.08	1.99	1.76	1.62	1.34	0.94
27 Aug	100.00	100.00	100.00	99.13	90.82	72.04	41.34	22.12	9.01	0.91	0.77	0.77	0.76	0.74	0.70	0.66	0.61	0.51	0.37
28 Aug	100.00	100.00	100.00	99.24	94.99	80.90	48.11	24.53	9.87	0.69	0.63	0.61	0.60	0.57	0.54	0.51	0.46	0.36	0.25
29 Aug	100.00	100.00	100.00	100.00	93.88	76.53	42.44	19.09	6.18	0.24	0.23	0.22	0.22	0.21	0.20	0.18	0.17	0.14	0.11
30 Aug	100.00	100.00	100.00	100.00	97.67	84.51	52.04	29.14	13.06	2.64	2.46	2.41	2.38	2.33	2.12	2.09	1.91	1.58	1.13
31 Aug	100.00	100.00	100.00	100.00	98.10	91.01	68.51	40.06	16.07	1.67	1.67	1.65	1.63	1.55	1.46	1.33	1.23	1.11	0.82
32 Aug	100.00	100.00	100.00	100.00	94.57	84.72	58.42	32.74	13.55	1.70	1.59	1.57	1.56	1.54	1.45	1.30	1.22	1.01	0.76

Table E-3 Continued. Individual sample data from particle size distribution analysis for June and August samples of 2014.

33 Aug	100.00	100.00	100.00	100.00	91.86	75.08	42.36	19.89	6.68	0.53	0.41	0.41	0.40	0.39	0.38	0.33	0.31	0.26	0.18
34 Aug	100.00	100.00	100.00	96.81	76.63	57.39	25.44	10.23	3.15	0.25	0.16	0.16	0.16	0.17	0.16	0.15	0.14	0.12	0.09
35 Aug	100.00	100.00	97.71	91.08	77.14	59.78	32.79	16.01	6.27	0.46	0.39	0.38	0.38	0.36	0.35	0.32	0.29	0.24	0.17
36 Aug	100.00	100.00	100.00	100.00	94.13	78.25	44.18	23.67	10.96	1.27	1.01	0.98	0.98	0.98	0.92	0.83	0.80	0.64	0.44
37.5 Aug	100.00	87.06	87.06	86.54	82.34	60.45	36.83	22.05	9.86	1.75	1.66	1.64	1.63	1.57	1.50	1.38	1.31	1.09	0.83
38 Aug	100.00	100.00	100.00	97.97	83.83	72.25	46.25	22.57	8.52	1.11	0.84	0.82	0.80	0.78	0.76	0.71	0.66	0.55	0.39
39 Aug	100.00	100.00	100.00	100.00	99.74	98.62	68.35	37.64	16.19	1.76	1.51	1.49	1.44	1.42	1.40	1.26	1.16	0.98	0.55
40 Aug	100.00	100.00	100.00	98.85	88.31	71.92	41.80	22.34	9.17	1.22	1.06	1.06	1.04	1.02	0.98	0.93	0.89	0.74	0.52
41 Aug	100.00	100.00	100.00	100.00	92.68	79.76	53.29	27.48	10.08	0.93	0.81	0.80	0.78	0.78	0.71	0.65	0.58	0.45	0.29
42 Aug	100.00	100.00	100.00	100.00	90.86	79.48	54.48	31.16	13.36	0.99	0.94	0.92	1.01	0.94	0.89	0.79	0.69	0.59	0.42
43 Aug	100.00	100.00	100.00	95.17	89.67	70.94	36.42	17.72	6.48	0.51	0.47	0.47	0.43	0.38	0.36	0.33	0.30	0.24	0.18
44 Aug	100.00	100.00	100.00	100.00	99.28	94.77	67.83	45.71	23.15	5.08	4.84	4.74	4.54	4.49	4.23	3.88	3.62	2.99	2.34
45 Aug	100.00	100.00	100.00	100.00	99.90	96.79	67.16	42.42	20.51	1.76	1.57	1.56	1.52	1.50	1.43	1.26	1.18	0.95	0.73
46 Aug	100.00	100.00	100.00	99.00	98.57	97.30	86.90	67.42	33.48	1.99	1.22	1.18	1.17	1.05	0.95	0.81	0.75	0.61	0.33
47 Aug	100.00	100.00	100.00	100.00	98.61	94.18	78.89	56.51	25.97	1.94	1.35	1.33	1.31	1.27	1.11	0.96	0.82	0.61	0.36
48 Aug	100.00	100.00	100.00	100.00	97.43	84.86	64.64	47.42	23.36	2.03	1.17	1.15	1.13	1.10	0.89	1.00	0.86	0.66	0.44